TECHNICAL REPORT N-77-6

CENSE EXPLOSION TEST PROGRAM

Report I

CENSE I, EXPLOSIONS IN SANDSTONE

by

James K. Ingram

Weapons Effects Laboratory
U. S. Army Engineer Waterways Experiment Station
P. O. Box 631, Vicksburg, Miss. 39180

September 1977

Report 1 of a Series

Prepared for Office, Chief of Engineers, U. S. Army
Washington, D. C. 20314

Under R&D Project 4A763734DT08, Task 09
Work Unit 006, Ground Shock from Multiple Bursts

Destroy this report when no longer needed. Do not return it to the originator.

DEPARTMENT OF THE ARMY
WATERWAYS EXPERIMENT STATION, CORPS OF ENGINEERS
P. O. BOX 631
VICKSBURG, MISSISSIPPI 39180

IN REPLY REFER TO: WESAR

14 October 1977

Errata Sheet

No. 1

CENSE EXPLOSION TEST PROGRAM

Report 1

CENSE 1, EXPLOSIONS IN SANDSTONE

Technical Report N-77-6

September 1977

1. The R&D Project, Task, and Work Unit numbers and titles on the cover, in Block 10 of the Form 1473, and in lines 8 and 9 of the Preface, page 2, should read as follows: R&D Project 4A762719AT40, Task A1, Work Unit 018, "Ground Shock from Multiple Bursts," and R&D Project 4A763734DT08, Task 09, Work Unit 008, "Ground Shock from Multiple Bursts."

Unclassified

SECURITY CLASSIFICATION OF THIS PAGE (When Data Entered)

REPORT DOCUMENTATION PAGE

READ INSTRUCTIONS BEFORE COMPLETING FORM

1. REPORT NUMBER: Technical Report N-77-6
2. GOVT ACCESSION NO.: WES-TR-N-77-6
3. RECIPIENT'S CATALOG NUMBER:
4. TITLE (and Subtitle): CENSE EXPLOSION TEST PROGRAM. Report 1. CENSE 1. EXPLOSIONS IN SANDSTONE.
5. TYPE OF REPORT & PERIOD COVERED: Report 1 of a series
6. PERFORMING ORG. REPORT NUMBER:
7. AUTHOR(s): James K. Ingram
8. CONTRACT OR GRANT NUMBER(s): 4A762719AT40
9. PERFORMING ORGANIZATION NAME AND ADDRESS: U. S. Army Engineer Waterways Experiment Station, Weapons Effects Laboratory, P. O. Box 631, Vicksburg, Miss. 39180
10. PROGRAM ELEMENT, PROJECT, TASK AREA & WORK UNIT NUMBERS: R&D Project 4A763734DT08, Task 09, Work Unit 008, Ground Shock from Multiple Bursts
11. CONTROLLING OFFICE NAME AND ADDRESS: Office, Chief of Engineers, U. S. Army, Washington, D. C. 20314
12. REPORT DATE: Sept 1977
13. NUMBER OF PAGES: 164
14. MONITORING AGENCY NAME & ADDRESS (if different from Controlling Office): 167 p.
15. SECURITY CLASS. (of this report): Unclassified
15a. DECLASSIFICATION/DOWNGRADING SCHEDULE:
16. DISTRIBUTION STATEMENT (of this Report): Approved for public release; distribution unlimited.
17. DISTRIBUTION STATEMENT (of the abstract entered in Block 20, if different from Report):
18. SUPPLEMENTARY NOTES:
19. KEY WORDS (Continue on reverse side if necessary and identify by block number):

Air blast waves	Ground shock
Cratering	High explosives
CENSE (Program)	Sandstones

20. ABSTRACT (Continue on reverse side if necessary and identify by block number):

CENSE (~~an acronym for~~ Coupling Efficiency of Near-Surface Explosions) was a high-explosive (~~HE~~) test program designed to obtain an understanding of the effects of burst position on cratering, ground shock, and related phenomena in several geologies. Results of these experiments will be published in a series of reports. Reports 1 through 3 are data reports; Report 1, CENSE 1, Explosions in Sandstone; Report 2, CENSE 2, Explosions in Soil; and Report 3, CENSE 3, Explosions in Soil over Sandstone. The final report of the series, Report 4,

(Continued) (over)

DD FORM 1 JAN 73 1473 EDITION OF 1 NOV 65 IS OBSOLETE

Unclassified

SECURITY CLASSIFICATION OF THIS PAGE (When Data Entered)

038 100

20. ABSTRACT (Continued) (of p 1473A) Report no. 4

Analysis and Summary of CENSE Data, will provide more complete analysis and data comparisons for the overall ~~test~~ program.

The objective of CENSE 1 was to study the effects of burst position on ground shock, airblast, and cratering in rock (sandstone). Eight tests were conducted using 1000-pound liquid nitromethane spheres. Burst positions ranged from an elevated (airburst, noncratering) charge position of 6 feet to depths of approximately 10.5 feet. Both apparent and true craters were measured for all events. Near-surface (2-foot depth) vertical and horizontal ground motions were measured on all ~~events~~ except the deepest shot. For ~~this~~ that shot, the near-surface gage array was repositioned at shot depth (10.5 feet). Surface airblast was measured for all but the deepest detonation. In addition to the near-surface motions, vertical motions were measured directly beneath the explosion on all events. No stress measurements were made on CENSE 1.

Data are presented in the form of time histories and amplitude-distance plots.

14 73B

THE CONTENTS OF THIS REPORT ARE NOT TO BE USED FOR ADVERTISING, PUBLICATION, OR PROMOTIONAL PURPOSES. CITATION OF TRADE NAMES DOES NOT CONSTITUTE AN OFFICIAL ENDORSEMENT OR APPROVAL OF THE USE OF SUCH COMMERCIAL PRODUCTS.

PREFACE

This report forms the first complete data report in a series of four reports on the CENSE (Coupling Efficiency of Near-Surface Explosions) explosion test program. Reports 1 through 3 are essentially data reports describing tests in sandstone, soil, and a layered soil/sandstone geology, respectively. Report 4 (in preparation at this writing) provides an analysis and summary of the entire test series.

The CENSE series was sponsored by the Office, Chief of Engineers (OCE) under R&D Project 4A763734DT08, Task 09, Work Unit 008, Ground Shock from Multiple Bursts, and conducted by the Weapons Effects Laboratory (WEL), U. S. Army Engineer Waterways Experiment Station (WES). Mr. D. S. Reynolds served as technical monitor for OCE.

Fieldwork for CENSE 1 was conducted by personnel in the Phenomenology and Effects Division (PED), WEL, in the fall of 1973 near the Mixed Company test site in western Colorado, under the direction of J. K. Ingram, Project Scientist, PED. Site preparation and instrument installation were accomplished by Messrs. W. M. Gay, T. P. Williams, and J. H. Stout. Explosive charges were prepared by Messrs. Gay and S. E. Bartlett. Craters were profiled by Mr. S. B. Price.

Support was provided by the WES Instrumentation Services Division. Messrs. L. T. Watson and E. W. Flowers provided field instrumentation support, and Messrs. F. P. Leake and E. L. Sadler provided instrument calibration.

Computer processing of the field data was coordinated by Mr. J. T. Brogan and Mrs. D. W. McAlpin, PED.

This effort was conducted under the general supervision of Messrs. J. L. Drake, Program Manager, PED; L. F. Ingram, Chief, PED; and W. F. Flathau, Chief, WEL.

COL G. H. Hilt, CE, and COL J. L. Cannon, CE, were Commanders and Directors of WES during the preparation and publication of this report. Mr. F. R. Brown was Technical Director.

CONTENTS

TABLES

FIGURES

CONVERSION FACTORS, U. S. CUSTOMARY TO METRIC (SI) UNITS OF MEASUREMENT

U. S. customary units of measurement used in this report can be converted to metric (SI) units as follows:

Multiply	By	To Obtain
feet	0.3048	metres
miles (U. S. statute)	1.609344	kilometres
cubic feet	0.02831685	cubic metres
pounds (mass)	0.4535924	kilograms
tons (short)	907.1847	kilograms
pounds (force) per square inch	6894.757	pascals
feet per second	0.3048	metres per second
inches	0.0254	metres

CENSE EXPLOSION TEST PROGRAM

CENSE 1, EXPLOSIONS IN SANDSTONE

CHAPTER 1

INTRODUCTION

1.1 BACKGROUND

Ground shock, airblast, and cratering are highly sensitive to burst position for near-surface explosions. Previous high-explosive (HE)[1] tests have indicated large increases in ground shock magnitudes and crater sizes when the height of burst (HOB) is varied from slightly elevated to buried configurations. Since MOLE (Reference 1), which was not adequately instrumented in the regions of interest, no systematic test program has been directed toward HOB effects. More than a score of large-scale HE tests have been conducted in recent years; however, wide variations in geology, yield, and burst configuration preclude a quantitative definition of HOB effects. Successful ground shock measurements on-axis below the explosion were very limited. Limited data are available for the Flat Top series (Reference 2); one point from Middle Gust Event 4 (References 3 and 4); and a few locations from a low-yield nuclear explosion in a granite cavity.

1.2 OBJECTIVE

The overall objective of the CENSE program (Coupling Efficiency of Near-Surface Explosions) was to study the influence of burst position on ground shock airblast and cratering in different geologic media, with particular emphasis on measurements directly beneath the explosion. The specific objective of CENSE 1 was to study these effects in a relatively uniform rock (sandstone).

---

[1] For convenience, symbols and unusual abbreviations used in this report are listed and defined in the Notation (Appendix C).

1.3 SCOPE

A preliminary treatment of the CENSE 1 data was published as Miscellaneous Paper N-75-3 in May 1975 (Reference 5). Effects of burst position were presented in terms of coupling factors, defined as the ratio of an effect magnitude to that for a standard containment condition.

This report is basically a data report. Detailed analysis and conclusions will be presented in Report 4 of this series, "Analysis and Summary of CENSE Data."

CHAPTER 2

APPROACH

2.1 DESCRIPTION OF TEST SITE

An exposed outcrop of Kayenta sandstone with 180- by 270-foot[1] dimensions, located about 4 miles south of Mixed Company test site, was selected for siting. Details of site location, geology, and test bed preparation are given in Appendix A.

2.2 EXPERIMENTAL PLAN

Eight 1000-pound spherical nitromethane (NM) charges (1140-pound TNT equivalent) were detonated at seven burst positions relative to the surface of the rock (Tables 2.1 and 2.2, Figure 2.1). Event 1 was an airburst (noncratering) shot with an HOB of 6 feet. (All burst positions refer to charge center of gravity (CG) relative to the surface of the rock.) Because of loss of certain data channels, Event 1 was reshot as Event 8. Events 2 through 7 were positioned respectively as: surface tangent (HOB = 1.5 feet), one-fourth buried (HOB = 0.75 foot), half buried (HOB = 0 foot), three-fourths buried (DOB = 0.75 foot), buried tangent (depth of burst (DOB) = 1.5 feet), and buried at 10.5 feet. The terms one-fourth buried, half buried etc., refer to that portion of the charge diameter positioned beneath the surface of the rock; i.e., one-fourth buried = one-fourth of charge diameter below rock surface, half buried = half in, half out, etc.

The explosive charges were contained in 3-foot-diameter fiberglass spheres. The charges were detonated at the geometric center of the sphere with a 0.75-pound C4 explosive booster initiated by a Reynolds RP-1M exploding bridge wire detonator.

2.3 INSTRUMENTATION LAYOUT

A total of 20 data channels were used for each test event to

---

[1] A table of factors for converting U. S. customary units of measurement to metric (SI) can be found on page 8.

measure ground shock and surface airblast: 5 channels for surface airblast, 5 channels for ground shock directly beneath the explosion, and 10 channels for near-surface ground shock. All signals were recorded in analog form on wide-band FM magnetic tape.

Five ground motion instrument positions were located directly beneath each explosion at distances of 20, 30, 40, 50, and 60 feet from the CG. The two elevated shots, Events 1 and 8, were exceptions to this rule; for these events, the gage positions were referenced to the surface of the rock.

In addition to the vertical instrument array, a horizontal array (termed near-surface) of two-axis (vertical and horizontal sensing) motion gages were placed near the ground surface, at a constant depth of 2 feet.

Five fixed positions were selected at horizontal ranges of 36, 48, 65, 85, and 100 feet from surface zero (SZ). These ranges were predicated by the expected maximum ground surface overpressures corresponding to 150, 70, 30, 15, and 10 psi. Surface airblast pressure gages were placed directly over the near-surface motion gages on all but Event 7. For Event 7, the horizontal instrument array was moved to charge depth (10.5 feet) to measure true radial motion. An additional horizontal gage station was added at 20 feet range for this event. No airblast measurements were made on Event 7.

2.4 TRANSDUCERS

Transducers used in this study were standard "off-the-shelf" instruments, i.e., Endevco Series 2200 piezoresistive accelerometers (Reference 6); Bytrex AB-200 diaphragm-type airblast gages (Reference 7); and the latest commercially available modification of the Sandia DX velocity gage (Reference 8). An expanded commentary on instruments and protective canisters is given in Appendix A.

All instrument packages were coupled to the rock at selected positions by use of rock-matching grout. Grout formulae are listed in Appendix A.

2.5 DATA RECORDING AND REDUCTION SYSTEMS

Signal conditioning systems were standard, i.e., 3-kHz carrier amplifier-demodulators built by the U. S. Army Engineer Waterways Experiment Station (WES) were used for the velocity gages (Reference 9) and dc-amplifiers were used for accelerometers and airblast gages. Wideband Sangamo Sabre IV 32-track FM magnetic-tape recorders were used to store the analog data signals. All recording systems were activated by a timing control countdown unit via hard-wire link.

Analog-to-digital data conversion was performed with the WES automatic data processing system. All integrations, filtering, baseline shifting, and other processings were performed on the WES GE 635 computer using various optional software routines developed at WES (References 10 and 11). Final computer output was in the form of analog plots of motions and pressure versus time.

Most of the records were baseline-shifted and filtered. A brief description of baseline correction techniques is given in Appendix B.

Table 2.1. LOCATION OF INSTRUMENTS DIRECTLY BENEATH EXPLOSION

Events 1, 2, 8 Depth from Rock Surface (ft)	Events 3-7 Depth from Charge CG (ft)	Measurement[a]
20	20	AV
30	30	AV
40	40	UV
50	50	UV
60	60	UV

[a]AV = vertical particle acceleration.
UV = vertical particle velocity.

Table 2.2. LOCATION OF INSTRUMENTS ALONG HORIZONTAL RADIAL

Range (ft)	Events 1-6		Event 8		Event 7	
	Depth (ft)	Measurement[a]	Depth (ft)	Measurement[a]	Depth (ft)	Measurement[a]
20	--	--	--	--	10.5	AH
36	0	AB	2	UV, UH	10.5	UH
48	0	AB	2	UV, UH	10.5	UH
65	0	AB	2	UV, UH	10.5	UH
85	0	AB	2	UV, UH	10.5	UH
100	0	AB	2	UV, UH	10.5	UH

[a]AB = surface airblast.
AH = horizontal acceleration.
UH = horizontal particle velocity.

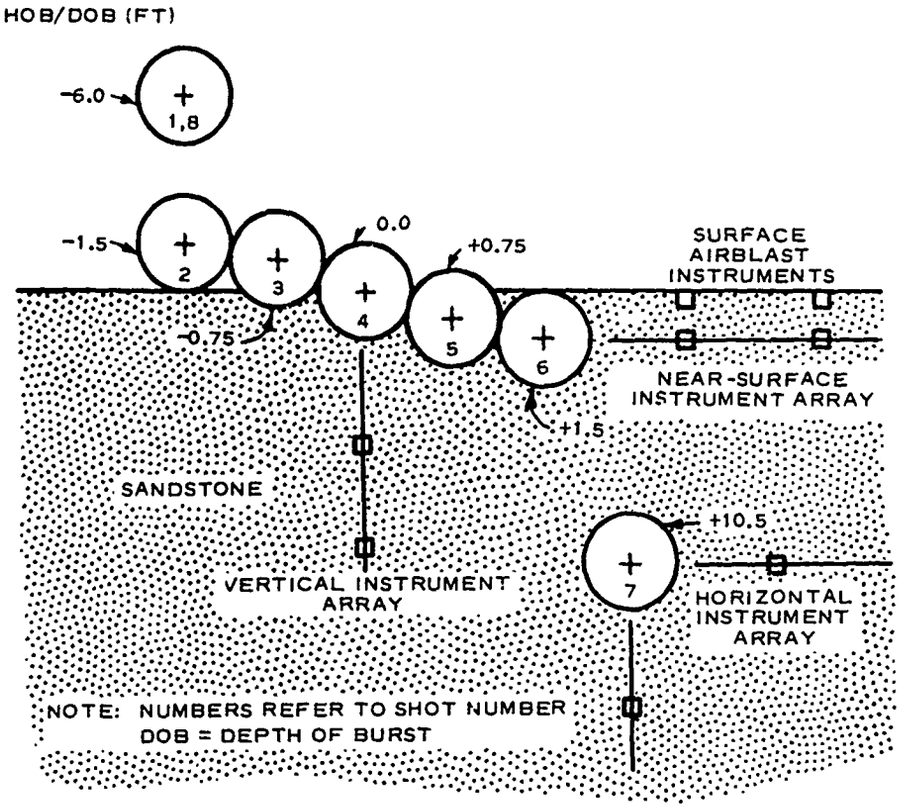

Figure 2.1. CENSE 1 experiment geometry, 1000-pound liquid NM explosive (1140-pound TNT equivalent).

CHAPTER 3

RESULTS

3.1 CRATERING

Both apparent and true craters were measured. No craters were produced by the elevated detonations (Events 1 and 8). Crater measurements are listed in Table 3.1. Apparent and true crater profiles are shown in Figure 3.1(a) and 3.1(b), respectively. The apparent crater profiles (Figure 3.1(a)) for Events 2 through 4 were either slightly mounded (positive crater) or relatively flat. A classical bowl-shaped crater was not achieved until the charge was buried 0.75 foot.

By contrast, the true craters increased with increasing DOB, Figures 3.1(b) and 3.2. An index of the cratering efficiency for a given burst position is obtained by plotting the ratio of the true crater volume to explosive charge weight versus scaled burst position, as in Figure 3.2. The cratering efficiency is seen to be a linear relationship when plotted in this manner. Cratering efficiencies ranged from 0.043 ft^3/lb for the surface tangent (Event 2) detonation to 6.02 ft^3/lb for the 10.5-foot DOB (Event 7) detonation, Table 3.1.

3.2 ARRIVAL TIME

First signal arrival times are listed in Tables 3.2, 3.3, and 3.4 for the vertical radial directly beneath the explosion, surface airblast, and motion horizontal radial, respectively. Arrival times are plotted versus depth for the vertical radial in Figure 3.3; surface airblast arrival time versus horizontal range in Figure 3.4, and motion-arrival time versus horizontal range in Figure 3.5.

The compression (P-wave) propagated downward at an average velocity of 7900 ft/s directly beneath the explosion (Figure 3.3, Table 3.2). This compares favorably with the 7500 ft/s seismic velocity previously determined (References 12-14) for the unweathered upper zone of the Kayenta sandstone.

The P-wave propagation along the horizontal motion radial was 8400 ft/s, some 500 ft/s faster than was measured along the vertical vector. Outrunning occurred at all near-surface motion gage locations.

3.3 VERTICAL GROUND MOTION DIRECTLY BENEATH THE EXPLOSION

3.3.1 Data Recovery

Practically no empirical ground shock data taken directly beneath the explosion existed prior to execution of the CENSE program. Several attempts had been made to acquire data from this region on a few preceding HE experiments, but almost all met with failure. Ground shock data recorded in CENSE 1 in this region were of excellent quality. Only data from two shallow gages were lost on Event 1, which was due to improper hookup; the shallowest gage data from Event 7, which was damaged by the shock; and the 60-foot depth station on Event 8.

3.3.2 Acceleration

Acceleration-time histories for all events are compared in Figures 3.6 and 3.7. Figure 3.6 compares waveforms from Events 8, 2, 3, and 4, while Figure 3.7 compares waveforms from Events 5, 6, and 7. The waveforms are similar for all events; namely, a predominant downward spike followed by a smaller longer duration upward pulse. Pulse durations increased with depth and amplitudes decreased.

Scaled peak downward acceleration directly beneath the explosion versus scaled depth is displayed in Figure 3.8. Since only two data points were available for any given event, the trend cannot be established; however, some observations can be made. Peak amplitudes increased with increasing charge DOB within the rock. Exception to this generality is noted at 30 feet from Event 7, which was about 30 percent lower than for the buried tangent shot (Event 6).

Based on the 30-foot depth data, an approximate increase in acceleration with increased DOB within the rock can be computed. Peak acceleration increased: 1.4 times from the 6-foot HOB (Events 1 and 8) to the surface tangent burst position (Event 6); 4.9 times from surface

tangent to 0.75-foot HOB; 2.3 times from 0.75-foot HOB to half buried; 1.2 times from half buried to 0.75-foot DOB; and 5.3 times from 0.75-foot DOB to 1.5-foot DOB (buried tangent position). A 40 percent reduction was observed for the peak acceleration measured on Event 7 (10.5-foot DOB) from that of the buried tangent shot.

3.3.3 Particle Velocity

Particle velocity-time histories for the two shallowest gage positions (i.e., 20 and 30 feet) for all events were obtained by numerical integration of the acceleration-time histories. Velocity waveforms for all events are shown in Figures 3.9 through 3.12. As was noted for the acceleration waveforms, the velocity waveforms exhibited a predominantly downward pulse followed by a lower amplitude, longer duration upward pulse. The amplitude ratio of the upward to downward velocity pulse increased with increasing depth, approaching a value of 0.6 at the 60-foot depth. Lower than expected signal levels, coupled with excessive system noise, caused distortion in the recorded velocity-time histories from the surface tangent shot (Event 2), Figure 3.9. Initial peaks were relatively unaffected; however, the lower amplitude, late-time portions of the waveforms were distorted. The zero baselines for the two integrated acceleration-time histories were significantly shifted by the low signal-to-noise ratio and an extraneous superimposed periodic noise. The estimated waveforms for the three deepest positions are indicated by dashed lines in Figure 3.9.

Peak downward particle velocity directly beneath the explosion versus scaled depth for all events is displayed in Figure 3.13. Attenuation of peak velocity with increasing depth was essentially constant for all events: approximately at the -3.67 power with depth. No significant enhancement in downward particle velocity was observed by moving the shot point from airburst to surface tangent. Significant increases in velocity amplitudes were noted for progressive burial of the explosive beyond the surface tangent (contact) burst position. Measured velocity increased approximately: 2 times from the surface tangent (1.5-foot HOB) to 0.75-foot HOB; 1.54 times from 0.75-foot HOB to half buried;

1.38 times from half buried to 0.75-foot DOB; 3.58 times from 0.75-foot DOB to buried tangent (1.5-foot DOB); and 2.86 times from buried tangent to 10.5-foot DOB. An overall increase in peak velocity of 43 times was attained at a DOB of 10.5 feet as compared with the 6-foot HOB detonations.

A comparison of true radial vertical and horizontal particle velocities from Event 7 (10.5-foot DOB) is presented in Figure 3.12. Horizontal velocity waveforms exhibited the characteristic shape as was noted for the near-surface (2-foot depth) measurements, the shape of the waveform being virtually independent of distance and burst position. The vertical waveforms, however, showed a peculiar double-peaked waveform. A single spike wave shape did not develop until a depth of 60 feet from the charge CG was reached. The peak downward velocity measured at the 60-foot depth appeared to be low by about a factor of 2. Peak particle velocities from the two radials are compared in the velocity-distance plot, Figure 3.14. Peak vertical (downward) particle velocity appeared to attenuate more rapidly than the outward velocity along the horizontal radial, as evidenced by the apparent slopes of the data (Figure 3.14), i.e., vertical at the slope of the data curve (velocity attenuated as the -3.4 power with range R) versus horizontal at $R^{-2.0}$.

3.3.4 Displacement

All displacements were derived from either singly integrating the velocity-time histories or doubly integrating the acceleration-time histories. The resulting displacement-time histories are presented in Appendix B. Peak downward displacements along the vertical radial are listed in Table 3.5. The maximum displacement recorded was less than 1 foot at a range of 20 feet from the charge center on Event 7.

The mininum downward displacement recorded was 0.00062 feet, 60 feet below the surface of the rock on Event 1. Vertical displacements were scaled by the cube root of the charge weight ($W^{1/3}$) and plotted as a function of scaled depth in Figure 3.15. Peak displacement directly beneath the explosion attenuated at similar slopes for all burst

positions, i.e., as $R^{-2.31}$. Displacements produced by the Events 1 and 8 airbursts and the surface tangent detonations were virtually identical. Only moderate increases in peak displacement were evident between the near-surface detonations, Events 3 through 5. Observed was: an increase in peak displacement of 1.7 times between surface tangent (1.5-foot HOB) and 0.75-foot HOB; a 1.5 times increase between 0.75-foot HOB and half buried (0 HOB); and a 1.2 times increase between half buried and 0.75-foot DOB positions. However, significant increases occurred for progressively deeper charge burial. An increase of 2.7 was obtained from the 0.75-foot DOB position to the buried tangent (1.5-foot DOB), and a factor of 10 increase was obtained from the buried tangent to the 10.5-foot DOB position. Peak displacement increased by a factor of 83 by moving the burst position from surface tangent above to a depth of 10.5 feet.

3.4 NEAR-SURFACE GROUND MOTION

3.4.1 Data Recovery

Generally, excellent data were obtained along the near-surface (2-foot depth) instrument radials. All near-surface motion data were recovered from Events 2 through 6. One vertical particle velocity data channel (36-2-UV)* was lost on Event 1 due to cable damage. Four horizontal particle velocity data channels (36-2-UH, 48-2-UH, 65-2-UH, and 85-2-UH) and three vertical particle velocity data channels (36-2-UV, 48-2-UV, and 65-2-UV) were lost on Event 8 due to a malfunction at the gage amplifier.

3.4.2 Horizontal Particle Velocity

Near-surface horizontal velocity waveforms at the nominal 70- and 10-psi overpressure region (48- and 100-foot ranges) are shown in Figure 3.16. Outrunning ground motion was evident at the closest gage station even for the airburst detonations (Events 1 and 8). The horizontal particle velocity waveforms per se appeared to be generally

---

* Refer to Appendix B for explanation of channel numbers.

independent of burst position in that they exhibited the same characteristic shape. However, the frequency content was inversely proportional to the charge depth, i.e., the greater the depth (less airblast energy fraction), the lower the frequency. The minimal airblast influence was observed in the composite waveforms (Figure 3.16), where arrival of the airblast is indicated by a vertical dashed line. The primary velocity contribution was provided by the shock propagating in the rock.

The inward-going, or rebound, velocity was generally higher than or equal to the outward-going (away from the explosive source) for all events.

Peak outward, near-surface velocity was highly sensitive to burst position, as illustrated by the velocity versus scaled range plot, Figure 3.17. The maximum increase in horizontal velocity occurred between the 6-foot HOB and surface tangent (1.5-foot HOB) detonations: an increase of 3.8 times. The increase was exactly half this value (1.9 times) between surface tangent and 0.75-foot HOB. Horizontal velocity increased by a factor of 2 between 0.75-foot HOB and half buried (0 HOB). Only slight increases were observed between the deeper burst positions. A maximum increase of 29 times was achieved by moving the burst position from surface tangent (1.5-foot HOB) to 10.5-foot DOB. The peak outward velocity attenuated as $R^{-1.21}$ for the 6-, 1.5-, and 0.75-foot HOB positions. The attenuation rate increased for the half buried (0 HOB) and deeper detonations, approximately as $R^{-1.85}$.

Peak-to-peak near-surface horizontal velocity, i.e., the absolute amplitude of the peak outward velocity, plus the absolute amplitude of the peak inward velocity, values are listed in Table 3.6 and shown below:

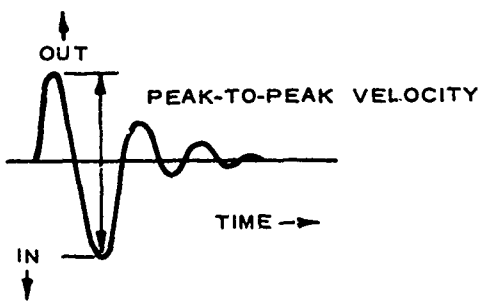

A plot of these peak-to-peak velocities versus scaled range is displayed in Figure 3.18. Horizontal velocity data thus treated appeared to attenuate at a constant rate of $R^{-1.33}$ for all burst conditions.

3.4.3 Vertical Particle Velocity

Near-surface vertical particle velocity waveforms (Figure 3.19) within the rock display a complicated wave pattern. Since outrunning has occurred at all measurement locations, discrete components of the motion signature are superimposed, resulting in a highly complicated, composite waveform. The character of each waveform is dependent upon the relative phasing of its individual components.

Downward airslap (airblast) was a principal contributor to the peak downward velocity only for the close-in measurement positions for the airburst, surface tangent, and one-fourth-buried detonations (Events 1 (8), 2, and 3). For detonations at depths in excess of one-fourth buried (0.75-foot DOB), this role was reversed, i.e., for the half-buried and deeper buried detonations, the significant peak velocity is seen to be upward, preceding the arrival of the surface airblast (Figure 3.19). Arrival of the surface airblast is indicated by dashed vertical lines on the velocity waveforms of Figure 3.19.

Analyses of the vertical data are difficult to make because of the extreme difficulty in separating the discrete components, i.e., airblast-induced motion, crater (direct)-induced motions, surface (Rayleigh) wave, etc. It appears pointless to present peak downward or upward particle velocity as a function of range when addressing different driving sources for the peaks. Instead, the data are taken peak-to-peak, i.e., the sum of the upward maxima plus downward maxima, peak upward to peak downward amplitudes. These peak-to-peak values are plotted as a function of scaled range in Figure 3.20. Table 3.7 lists the peak-to-peak values for the vertical data, Events 1 through 6 and 8. Definite trends appear in this plot (Figure 3.20). The velocity is seen generally to attenuate at a rate of the -2.5 power of range between the scaled range of 3.4 and 6.2 $W^{1/3}$ (except for the aboveground detonations, Events 1

and 8). A velocity increase occurred at a range of $8.1\ W^{1/3}$. Velocity again attenuated as $R^{-2.5}$ beyond $8.1\ W^{1/3}$.

3.4.4 Horizontal Displacement

Near-surface horizontal displacement waveforms for the 48- and 100-foot range locations for Events 1 through 6 are shown in Figure 3.21. The displacement waveforms are similar in ch -acter to their velocity counterparts (see Section 3.4.2). Surface airblast had no significant influence on horizontal displacement. No structure within the displacement waveform appeared to have an association with the airblast phasing (note that surface airblast arrival is indicated by a vertical dashed line in Figure 3.21). The horizontal displacement was produced exclusively by the shock propagating in the rock. Little permanent displacement was observed over the region studied. The response of the site material appeared to have been highly elastic in behavior. Peak outward displacements for all events, scaled by $W^{1/3}$, are plotted as functions of scaled horizontal distance in Figure 3.22. Peak amplitudes increased progressively with increasing charge DOB. Slopes of the attenuation curves progressively steepened with increasing charge DOB. Practically no attenuation was observed in the displacement data from Event 1, which was detonated at a HOB of 6 feet. Maximum data scatter was present in the Event 4 (half-buried) data.

The initial outward going transient displacement in some instances was greater than the inward rebound displacement pulse; in other instances the rebound displacement was of a higher amplitude. The displacement relationship between events is more readily seen by plotting scaled peak-to-peak displacements versus scaled distance, Figure 3.23. In this figure, definite attenuation trends are evident for all events. Again, peak amplitudes increased proportionally with increasing charge DOB; however, note that the slopes are essentially equal for all events. Based on Figure 3.23, peak displacement was 18 times greater for the 10.5-foot DOB shot (Event 7) than for the surface tangent burst position. Peak displacement was 8 times greater for the buried tangent shot (Event 6) than for the surface tangent event.

3.4.5 Vertical Displacement

Near-surface vertical displacement waveforms for the 48- and 100-foot range locations for Events 1 through 6 are shown in Figure 3.24. Surface airblast influenced the vertical displacement minimally at the two closest-in gage notations (36- and 42-foot horizontal range) for Events 1 through 3. Surface airblast had little influence at ranges greater than 48 feet for Events 1 through 3, or at any range instrumented for deeper buried shots.

3.5 SURFACE AIRBLAST

3.5.1 Data Recovery

No airblast data were recorded for Event 1 due to a malfunction in the recording electronics. No airblast measurements were attempted for the deeply buried shot (Event 7). Good quality airblast data were attained on all other events for the test program.

3.5.2 Airblast Pressure-Time Histories

Airblast pressure-time histories from Events 2 through 6 and 8 are composited in Figures 3.25, 3.26, and 3.27. (See Appendix B for complete time histories and impulse.) Figure 3.28 displays peak surface airblast as a function of scaled range and burst position.

3.5.3 Airblast Impulse

Surface airblast impulses were derived by numerically integrating the airblast time histories (see Appendix B). Peak impulse values are listed in Table 3.8. Peak surface airblast impulse as a function of λ_r and burst condition is shown in Figure 3.29. With the exception of the surface tangent shot, impulse values decreased progressively with increased charge burial. Impulses were relatively constant over a horizontal range of 3.4 to 6.2 $W^{1/3}$ for the 0.75- and 1.5-foot DOB tests (Events 5 and 6, respectively).

Table 3.1. CRATER MEASUREMENTS.

Event No.	HOB/DOB (-)/(+)[a] (ft)	R_c [b]	$W^{1/3}$ [c]	Apparent Crater Radius r_a (ft)	Apparent Crater Depth d_a (ft)	Apparent Crater Volume v_a (ft^3)	True Crater Radius r_t (ft)	True Crater Depth d_t (ft)	True Crater Volume v_t (ft^3)	Cratering Efficiency $\frac{v_t}{W}$ (ft^3/lb)
1(8)	-6.0	-4.0	-0.57				No crater produced			
2	-1.5	-1.0	-0.14	4.0[d]	-1.0[d]	-33[d]	4.0	1.7	49	0.043
3	-0.75	-0.5	-0.072	3.6	1.0	46	9.0	4.0	395	0.346
4	0	0	0	5.3[d]	-1.2[d]	10	10.0	4.5	680	0.596
5	+0.75	+0.5	+0.072	7.5	3.5	339	12.5	4.7	1155	1.01
6	+1.5	+1.0	+0.14	12.0	3.3	636	15.5	4.5	1457	1.28
7	+10.5	+7.0	+1.00	12.7	7.0	2055	22.0	12.3	6868	6.02

[a] (-) = elevated charge.
(+) = buried charge.

[b] R_c = charge radius.

[c] $W^{1/3}$ = scaled burst position.

[d] Mound, positive crater.

Table 3.2. FIRST SIGNAL ARRIVAL TIMES (MILLISECONDS) ALONG THE VERTICAL RADIAL DIRECTLY BENEATH THE EXPLOSION.

Depth (ft)	Event Designation 1/8 (Airbursts)	2 (Surface Tang.)	3 (1/4 Buried)	4 (1/2 Buried)	5 (3/4 Buried)	6 (Buried Tang.)	7 (Buried 1W1/3)
20	2.50/3.70	1.85	2.00	1.95	1.75	1.50	1.90
30	3.85/5.00	3.20	3.30	3.00	2.90	2.70	3.00
40	5.20	4.50	4.50	4.10	4.05	3.80	4.05
50	6.30	6.00	6.25	5.25	5.35	5.15	5.35
60	7.40	7.15	6.65	6.05	6.75	6.35	7.00

Table 3.3. FIRST SIGNAL SURFACE AIRBLAST ARRIVAL TIMES (MILLISECONDS).

Range (ft)	Event Designation 1/8 (Airburst)	2 (Surf. Tang.)	3 (1/4 Buried)	4 (1/2 Buried)	5 (3/4 Buried)	6 (Buried Tangent)
36	5.80/4.85	4.60	5.00	7.60	16.6	11.2
48	9.50/8.65	8.30	9.00	13.2	24.0	19.0
65	17.0/16.2	16.0	17.6	22.9	35.0	30.5
85	28.7/27.8	27.6	29.7	35.6	49.0	45.0
100	38.5/37.4	37.7	39.8	46.0	60.0	56.2

Table 3.4. FIRST MOTION SIGNAL ARRIVAL TIMES (MILLISECONDS) ALONG THE HORIZONTAL INSTRUMENT RADIAL.

Range (ft)	Event Designation 1/8 (Airburst)	2 (Surf. Tang.)	3 (1/4 Buried)	4 (1/2 Buried)	5 (3/4 Buried)	6 (Buried Tang.)	7 (Buried $1W^{1/3}$)
20							2.0
36	4.6	4.9	5.0	5.0	4.85	5.05	5.2
48	5.8	6.0	6.2	6.1	6.20	6.45	6.0
65	8.1	8.0	8.8	8.6	8.75	8.50	8.0
85	10.8	10.5	10.8	10.6	10.50	11.10	10.0
100	12.1/13.2	11.9	12.0	12.1	12.40	12.50	12.8

Table 3.5. PEAK DOWNWARD DISPLACEMENT (FEET), VERTICAL INSTRUMENT RADIAL DIRECTLY BENEATH EXPLOSION.

Depth (ft)	Event 1 (Airburst)	Event 8 (Airburst)	Event 2 (Surface Tangent)	Event 3 (1/4 Buried)	Event 4 (1/2 Buried)	Event 5 (3/4 Buried)	Event 6 (Buried Tangent)	Event 7 (Buried $1W^{1/3}$)
20[a]	b	0.01050	0.01600	0.01000	0.00060[c]	0.02300	0.2000[c]	>>0.4900[d]
30[a]	b	0.00200	0.00150	0.00600	0.01200	0.00300[c]	0.01100[c]	0.4360
40[e]	0.00135	0.00275	0.00170	0.00250	0.00265	0.00420	0.00760	0.1610
50[e]	0.00092	0.00160	0.00083	0.00190	0.00240	0.00300	0.00750	0.0750
60[e]	0.00062	f	0.00071	0.00120	0.00070	0.00220	0.00700	0.0078

[a] Data from these depths derived from doubly integrated acceleration.

[b] No data recorded.

[c] Questionable data.

[d] Gage failed at early time, data questionable.

[e] Data from these depths derived from singly integrated velocity.

[f] No useable data.

Table 3.6. PEAK-TO-PEAK NEAR-SURFACE HORIZONTAL PARTICLE VELOCITY.

Horizontal Range (ft)	Event 1 (Airburst) (ft/s)	Event 8 (Airburst) (ft/s)	Event 2 (Surface Tangent) (ft/s)	Event 3 (1/4 Buried) (ft/s)	Event 4 (1/2 Buried) (ft/s)	Event 5 (3/4 Buried) (ft/s)	Event 6 (Buried Tangent) (ft/s)	Event 7 (Buried $+1W^{1/3}$) (ft/s)
20	--	--	--	--	--	--	--	64.00
36	0.85	a	2.10	3.40	5.00	7.99	9.10	7.70
48	0.66	a	1.52	2.43	5.75	5.02	7.05	7.40
65	0.42	a	1.10	1.40	3.16	3.16	3.50	5.10
85	0.27	a	0.69	1.15	2.38	2.69	2.65	2.95
100	0.24	0.40	0.59	0.86	1.37	1.73	1.94	1.68

[a]No data recorded.

Table 3.7. PEAK-TO-PEAK NEAR-SURFACE VERTICAL PARTICLE VELOCITY.

Horizontal Range (ft)	Event 1 (Airburst) (ft/s)	Event 8 (Airburst) (ft/s)	Event 2 (Surface Tangent) (ft/s)	Event 3 (1/4 Buried) (ft/s)	Event 4 (1/2 Buried) (ft/s)	Event 5 (3/4 Buried) (ft/s)	Event 6 (Buried Tangent) (ft/s)
36	a	a	1.75	2.00	1.35	2.55	2.11
48	0.59	a	0.61	0.84	0.95	0.70	1.42
65	0.54	a	0.59	0.46	0.37	0.35	0.57
85	0.37	0.52	0.47	0.37	0.46	0.57	0.53
100	0.29	0.36	0.34	0.30	0.32	0.36	0.44

[a]No data recorded.

Table 3.8. PEAK SURFACE AIRBLAST IMPULSE.

Horizontal Range (ft)	Event Designation 8 (Airburst)	2 (Surf. Tang.)	3 (1/4 Buried)	4 (1/2 Buried)	5 (3/4 Buried)	6 (Buried Tang.)
36	0.190	0.310	0.300	0.210	0.062	0.039
48	0.120	0.125	0.140	0.081	0.055	0.039
65	0.093	0.140	0.086	0.071	0.050	0.038
85	0.055	0.060	0.056	0.043	0.025	0.020
100	0.063	0.056	0.058	0.050	0.045	0.030

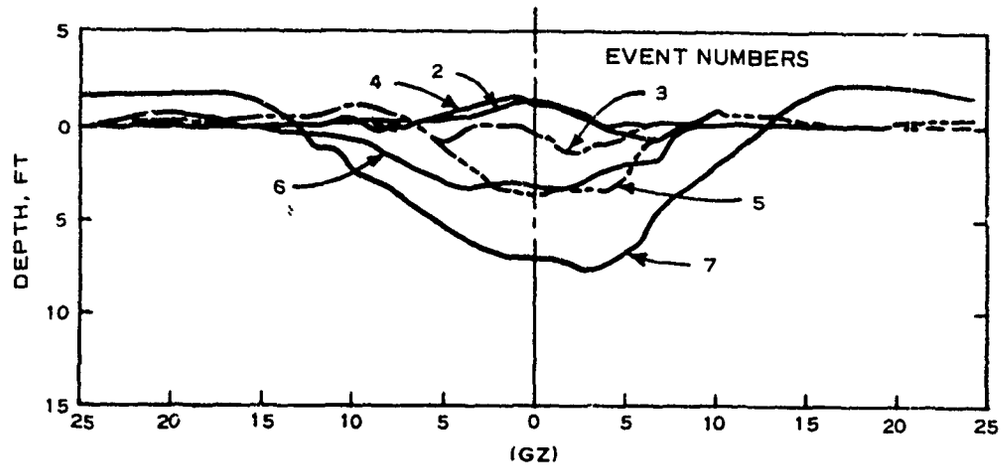

a. APPARENT CRATER PROFILES

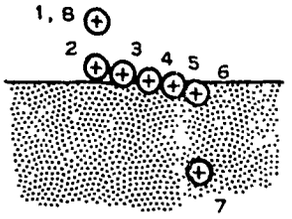

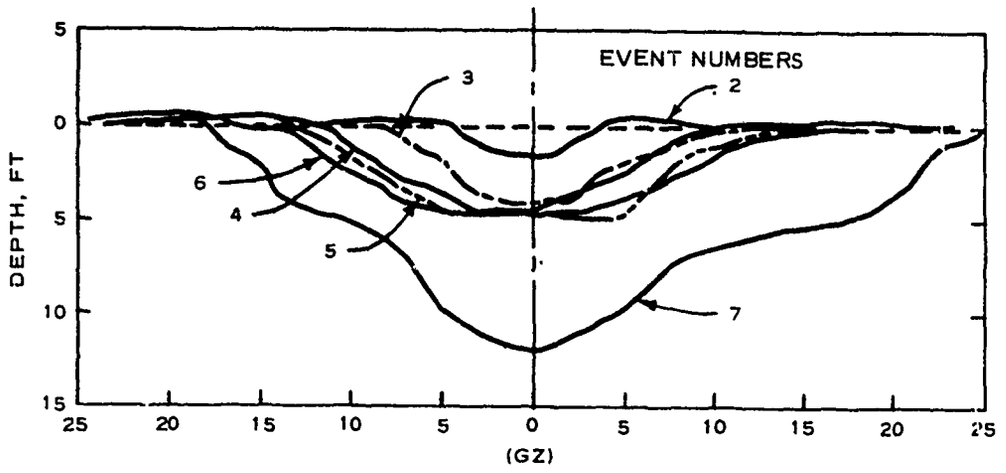

b. TRUE CRATER PROFILES

NOTE: GZ = GROUND ZERO

Figure 3.1. Apparent and true crater profiles.

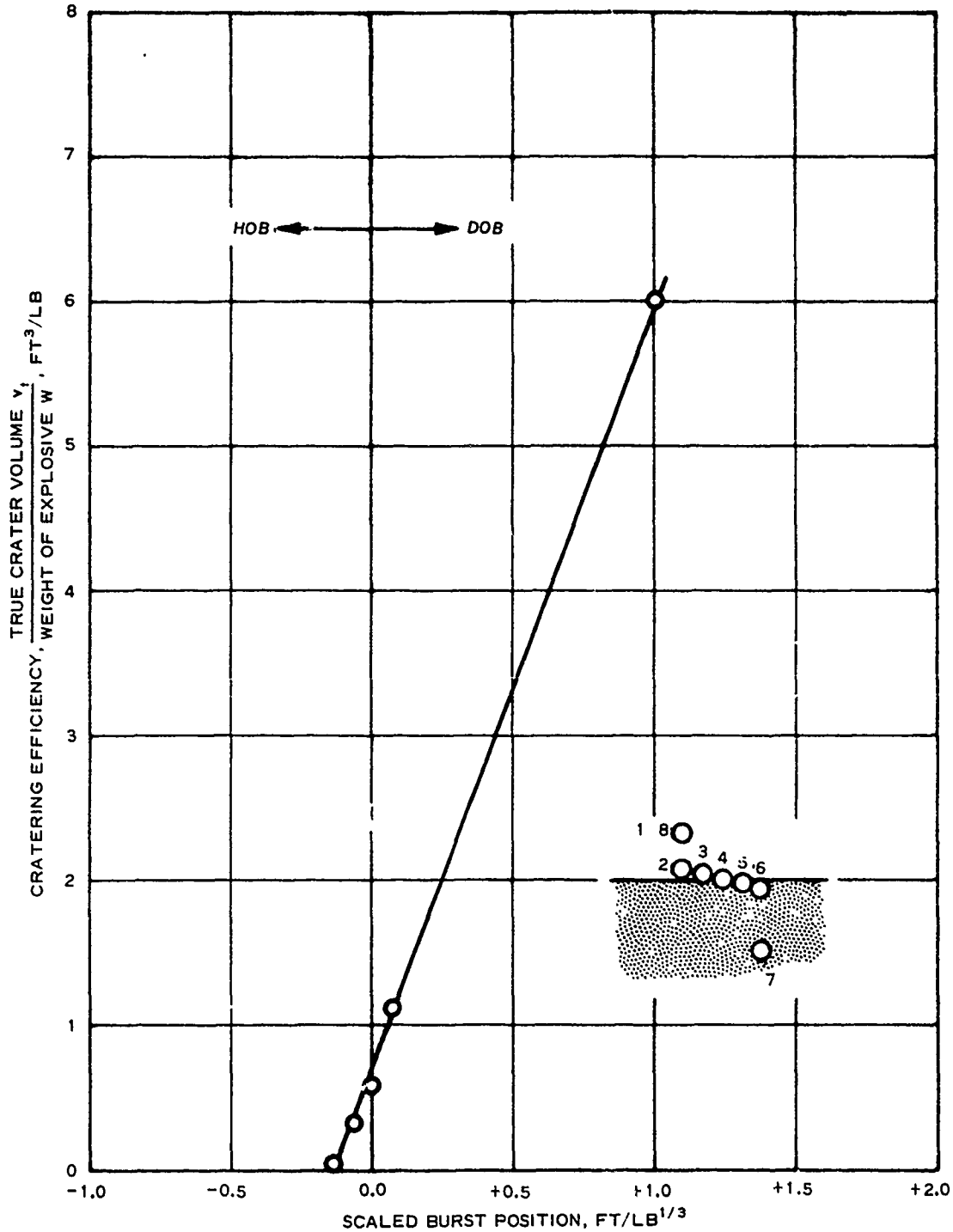

Figure 3.2. Cratering efficiency as a function of scaled burst position.

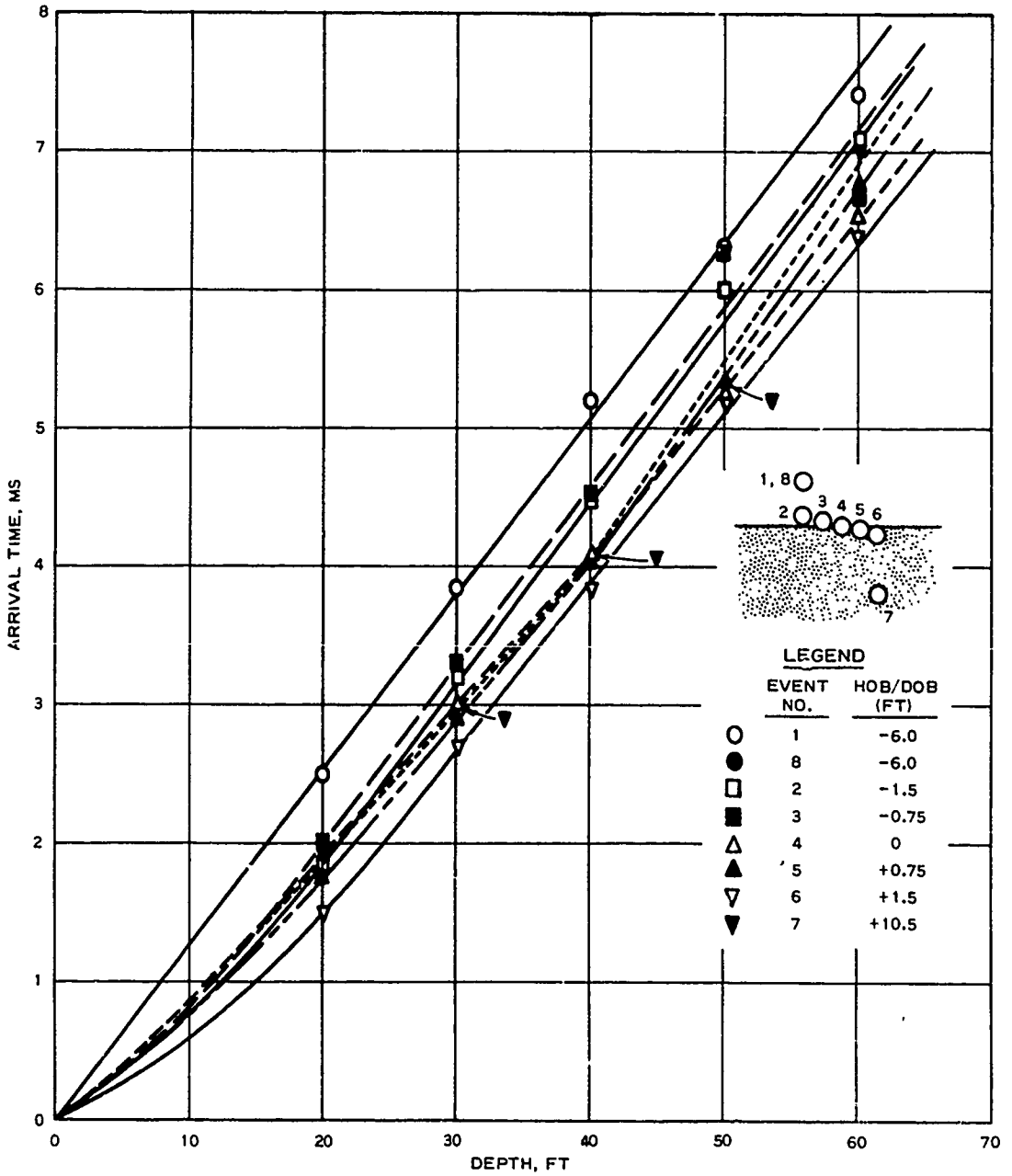

Figure 3.3. First signal arrival times along the vertical radial directly beneath the explosion versus depth.

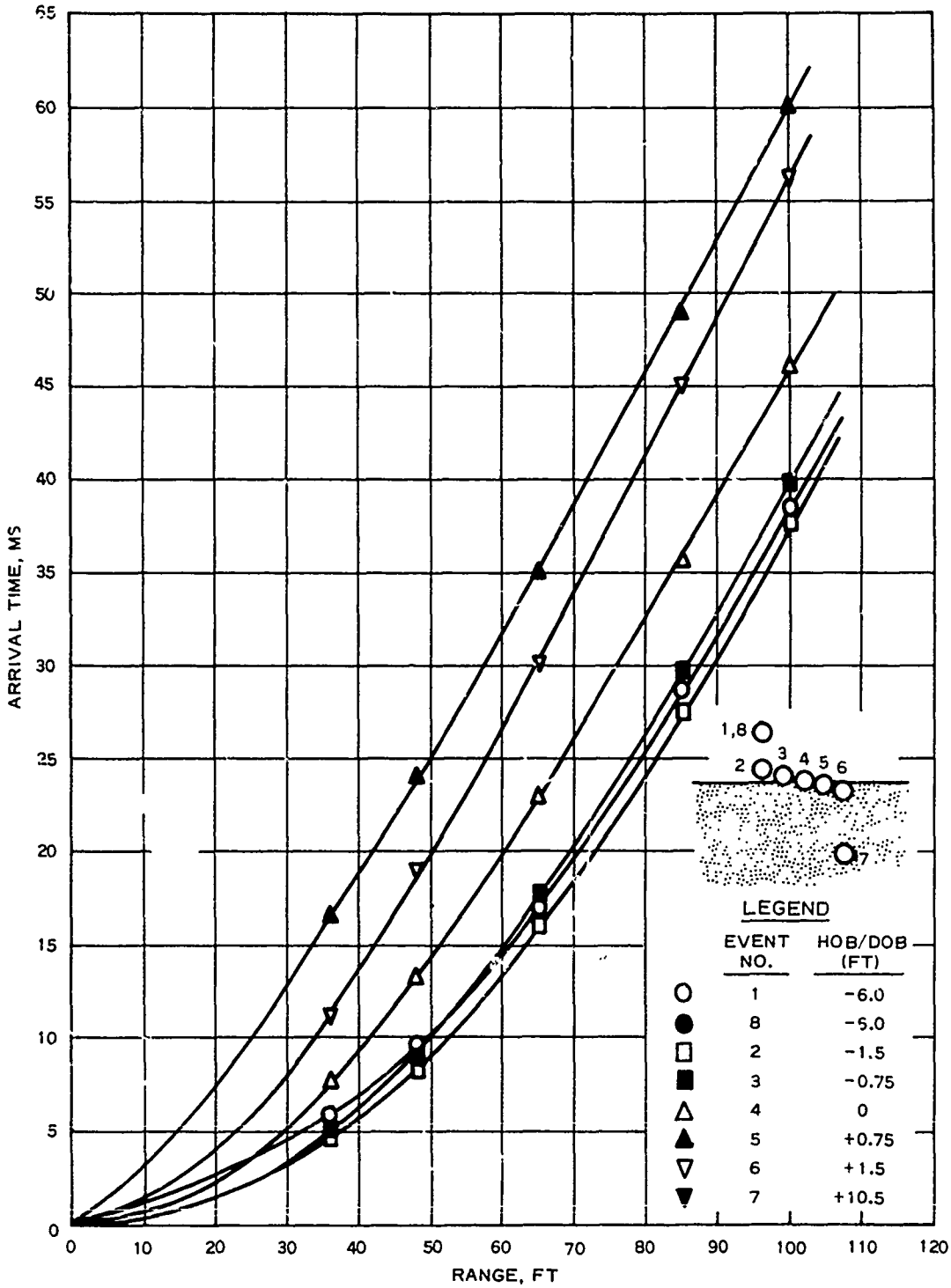

Figure 3.4. Surface airblast arrival times along horizontal instrument radial versus range.

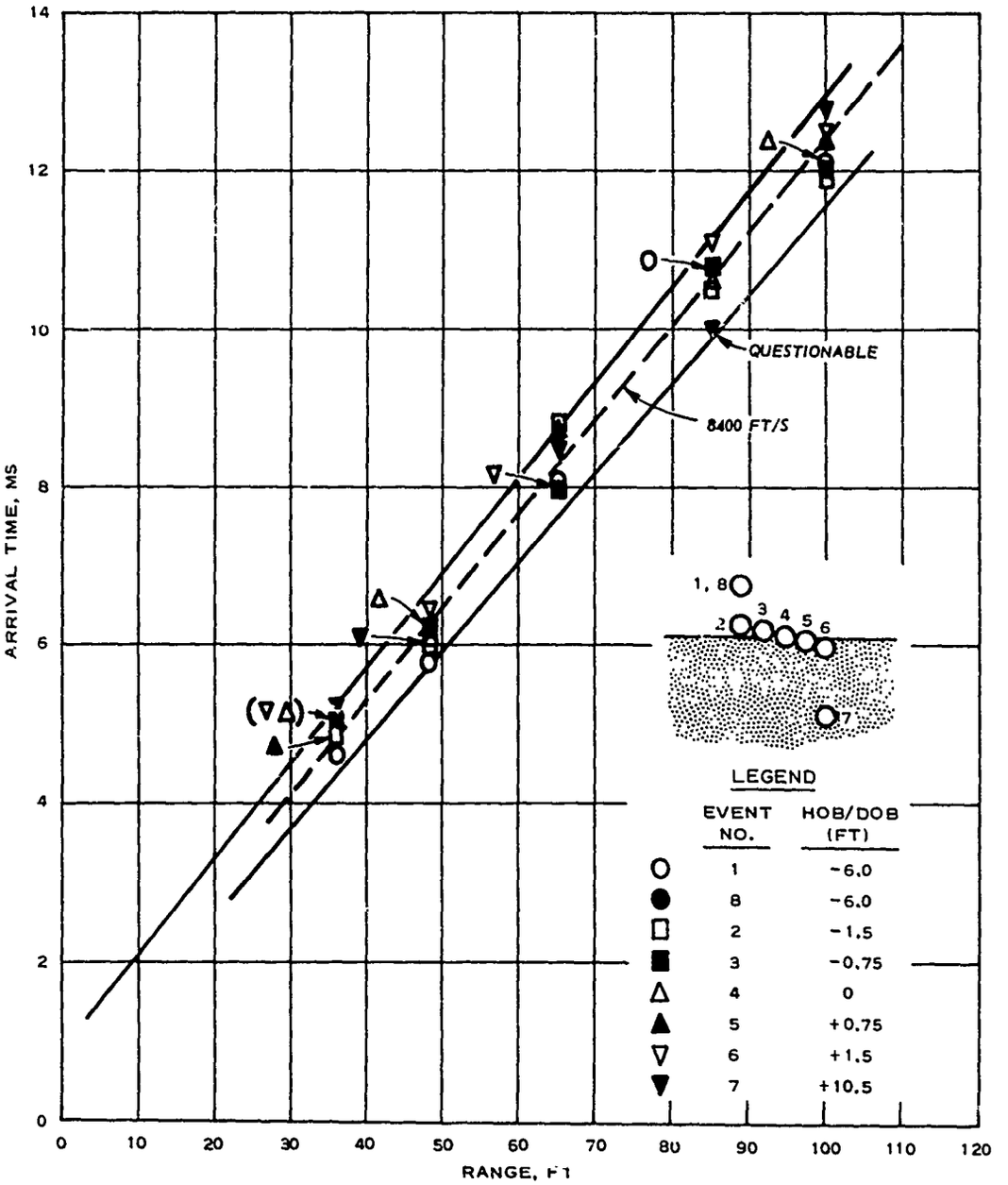

Figure 3.5. First motion signal arrival times along the horizontal instrument radial versus range.

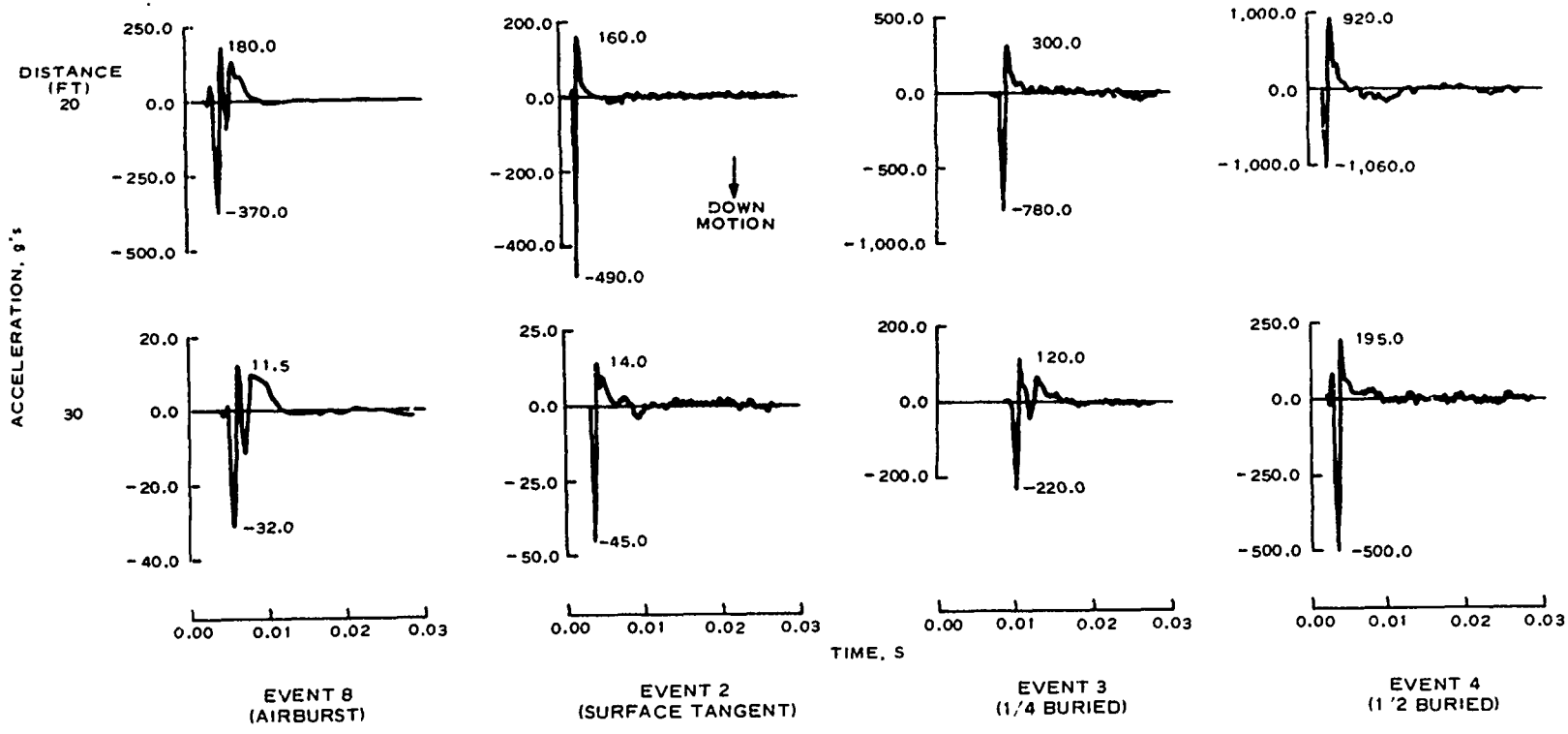

Figure 3.6. Comparison of acceleration waveforms along the vertical radial directly beneath the explosion at 20- and 30-foot depths, Events 8, 2, 3, and 4.

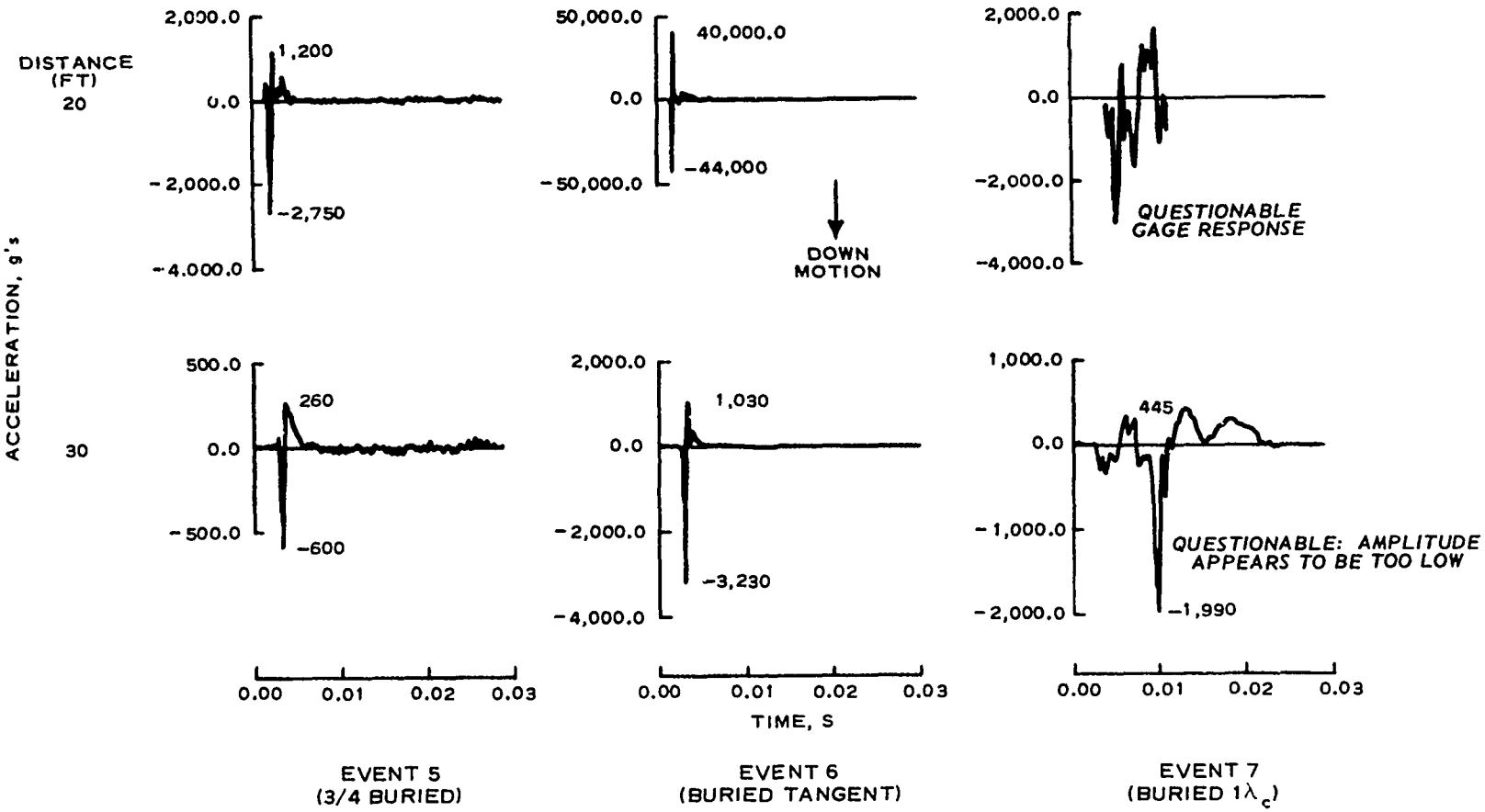

Figure 3.7. Comparison of acceleration waveforms along the vertical radial directly beneath the explosion at 20- and 30-foot depths (from charge CG), Events 5 through 7.

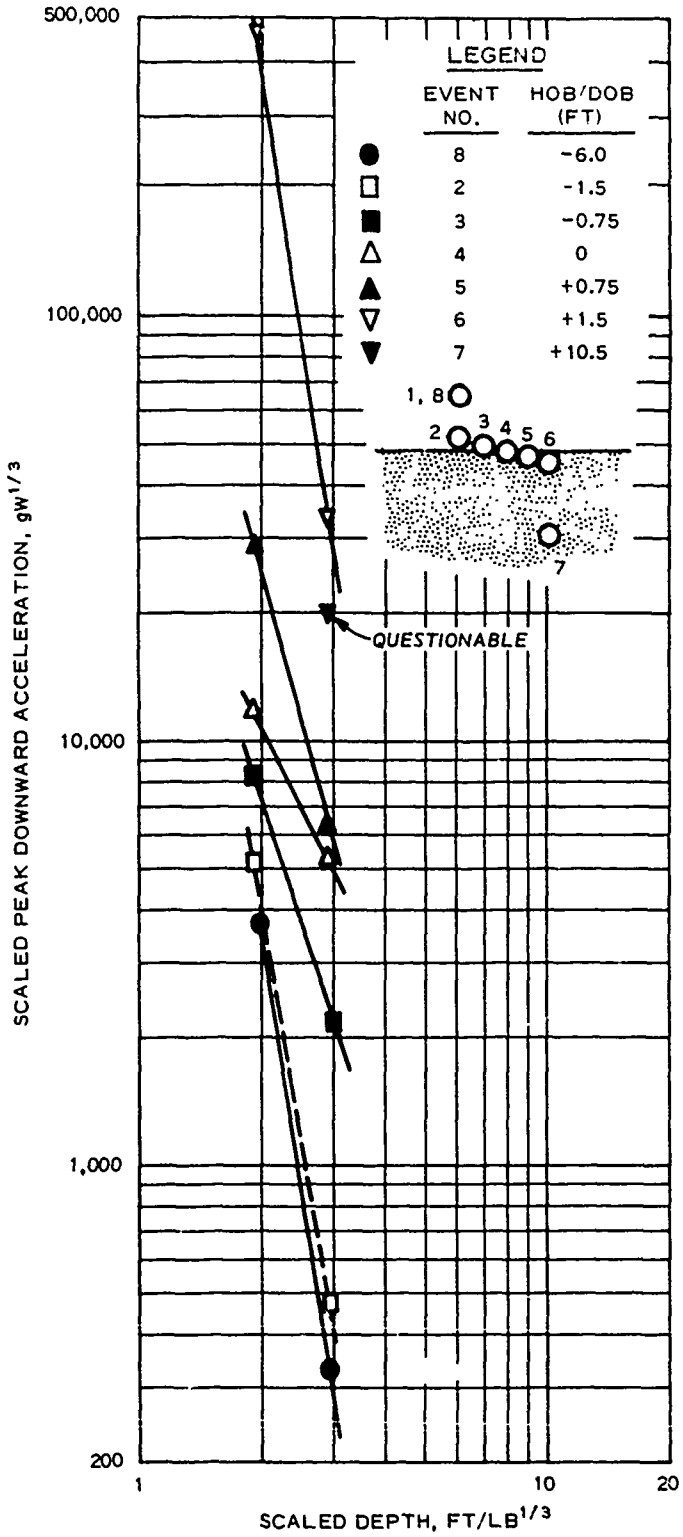

Figure 3.8. Scaled peak downward acceleration directly beneath the explosion versus scaled depth.

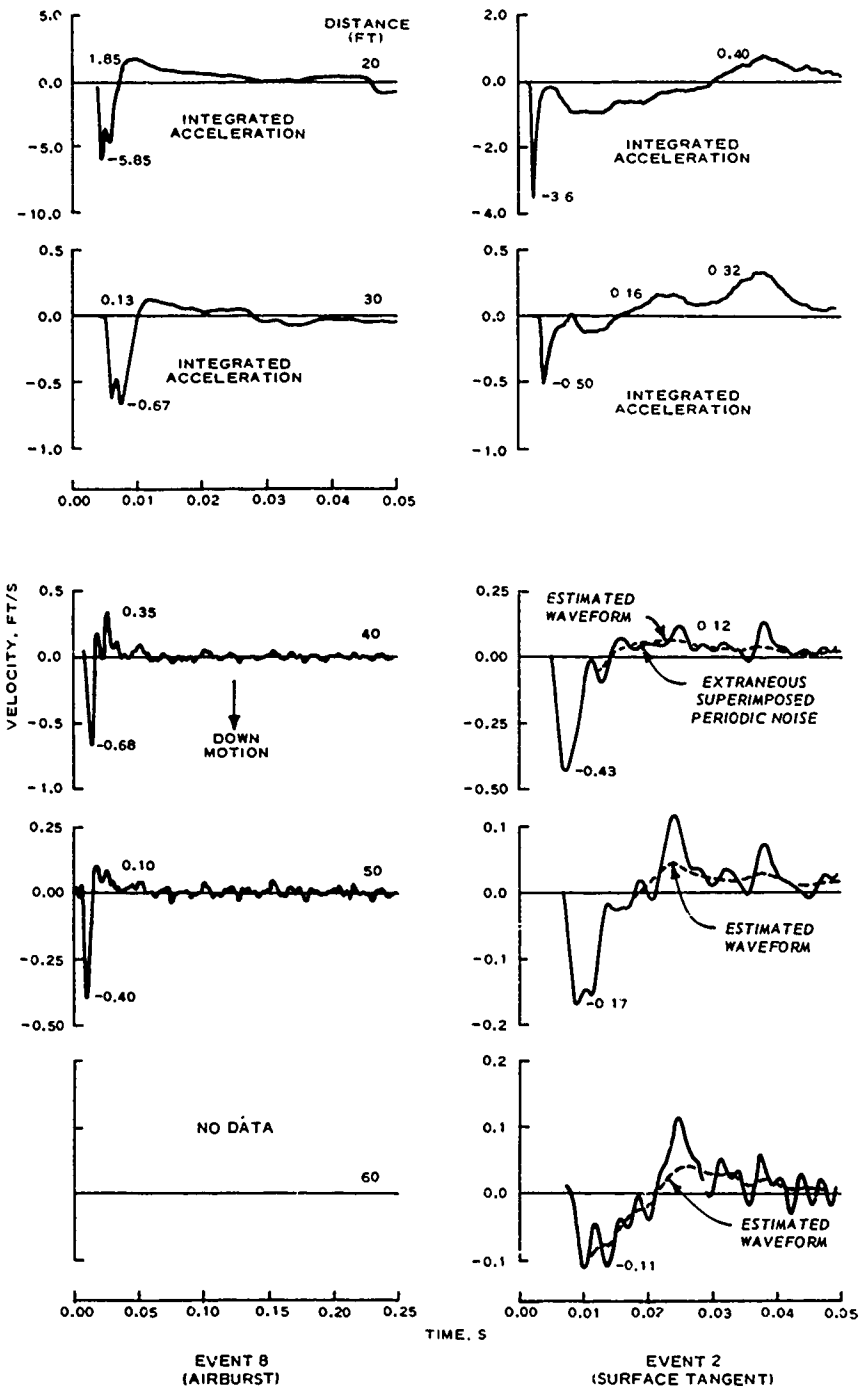

Figure 3.9. Comparison of particle velocity waveforms along the vertical radial directly beneath the explosion at 20-, 30-, 40-, 50-, and 60-foot depths (from charge CG), Events 8 and 2.

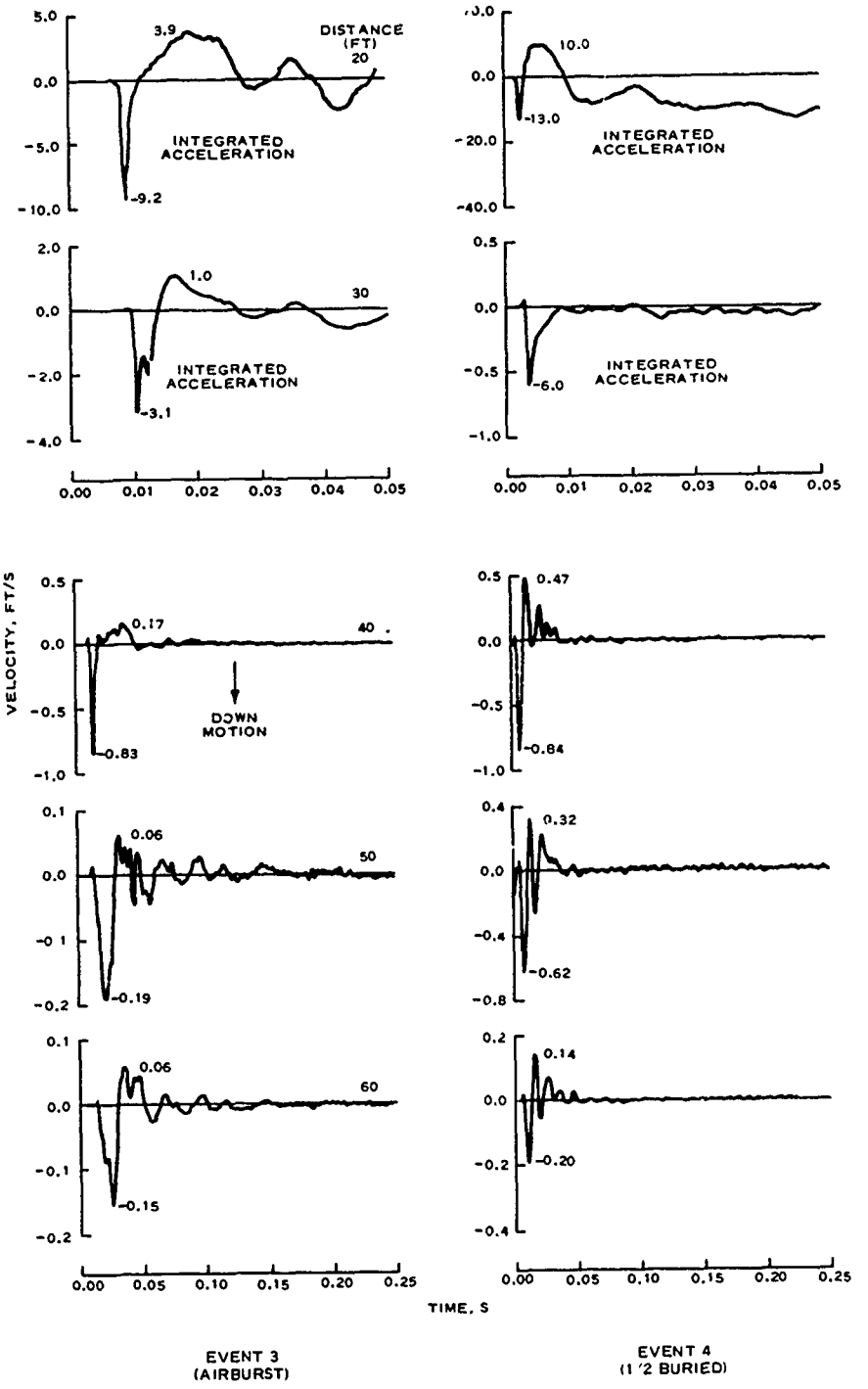

Figure 3.10. Comparison of particle velocity waveforms along the vertical radial directly beneath the explosion at 20-, 30-, 40-, 50-, and 60-foot depths (from charge CG), Events 3 and 4.

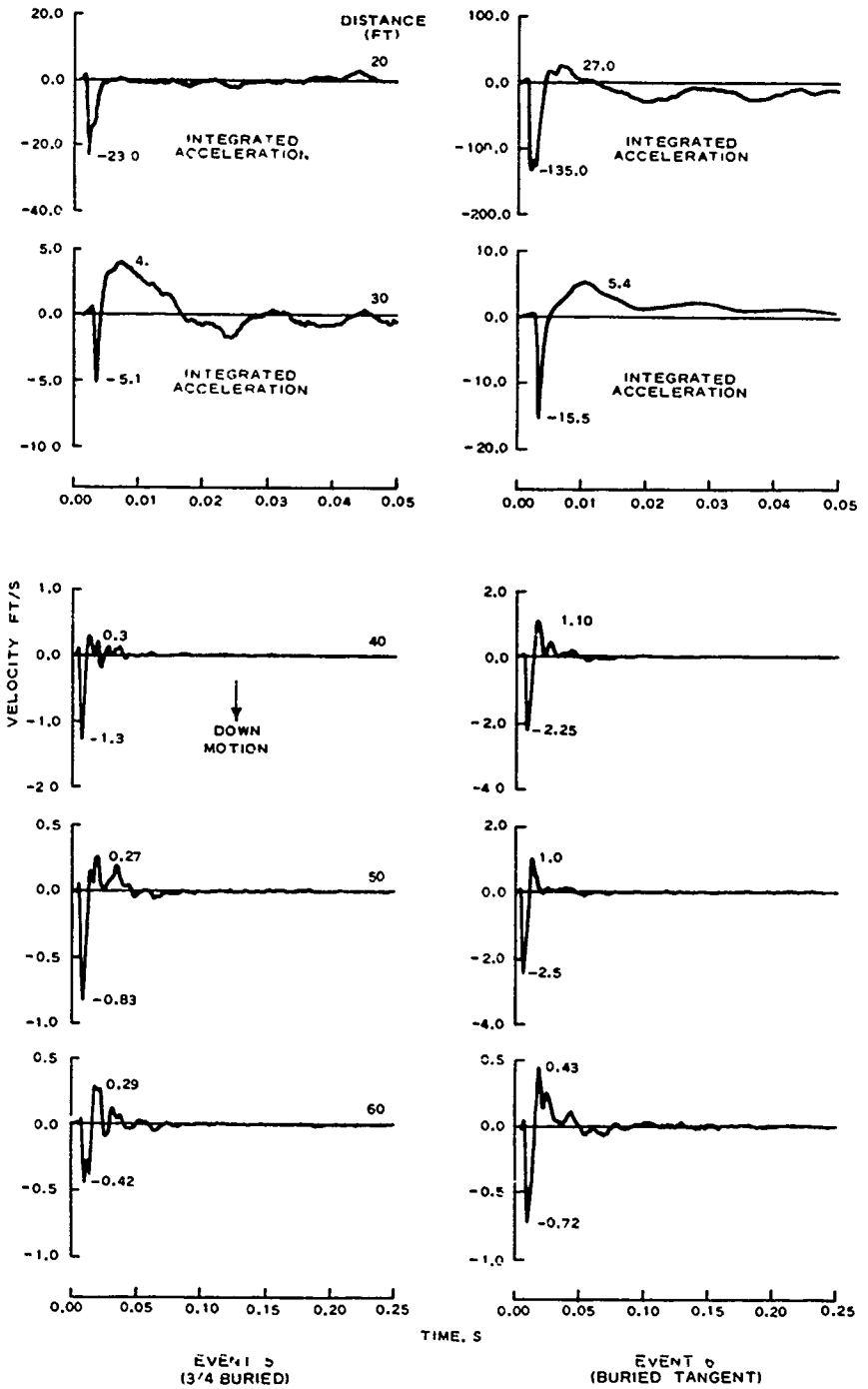

Figure 3.11. Comparison of particle velocity waveforms along the vertical radial directly beneath the explosion at 20-, 30-, 40-, 50-, and 60-foot depths (from charge CG), Events 5 and 6.

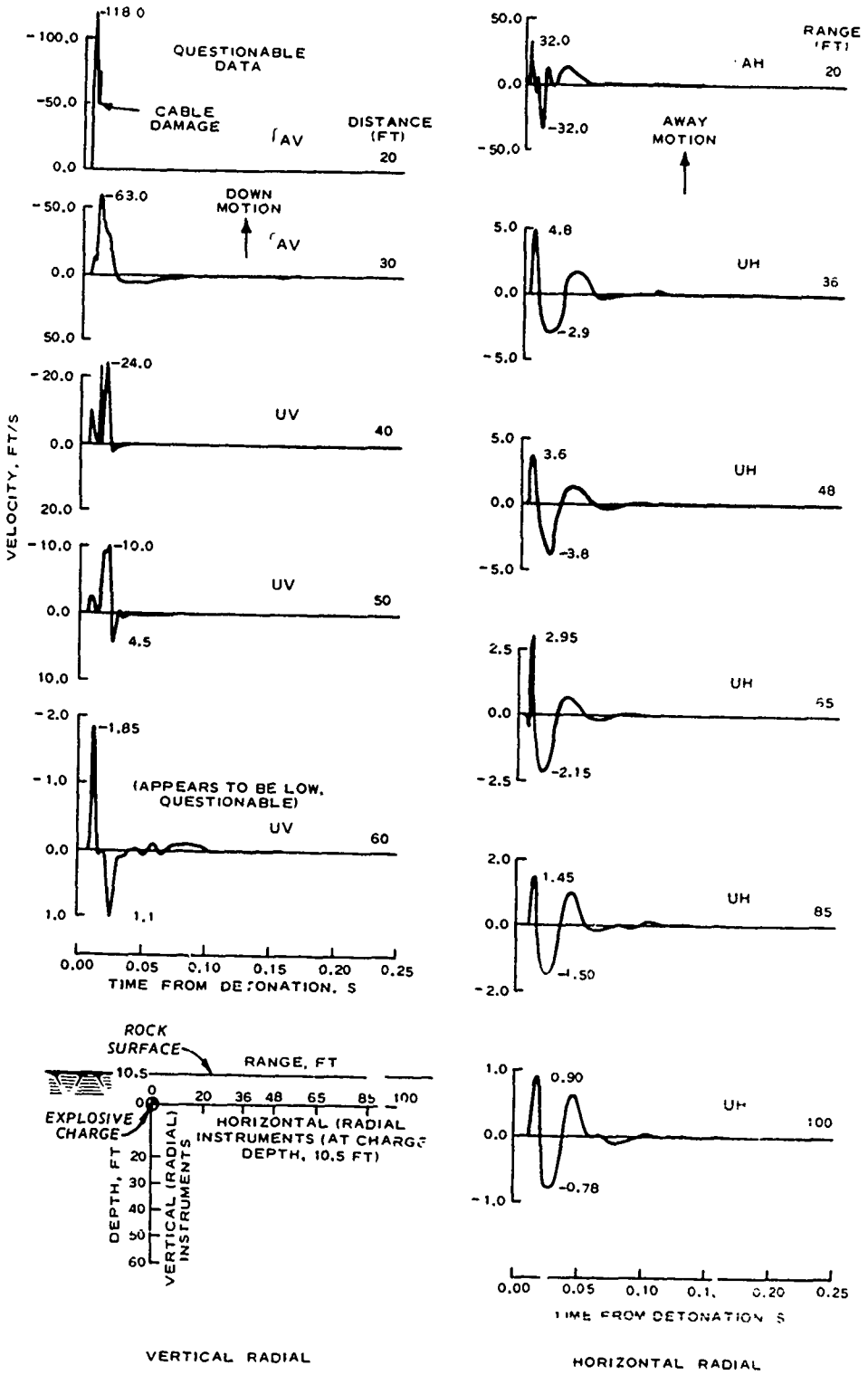

Figure 3.12. Velocity waveform comparison between vertical and horizontal instrument radials, Event 7.

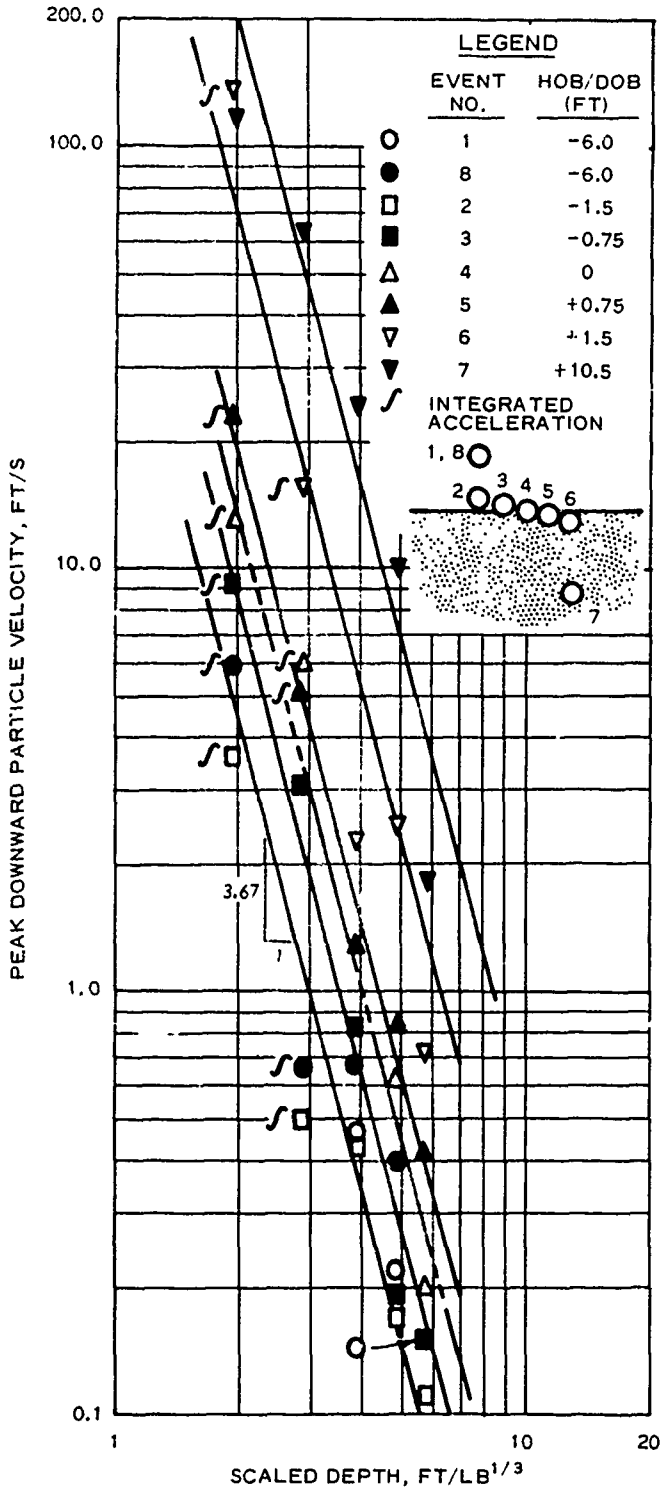

Figure 3.13. Peak downward particle velocity directly beneath the explosion versus scaled depth.

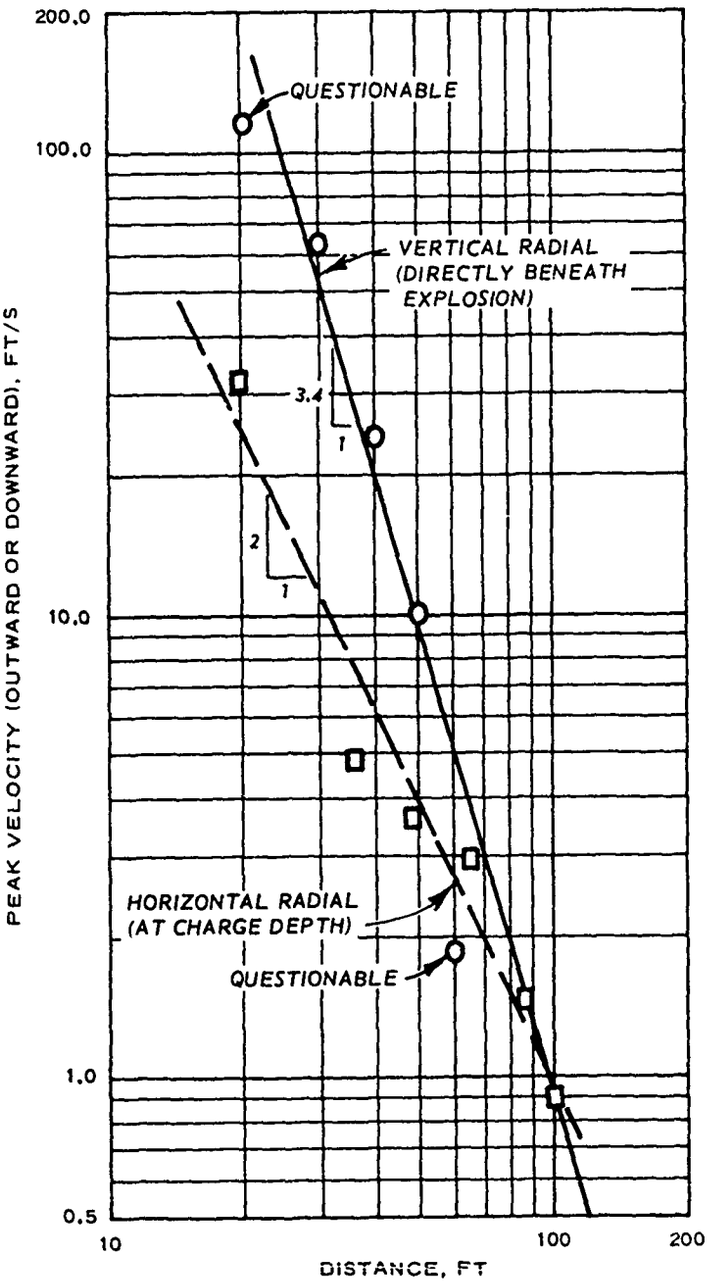

Figure 3.14. Comparison of peak velocities between the vertical radial directly beneath the explosion and the horizontal radial at charge depth, Event 7.

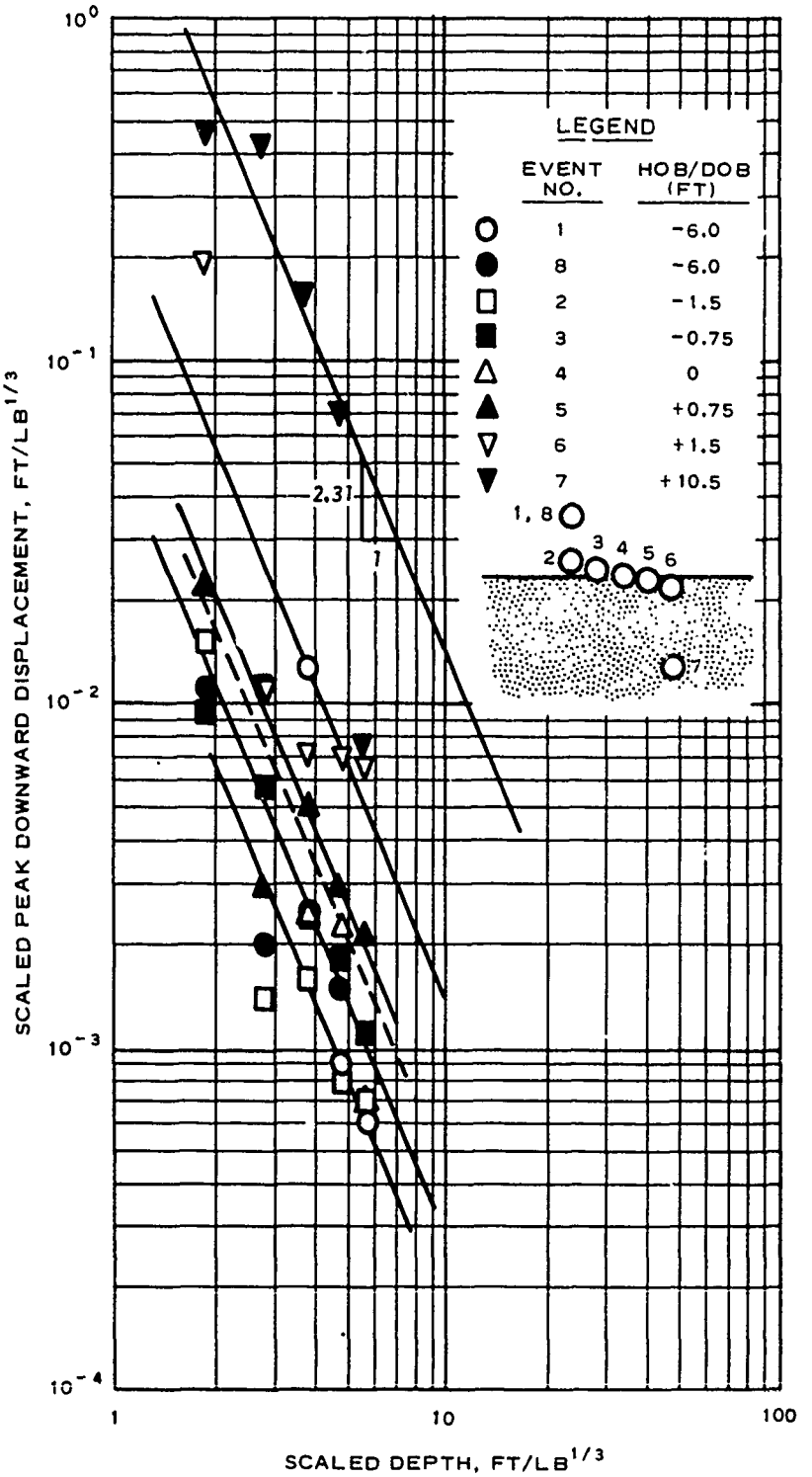

Figure 3.15. Scaled peak downward displacement along the vertical radial directly beneath the explosion versus scaled depth.

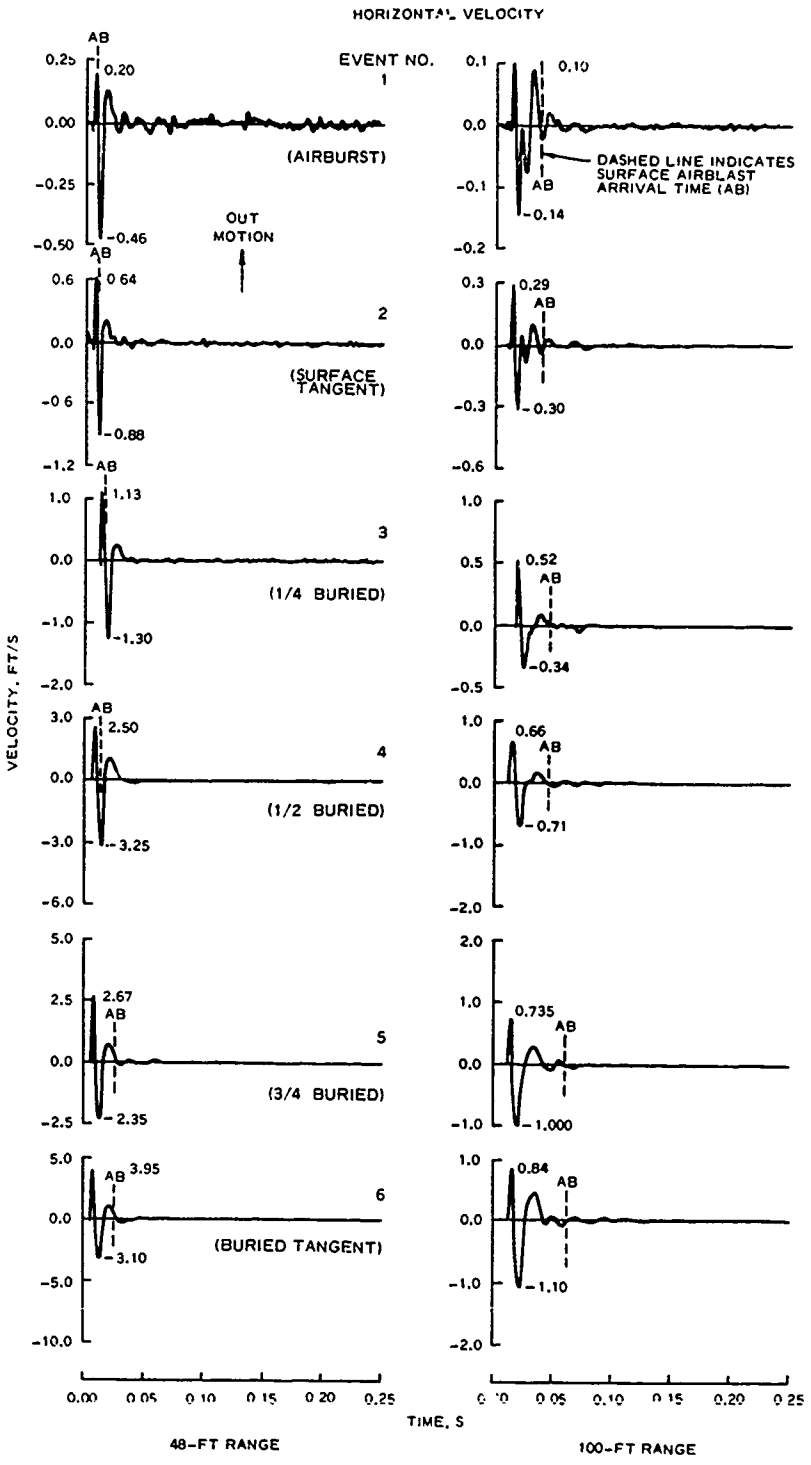

Figure 3.16. Near-surface (2-foot depth) horizontal velocity waveforms, Events 1 through 6, at 48- and 100-foot range locations.

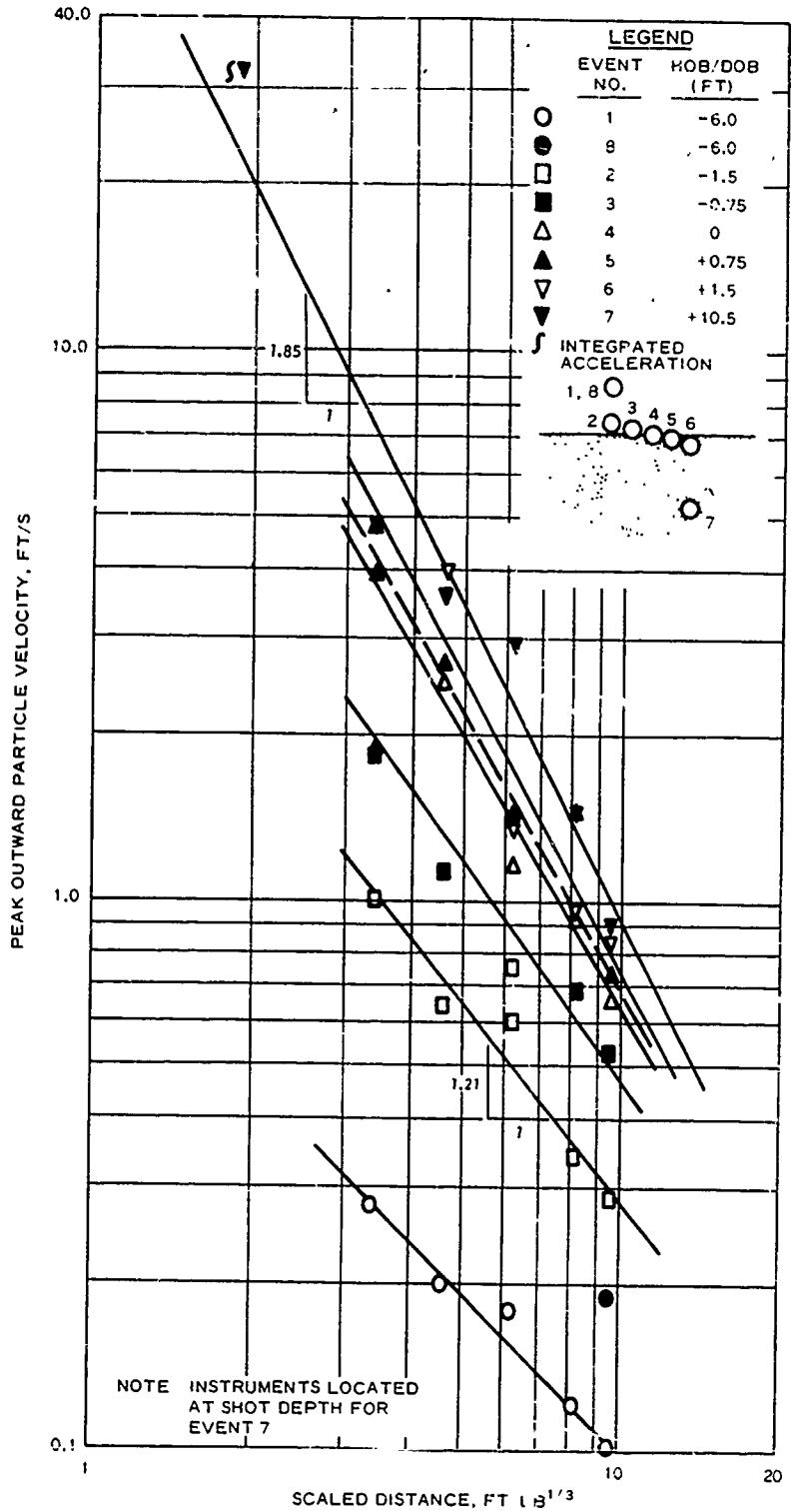

Figure 3.17. Peak outward near-surface particle velocity versus scaled distance.

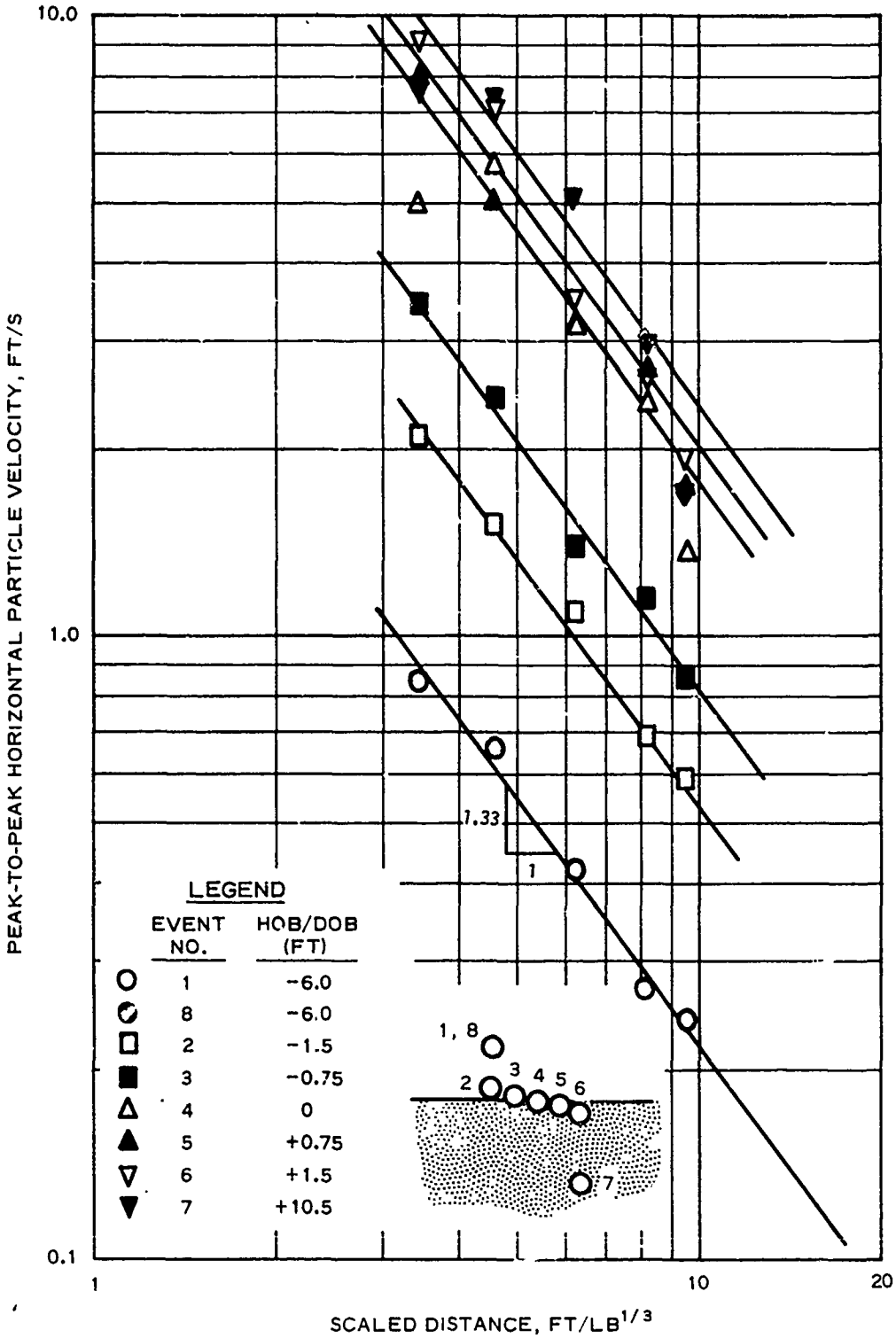

Figure 3.18. Peak-to-peak near-surface horizontal particle velocity versus scaled distance.

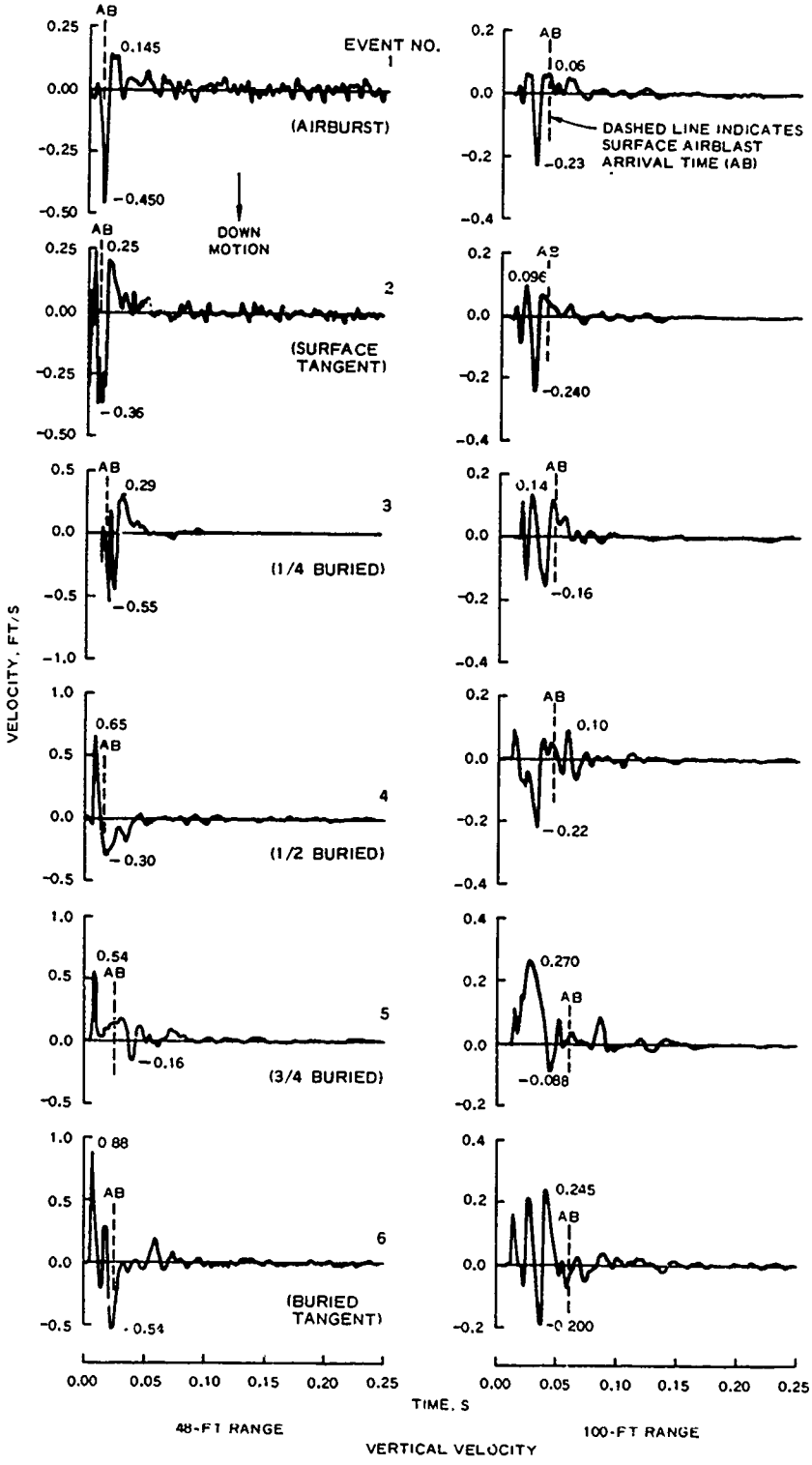

Figure 3.19. Near-surface (2-foot depth) vertical velocity waveforms, Events 1 through 6, at 48- and 100-foot range locations.

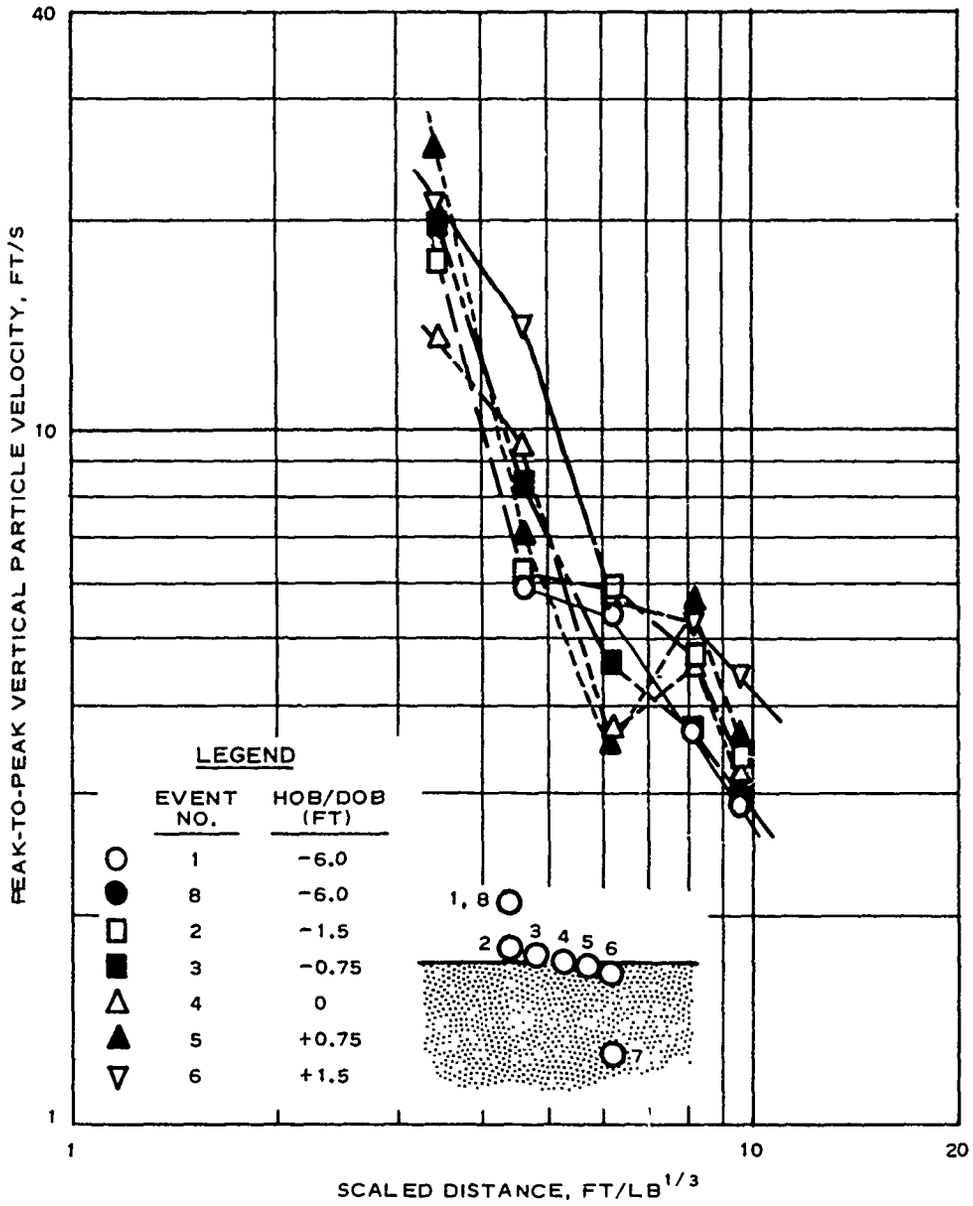

Figure 3.20. Peak-to-peak near-surface vertical particle velocity versus scaled range.

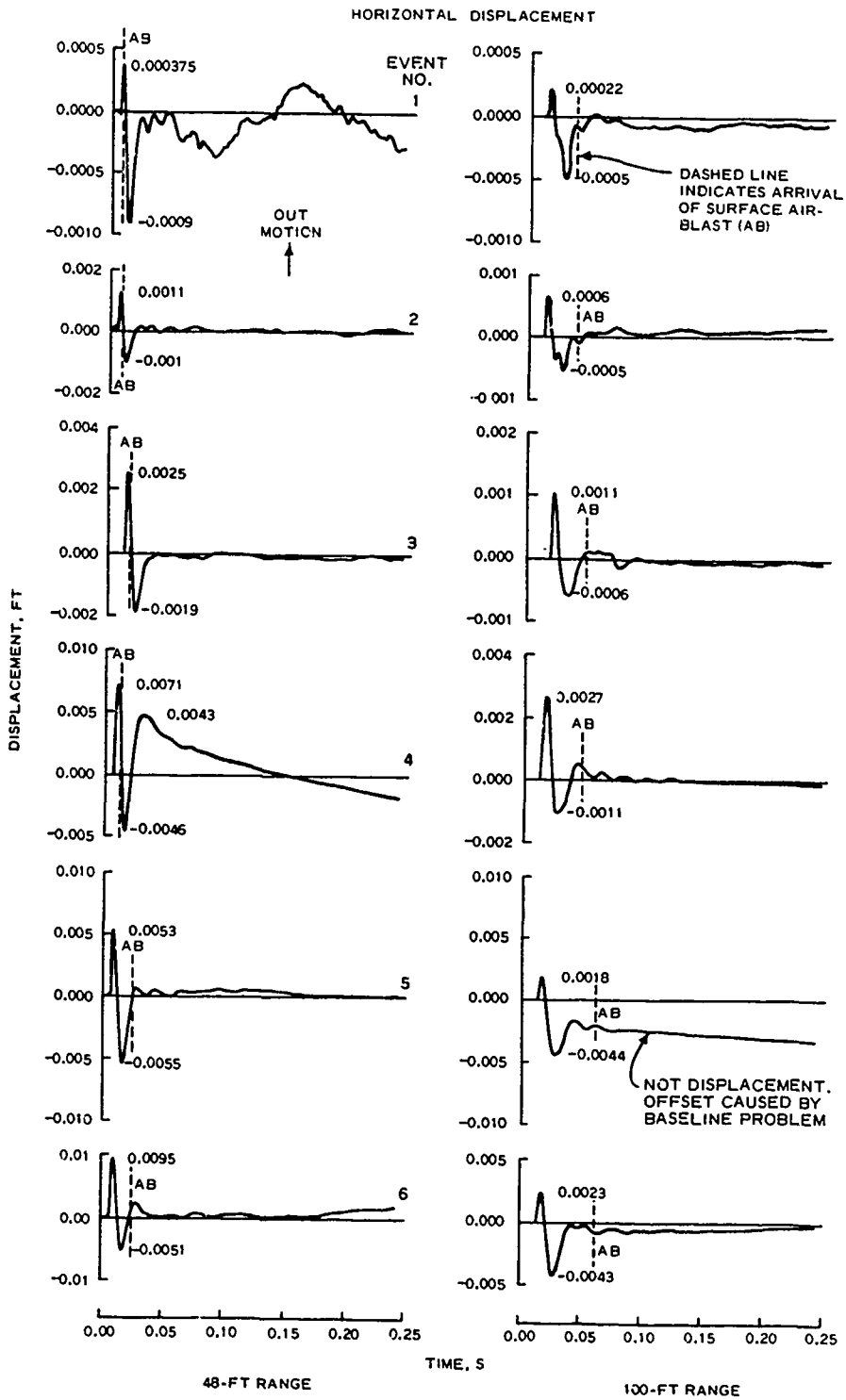

Figure 3.21. Near-surface (2-foot depth) horizontal displacement waveforms, Events 1 through 6, at 48- and 100-foot range locations.

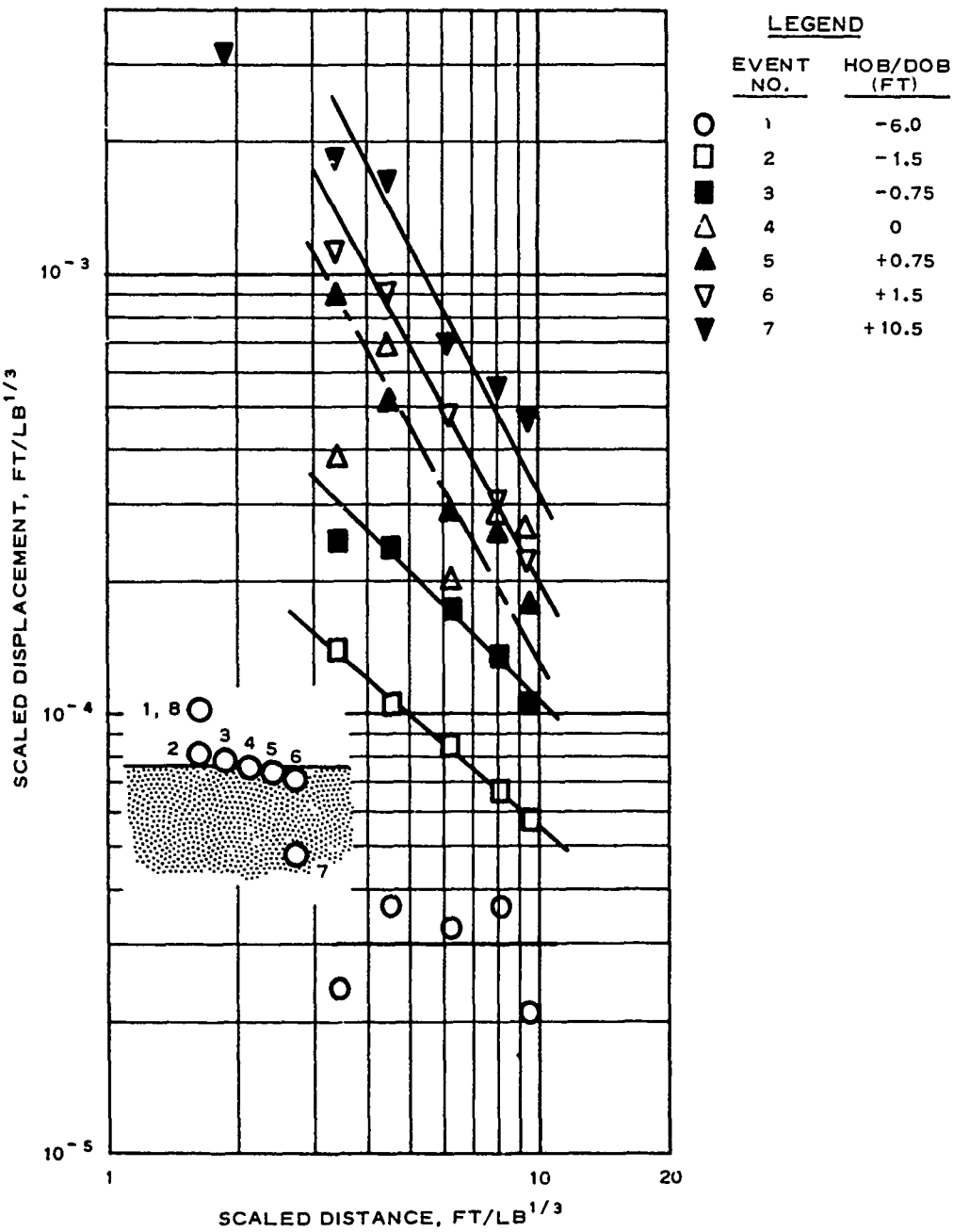

Figure 3.22. Scaled peak outward displacement versus scaled distance.

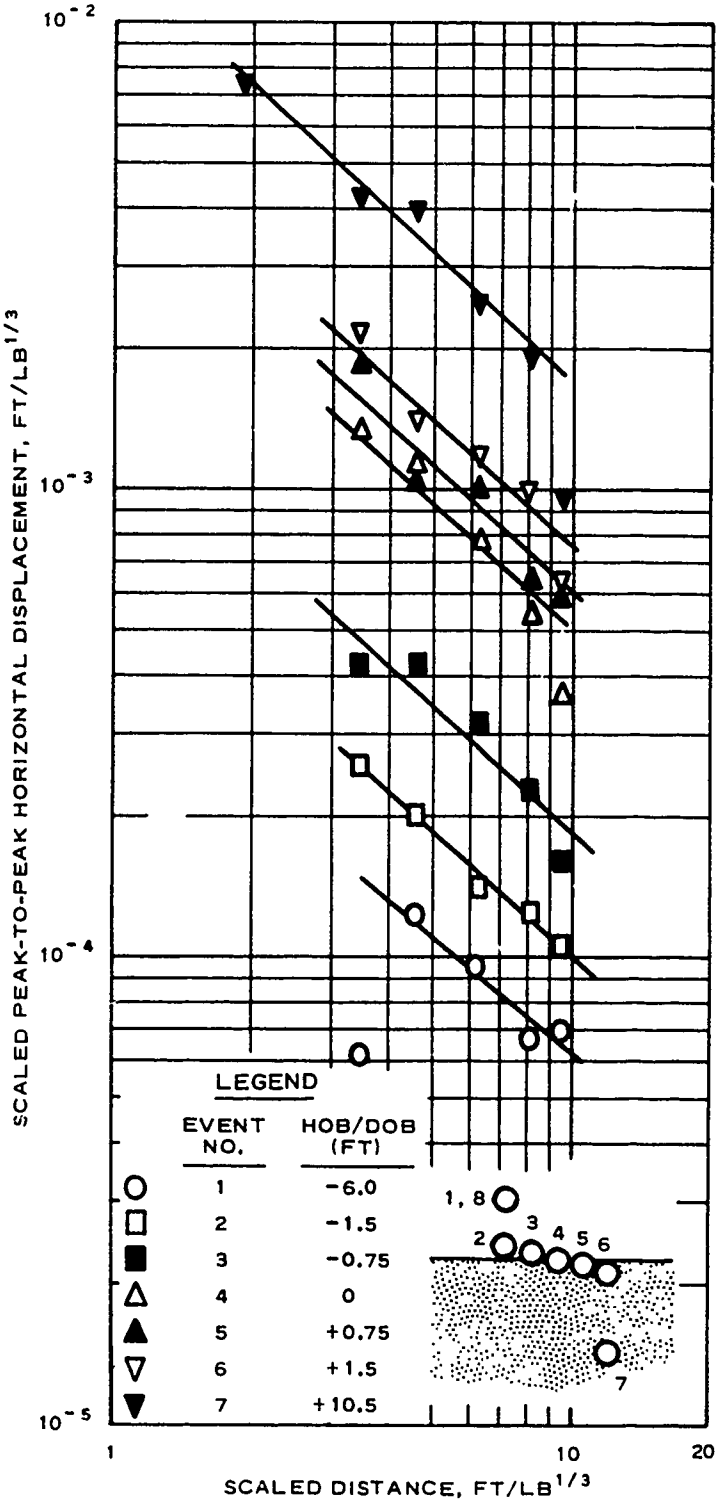

Figure 3.23. Scaled peak-to-peak horizontal displacement versus scaled distance.

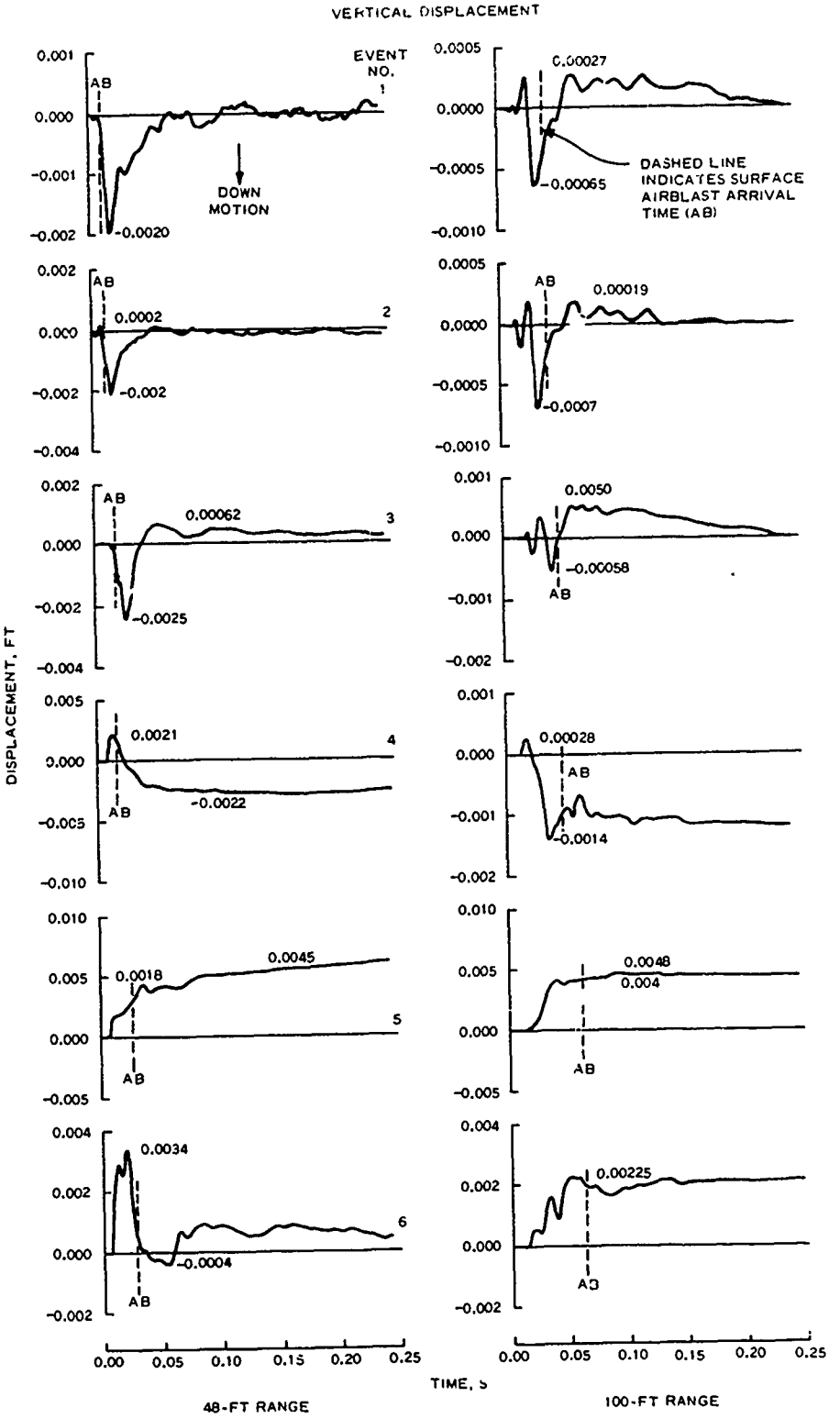

Figure 3.24. Near-surface (2-foot depth) vertical displacement waveforms, Events 1 through 6, at 48- and 100-foot range locations.

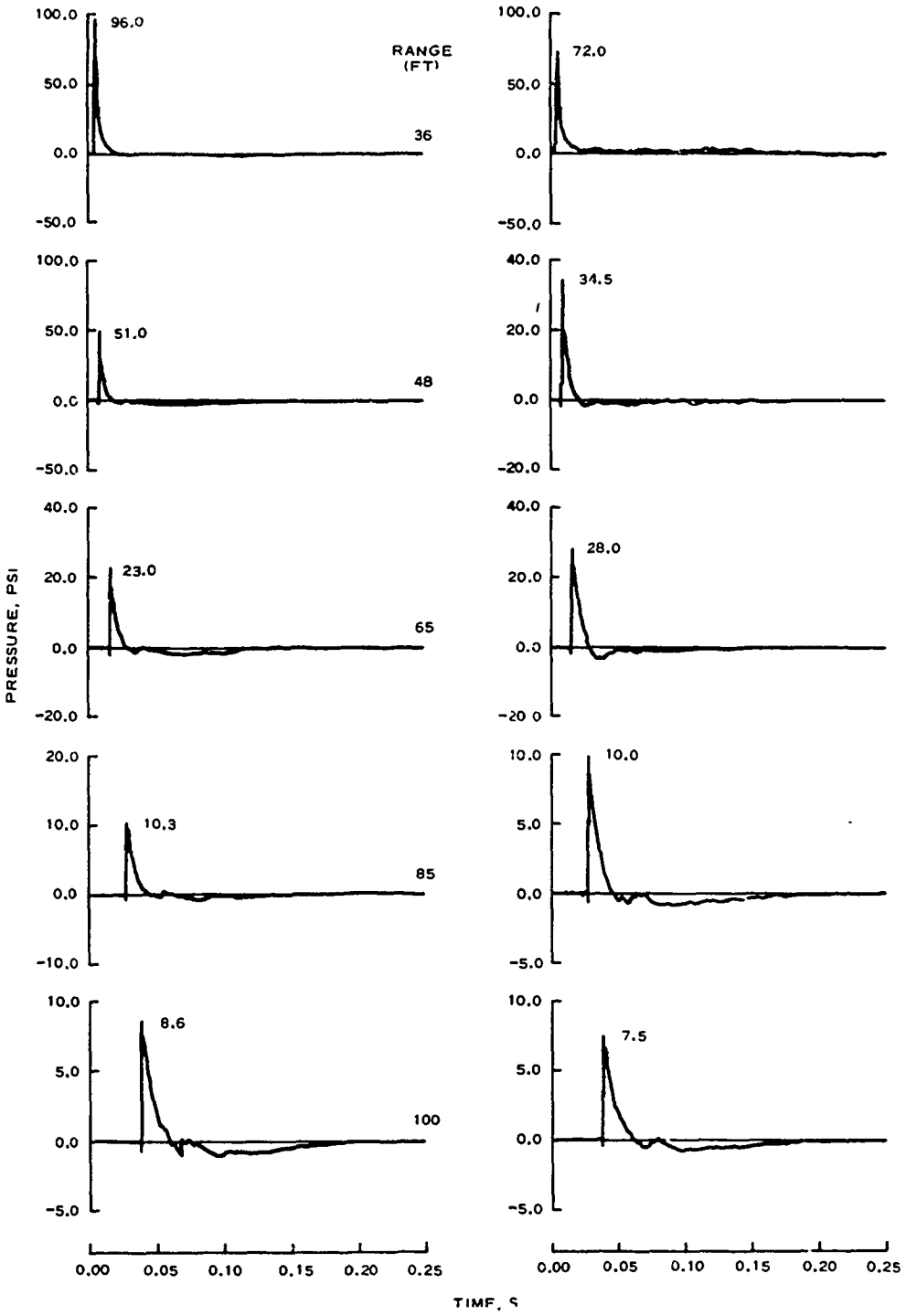

Figure 3.25. Surface airblast waveforms, airburst and surface tangent detonations (Events 8 and 2).

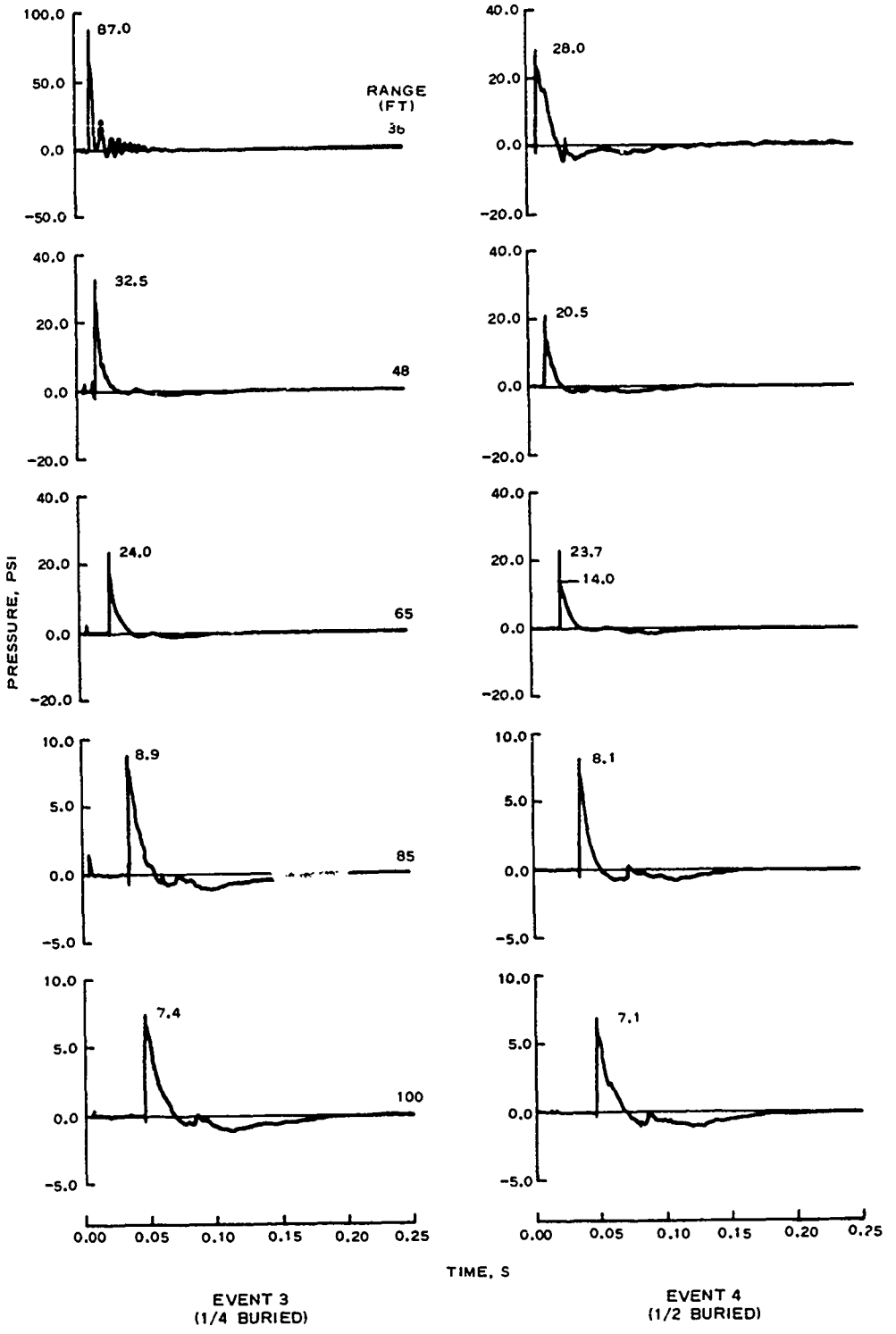

Figure 3.26. Surface airblast waveforms, 1/4- and 1/2-buried detonations (Events 3 and 4).

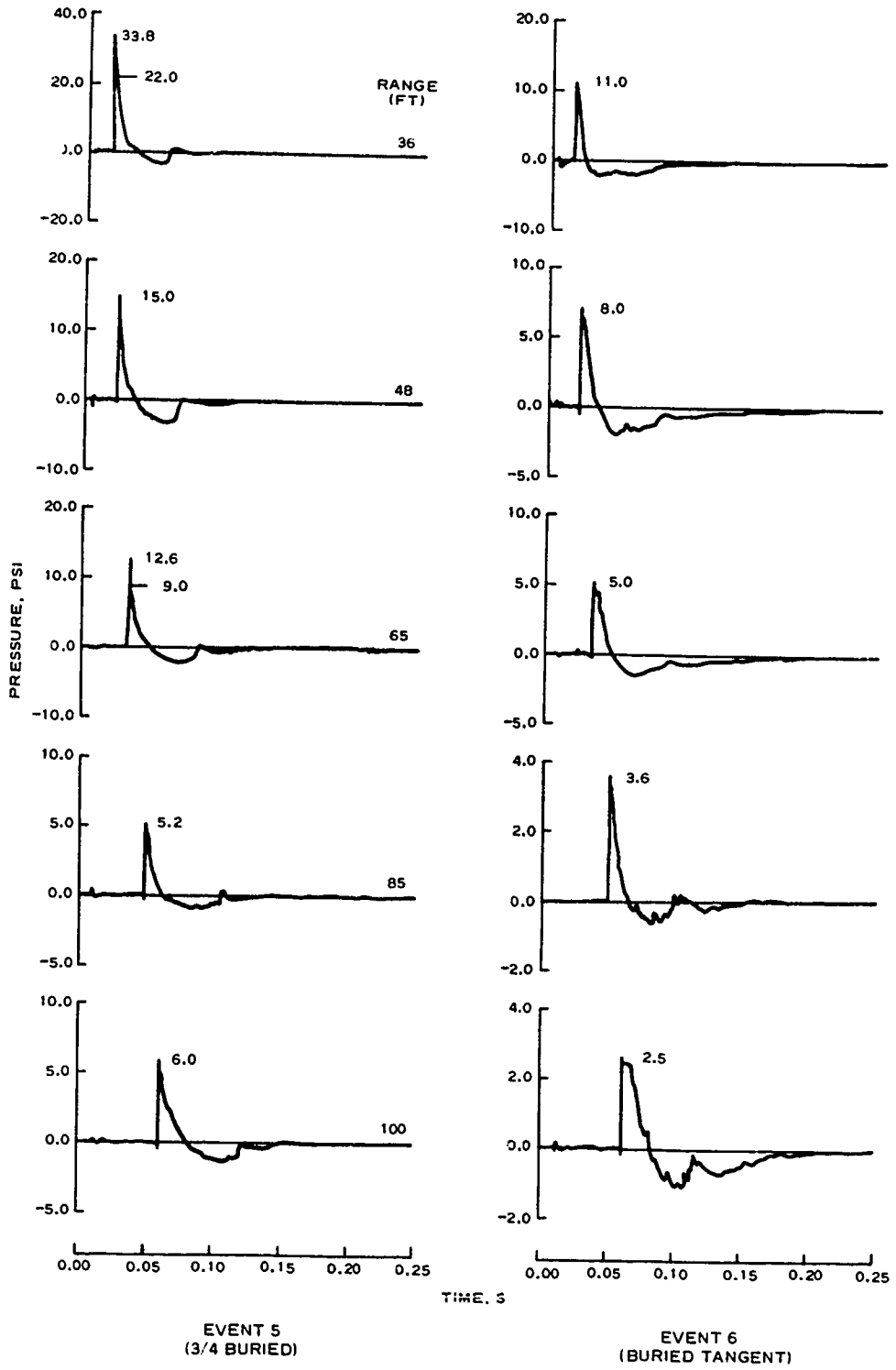

Figure 3.27. Surface airblast waveforms, 3/4-buried and buried tangent detonations (Events 5 and 6).

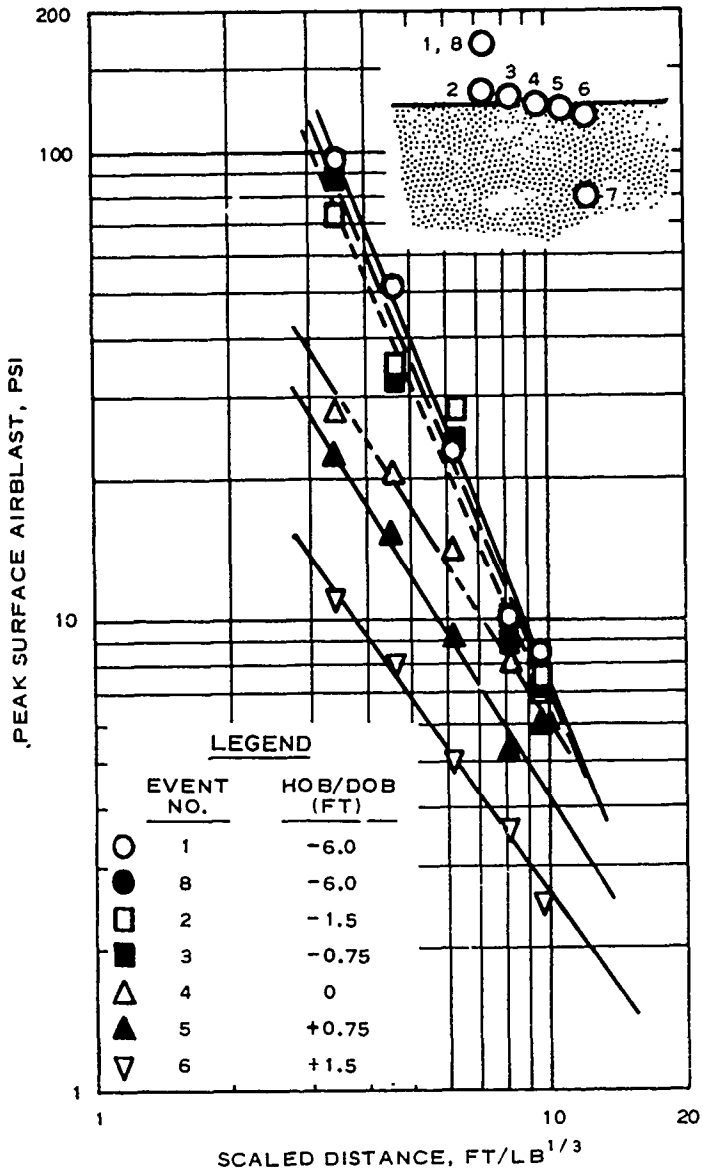

Figure 3.28. Peak surface airblast versus scaled distance.

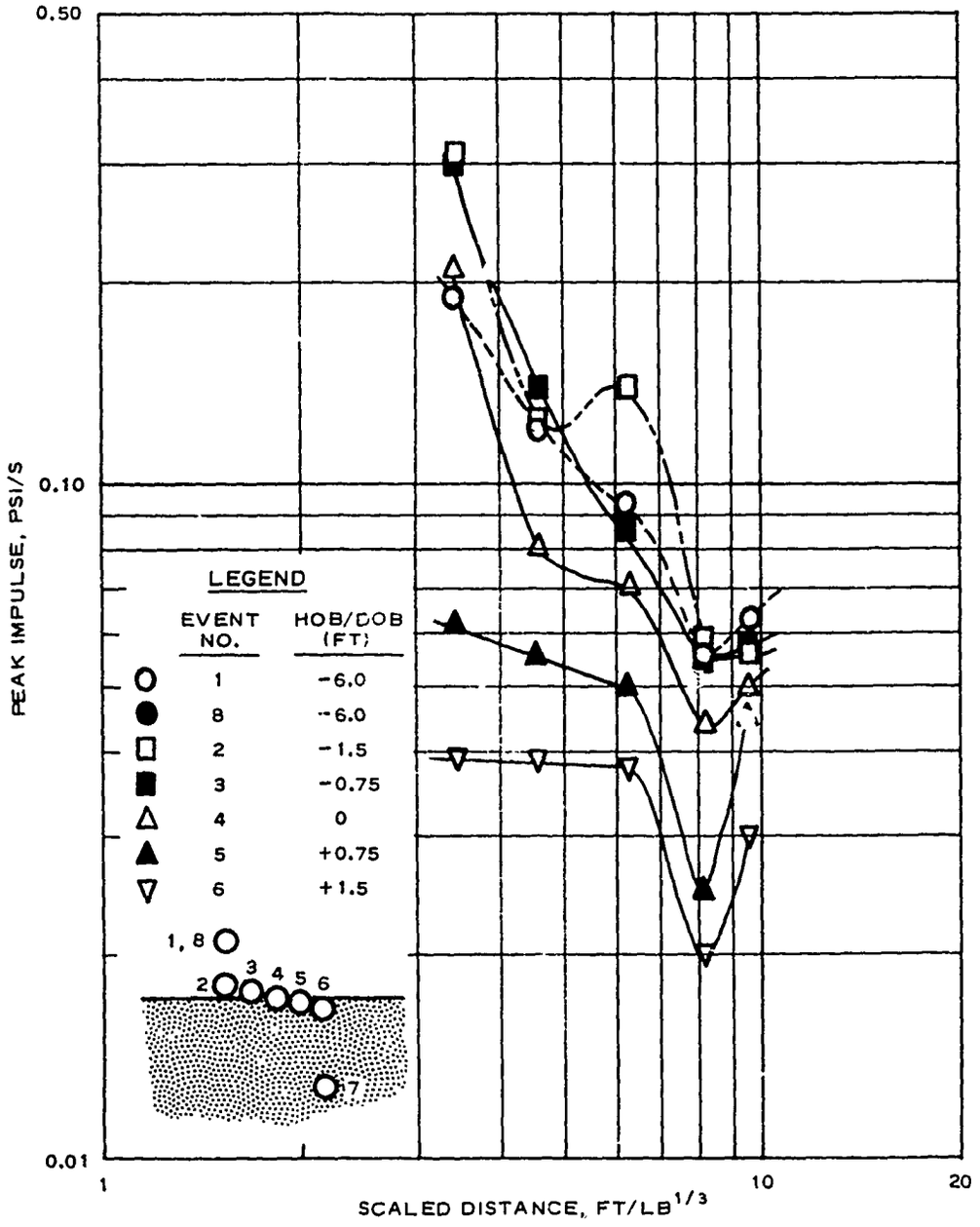

Figure 3.29. Peak surface airblast impulse versus scaled distance.

CHAPTER 4

OBSERVATIONS AND RECOMMENDATIONS

4.1 OBSERVATIONS

This chapter presents pertinent observations of the results from the CENSE 1 experiment. Detailed conclusions will be appropriately treated in Report 4 of this series, "Analysis and Summary of CENSE Data."

The primary objective of the CENSE 1 program was to determine the influence of burst position on ground shock in rock. Airblast and cratering were of secondary interest. Particular emphasis was placed on measurements directly beneath the explosion. The objectives were achieved. Excellent quality ground motion data were recorded.

The CENSE HOB/DOB experiment concept has provided critical insight into the shock physics and wave propagation in the region directly beneath an explosion detonated in rock. The information retrieved has already had major impact on weapons effects tests design and hardness assessments.

4.1.1 Cratering

No craters were produced by the airbursts, Events 1 and 8. The near-surface burst produced mounds of crushed and pulverized rock. (This same rebound phenomenon was also observed on the 20-ton Mixed Company surface tangent shot.) Because of the mounding effect for the shallow bursts, apparent crater parameters, especially volumes, are anomalous and do not scale. However, the true craters behaved in a consistent fashion with size increasing with DOB. Although the optimum DOB was not achieved in this test series, it is believed to occur at a scaled depth of approximately 1.5 $W^{1/3}$ (15 ft) where the true cratering efficiency is estimated to be at least 7.5 ft^3/lb. A comparison of the cratering efficiencies shows about 10 percent of optimum for a surface burst and 1.5 percent for a tangent sphere. (These values were derived from an analysis of CENSE-1 and Mixed Company data.)

4.1.2 Airblast

The airblast suppression (enhancement) was strongly influenced by the burst position in the region HOB = 0.29 $W^{1/3}$ to DOB = 0.14 $W^{1/3}$. For HOB's higher than 0.29 $W^{1/3}$ the enhancement asymptotically approached a maximum value twice the value of the free-air condition. Suppression was substantial for burst positions within the rock where DOB was greater than half buried. Increasing containment caused a progressive flattening of the peak pressure attenuation with range, limiting conclusions about airblast suppression to shallow-buried bursts (DOB about 0.14 $W^{1/3}$ or less). Extrapolation to greater DOB and ranges is not warranted with this data base.

4.1.3 Ground Shock

4.1.3.1 WAVE SPEED. The compressional wave propagated downward directly beneath the explosion at a velocity of 7900 ft/s. Propagation along the horizontal radial was 8400 ft/s. The seismic velocity previously determined for Kayenta sandstone in this area was 7500 ft/s. Outrunning occurred at all near-surface motion gage locations.

4.1.3.2 ACCELERATION MEASUREMENTS. Burst position significantly influenced acceleration measured directly beneath the explosion. Peak amplitudes increased rapidly with increasing charge DOB. Peak downward acceleration from the buried tangent detonation was 115 times that from the surface tangent detonation.

4.1.3.3 PARTICLE VELOCITY. Significant increases in particle velocity directly beneath the explosion occurred for progressive charge burial within the rock. Maximum downward particle velocity, which was produced from the charge DOB of 10.5 feet, was some 42 times greater than that produced by the surface tangent detonation.

Distinct differences were observed in both the amplitude and the shape of the particle velocity waveforms beneath the charge and near the surface from the deepest shot, Event 7. The vertical velocity waveform was characterized by a double-spiked initial peak, whereas the horizontal waveform showed a characteristic single peak profile that was

present in all the near-surface (2-foot depth) horizontal waveforms. Velocities were higher beneath the charge, yet attenuated more rapidly with distance compared to the surface motions. This difference might be associated with the almost horizontally bedded structure of the sandstone and the burst position.

Near-surface horizontal particle velocity exhibited a characteristic shape at all ranges (including the 10.5-foot depth horizontal radial of Event 7) in all HOB/DOB detonations. Horizontal particle velocity was independent of localized surface airblast influence and appeared to be related to a body wave phenomenon. Horizontal motion apparently originated at or very near GZ from the airblast loading. Because of the high strength of the rock and relatively low surface airblast pressures over the horizontal range instrumented, little airslap was transmitted directly to the sensors. Burst position significantly influenced horizontal particle velocity amplitudes. Maximum near-surface horizontal particle velocity measured from the buried tangent detonation (Event 6) was 5 times greater than from the surface tangent detonation. Maximum horizontal particle velocities were measured at charge depth from Event 7. The amplitudes were 8 times those from the surface tangent detonation at comparable distances.

Near-surface vertical velocity waveforms were highly complex and, therefore, difficult to interpret. Surface airblast significantly influenced peak downward velocity only at the closest gage position for the 0.75-foot HOB and shallower events. For all other burst positions, the direct-induced motion was the primary source influencing the vertical velocity.

4.1.3.4 DISPLACEMENT. Vertical displacement directly beneath the explosion responded in a manner similar to the vertical particle velocity. Maximum downward displacement produced by Event 7 (DOB 10.5 feet) was 84 times greater than for the surface tangent detonation.

Surface airblast had no significant influence on near-surface horizontal displacement. The horizontal displacement was produced

exclusively by the shock propagating in the rock, even in the air-bursts (Events 1 and 8). Peak horizontal displacement increased proportionally with increasing charge DOB. Near-surface horizontal displacement was 8 times greater from the buried tangent detonation (Event 6) than the surface tangent shot. This enhancement increased to 18 times for the 10.5-foot DOB detonation.

4.2 RECOMMENDATIONS

It is recommended that similar tests be performed in soil and in layered geologies, including soil over rock.

REFERENCES

1. D. C. Sachs and L. M. Swift; "Small Explosion Tests, Project Mole"; Final Report AFSWP-291, Vols I & II, Dec 1955; Stanford Research Institute, Menlo Park, Calif.

2. F. M. Sauer and C. T. Vincent; "Ferris Wheel Series, Flat Top Event, Project Officer's Report, Project 1.2/1.3a; Earth Motion and Pressure Histories"; POR-3002 (WT-3002), 12 Apr 1967; Stanford Research Institute, Menlo Park, Calif.

3. E. E. Jaramillo and R. G. Pozega; "Middle Gust Free-Field Data Analysis"; AFWL TR-73-251, Apr 1974; Air Force Weapons Laboratory, Air Force Systems Command, Kirtland Air Force Base, N. Mex.

4. D. W. Murrell; "Middle Gust Series, Ground Motion Measurements" (in preparation); U. S. Army Engineer Waterways Experiment Station, CE, Vicksburg, Miss.

5. J. K. Ingram, J. L. Drake, and L. F. Ingram; "Influence of Burst Position on Airblast, Ground Shock, and Cratering in Sandstone"; Miscellaneous Paper N-75-3, May 1975; U. S. Army Engineer Waterways Experiment Station, CE, Vicksburg, Miss.

6. "Endevco 2200 Series Piezoresistive Accelerometer Specifications Bulletin"; Endevco, Dynamic Instrument Division, Pasadena, Calif.

7. "Series Blast Pressure Transducers"; Instruction Manual AB-200," 1968; Bytrex, Inc., Waltham, Mass.

8. J. W. Wister; "An Extended Range Velocity Gage for Measurements in High-Shock Environment"; Sandia Corporation, Albuquerque, N. Mex.

9. F. P. Hanes; "Signal Conditioning System for Velocity Gages, Instrumentation for Nuclear Weapons Effects Simulation Symposium, Shock Effects"; Technical Report No. AFSWC-TR-70-5, Vol II, Mar 1970; Air Force Special Weapons Center, Kirtland Air Force Base, Albuquerque, N. Mex.

10. H. D. Carleton; "Digital Filters for Routine Data Reduction"; Miscellaneous Paper N-70-1, Mar 1970; U. S. Army Engineer Waterways Experiment Station, CE, Vicksburg, Miss.

11. H. D. Carleton; "Digital Filters for Explosion Effects Analysis"; Technical Report N-71-7, Jun 1971; U. S. Army Engineer Waterways Experiment Station, CE, Vicksburg, Miss.

12. J. Q. Ehrgott; "Preshot Material Property Investigation for the Mixed Company Site: Summary of Subsurface Exploration and Laboratory Test Results"; Miscellaneous Paper S-73-62, Oct 1973; U. S. Army Engineer Waterways Experiment Station, CE, Vicksburg, Miss.

13. J. Q. Ehrgott and J. G. Jackson, Jr.; "Material Properties for Postshot Mixed Company Analysis: Recommendations Based on Recent Laboratory and In Situ Test Data"; Miscellaneous Paper S-74-1, Jan 1974; U. S. Army Engineer Waterways Experiment Station, CE, Vicksburg, Miss.

14. J. B. Palmerton and J. B. Warriner; "Postshot In Situ Material Property Tests at the Mixed Company Site, Colorado"; Miscellaneous Paper S-74-8, May 1974; U. S. Army Engineer Waterways Experiment Station, CE, Vicksburg, Miss.

15. A. Peekna; "Ground Motion Canister Design and Evaluation" (in preparation); U. S. Army Engineer Waterways Experiment Station, CE, Vicksburg, Miss.

APPENDIX A

TEST SITE PREPARATION

A.1 SITE LOCATION

The test series was conducted on private land in the NW quadrant of Section 33, Township 12 South, Range 102 West, Mesa County, Colo. (Figures A.1 and A.2). The site was located about 4 miles west of Glade Park, which is approximately 15 miles southwest of Grand Junction.

A.2 GEOLOGY

The exposed rock of the test site is part of the approximately 70-foot-thick Kayenta Formation of the Glen Canyon Group, Triassic period. This formation is a fluvial deposit consisting of lenticular to irregularly bedded layers of fine- to medium-grained sandstone, siltstone, and conglomerate with occasional layers or lenses of shale (References 11, 12, and 13).[1]

The Wingate Formation lies beneath the Kayenta and extends from approximately 70 to 400 feet in depth. It is predominately eolean deposited, crossbedded, fine-grained massive sandstone. A geologic profile of the CENSE 1 site is shown in Figure A.3.

An exposed massif north of the test site is composed of sandstone of the Entrada Formation, similar to the Wingate in character, but considerably harder (better cemented).

Only a few surface faults were observed in the area selected as the test bed. The major visible feature was a N-NW striking fault that extended through the test bed (extending to an unknown depth) to the north bounding massif.

Borings to depths of 85 feet did not indicate obvious faulting in the area planned for testing. However, a layer of relatively uncemented

---

[1] Raised numbers refer to similarly numbered items in the References at the end of the main text.

sand or very friable sandstone was encountered at a nominal depth of 65 feet, and may mark the Kayenta-Wingate Formation contact zone. These borings revealed a finely layered structure with the bedding plane dipping 10 degrees to the north.

A.3 INSTRUMENT INSTALLATION

A.3.1 Instrument Packages

Motion instruments were protected by cylindrical aluminum canisters. Two sizes were used. A small "micro" can was used for the accelerometers and a larger "combination" can was used for the velocity gages. Specifications for these canisters are given in Reference 15.

Surface airblast gages were mounted in 2-1/2-inch-diameter steel pipe nipples and potted with Biwax 601 potting compound.

A.3.2 Vertical Radial Directly Beneath the Explosion

Ground Zero (GZ) instruments were prealined on the ground surface at specified intervals. The instrument canisters were then clamped to lengths of 1/8-inch-diameter stainless steel aircraft cable. A 25-pound steel deadman was used for stability. Signal cables were looped around the canisters and protected from sharp edges by short lengths of Tygon tubing. Signal cables were than taped to the steel cable between instrument canisters. Figure A.4 shows the details. After checkout, the signal cables were disconnected and strung down the vertical instrument hole and brought back to the surface via the slant hole that intersected the vertical hole some 10 feet below the deepest canister. Signal cables were reconnected and all channels were monitored as the instruments were placed and grouted.

Grout was injected into the instrument hole from the bottom through a 1-inch diameter hose. The gage stringer was secured at the surface and the deadman grouted in. Sufficient grout was placed to not only secure the deadman, but also seal off the intersecting slant hole. After the initial grout pour was set, the remainder of the vertical hole was grouted in a single operation.

To provide good ground motion measurements, rigid coupling to the native earth is mandatory. Chemical grouting provided a positive coupling to the in situ rock. Although slight variances in materials and associated properties probably existed throughout the depths instrumented on CENSE 1, a single grout type was used for coupling the instrument packages to the rock. The grout formula by weight percentage is given in Table A.1.

A.3.3 Horizontal Radial

Thin cement grout pads approximately 110 feet long by 4 feet wide and an average 4 inches thick were poured for surface airblast gages (Figure A.5). An expanded pad area was provided around GZ to ensure a smooth path for surface air shock runout. Since both surface airblast and near-surface motion gages were used at the same fixed horizontal ranges, a single placement hole was augered vertically through the pad at its center (Figure A.5). The near-surface motion instruments were positioned at the bottom of the boreholes (canister midpoint at a depth of 2 feet), locally grouted at the base, and the holes backfilled with damp tamped masonry sand.

Surface airblast gages were positioned in the top center of the hole flush with the pad surface and grouted in place.

One-inch-diameter polyvinylchloride pipe was placed in the pad for instrument cable access and protection. All surface airblast and near-surface ground motion instruments were recovered and reused for all events except Event 7.

The Event 2 (surface tangent) GZ area had to be cleared and rebuilt before testing of Event 6 (buried tangent). A large volume of grout was required that was greatly in excess of the existing supply of instrument canister grout. As an alternative, a commercial grout was purchased and used as backfill. This crater backfill grout mix formula is given in Table A.1.

Grout components are described in Table A.2.

A.4 CHARGE INSTALLATION

The explosive charges for the elevated shots were suspended from a wire rope supported by two poles. The poles were grouted into the rock. The explosive was suspended from the wire rope by a nylon sling.

The charge for the surface tangent shot was supported by a Styrofoam ring. Charges for Events 3 through 6 were placed in shaped cavities chiseled into the rock. A thin layer of rock-matching grout was used to couple the charge to the rock.

The charge for Event 7 was positioned in a 40-inch-diameter calyx hole. The charge container was filled with water and weighted down with sandbags. A layer of rock-matching grout was placed to an elevation just above the centerline. After the first lift of grout had set, a second lift was placed to cover the charge. The water was pumped out of the container and the container was blown dry. Filling, vent, and arming ports were attached to the container and the booster explosive (3/4-pound C4) and exploding bridge wire detonators were installed. The top parts were sealed and the remaining volume of the charge hole was grouted in a single pour. The charge container was filled with nitromethane just prior to execution of the event (T-2 hours).

Table A.1. GROUT FORMULAE.

Component	Weight Percentage
Instrument and Charge Backfill Mix	
ChemComp cement	18.13
Fly ash	7.68
Sand (masonry)	52.33
Gel	0.28
Barite	6.89
CFR-2	0.14
Water	14.55
Crater Backfill Mix	
Portland cement, type II	21.95
Sand (masonry)	57.72
Gel	0.01
Water	20.32

Table A.2. GROUT COMPONENT DESCRIPTIONS.

Material	Description
Portland cement	Common type II portland cement.
Fly ash	Pozzolan, used for filler, retards heat of hydration, provides long-term strength. Distributed by Halliburton Oil Well Cementing Company, Mopa, Nev.
ChemComp	Shrinkage compensating cement.
Sand	Locally available, fine gray sand, washed. Whitewater Materials Company, Grand Junction, Colo.
Gel	Bentonite clay, used to hold other materials in suspension during pumping and curing.
Barite	Barium sulfate, used as filler to increase weight of grout. Proprietary product of Baroid Division, National Lead Company, Jackson, Miss.
CFR-2	Friction-reducing admixture. Proprietary product of Halliburton Oil Well Cementing Company, Nevada Test Site, Mercury, Nev.
Water	Local reservoir water, furnished by commercial supply truck.

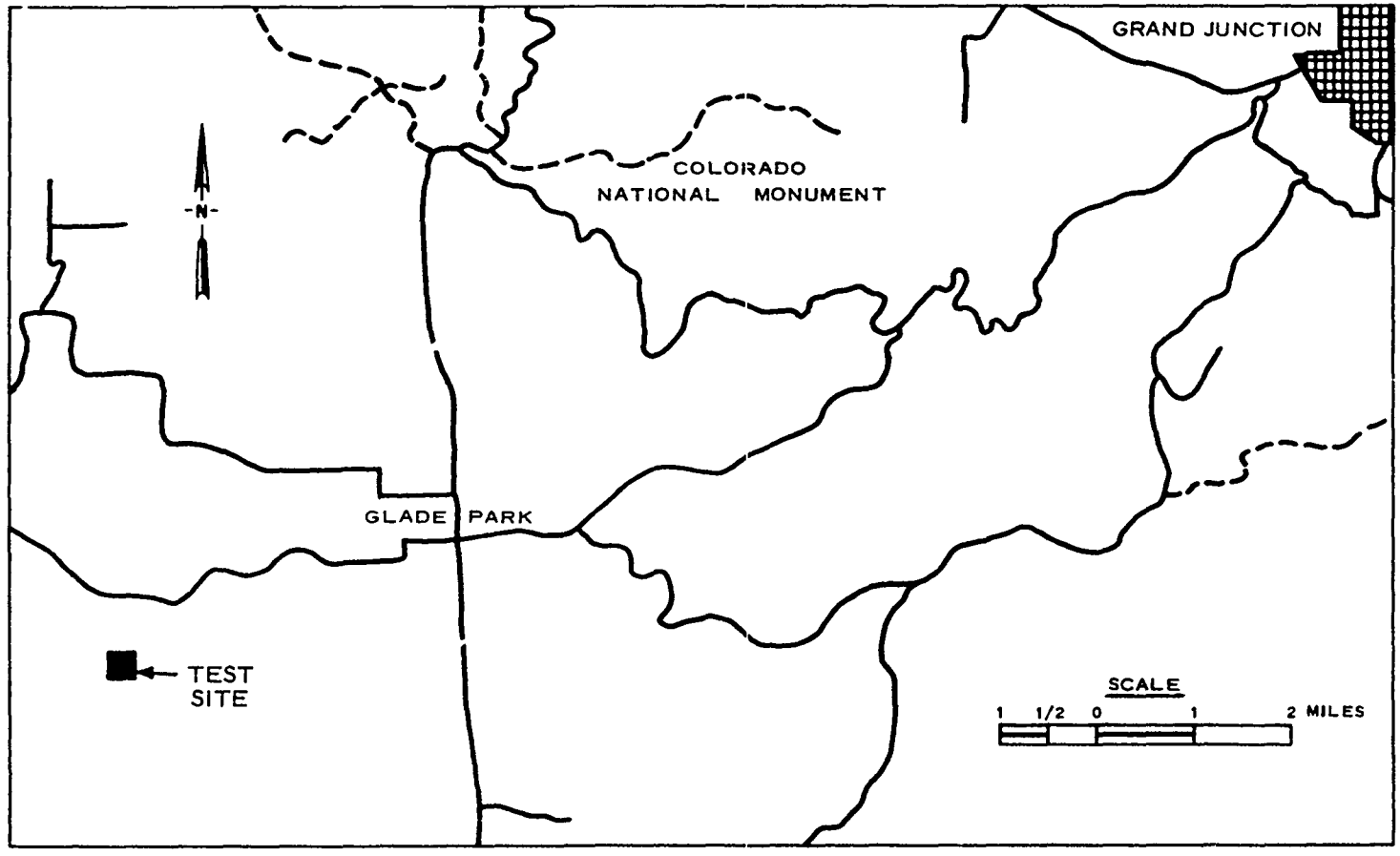

Figure A.1 Site area location map.

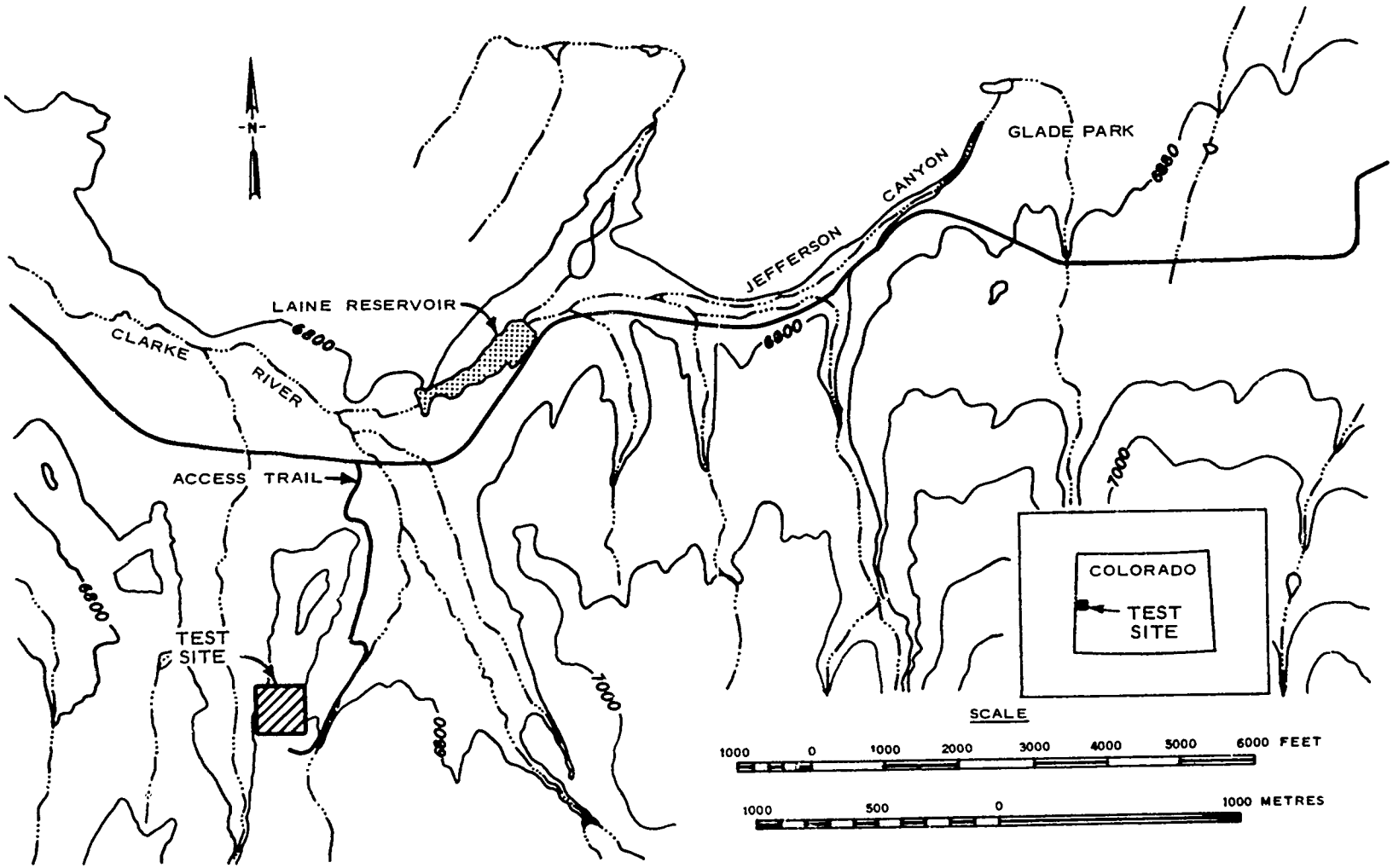

Figure A.2 Test site detailed topographic map.

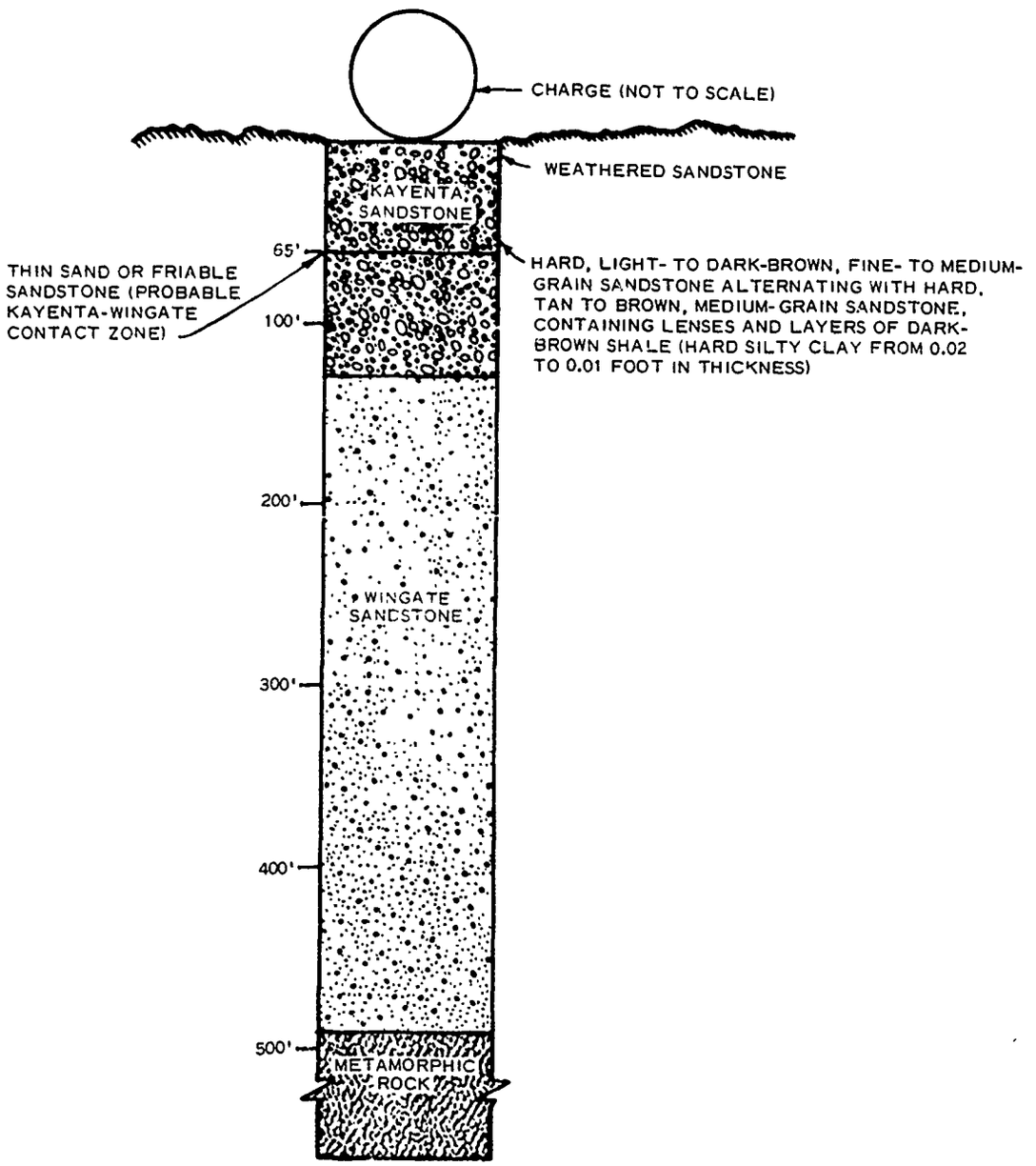

Figure A.3. CENSE 1 geologic profile (Reference 12).

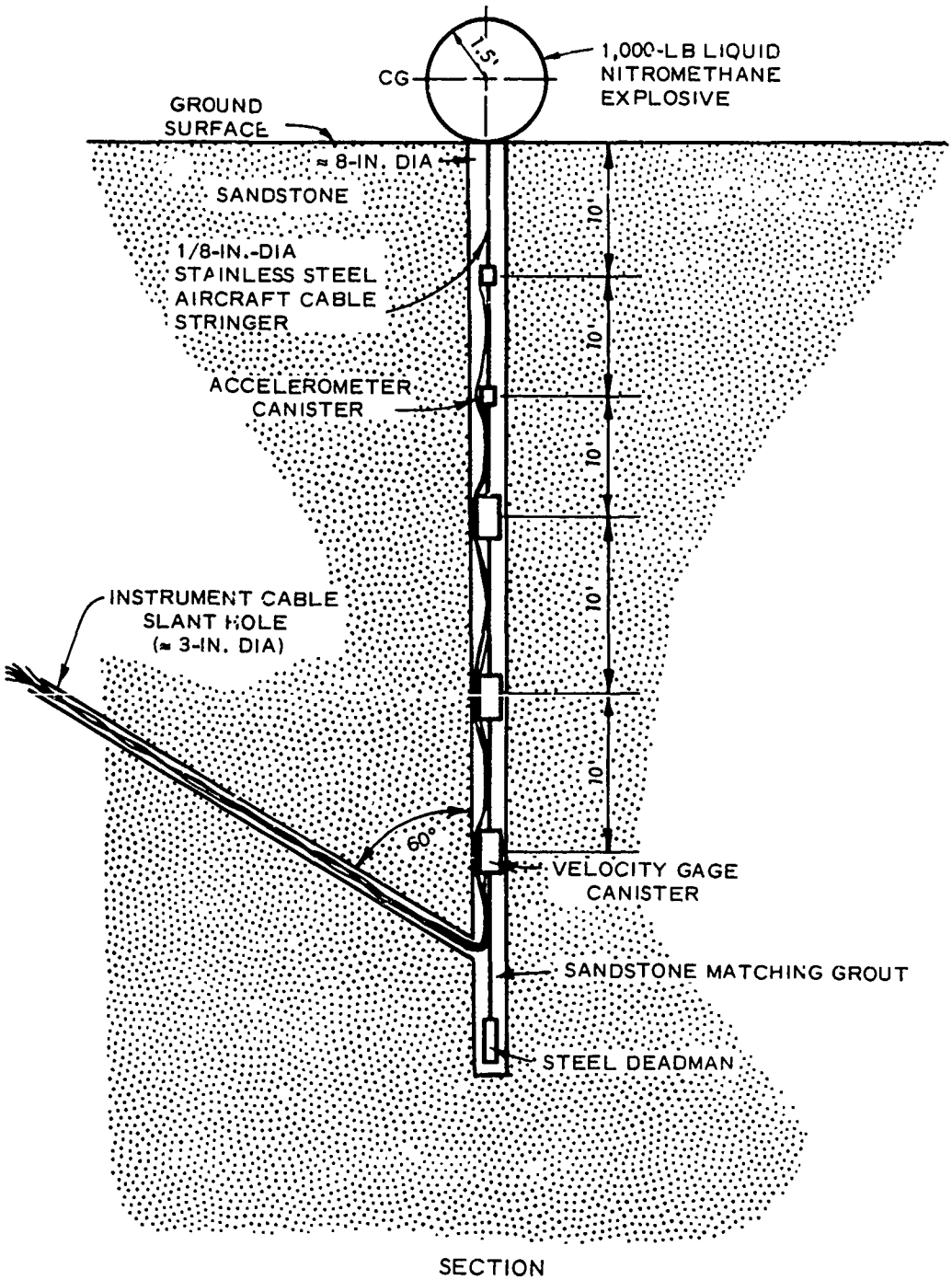

Figure A.4. Installation detail of motion instruments along the vertical radial directly beneath the explosion (not to scale).

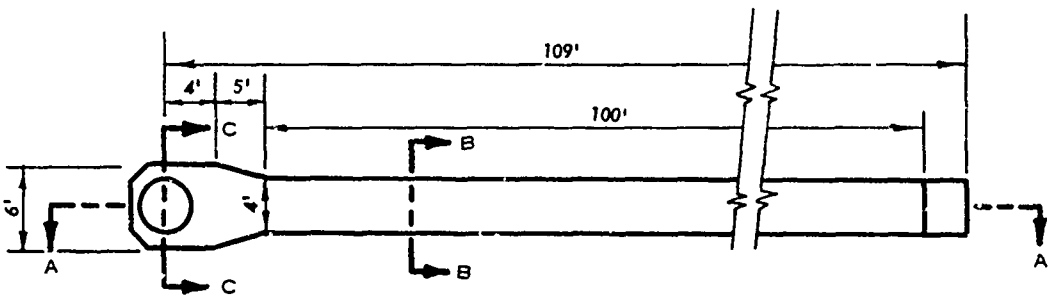

PLAN

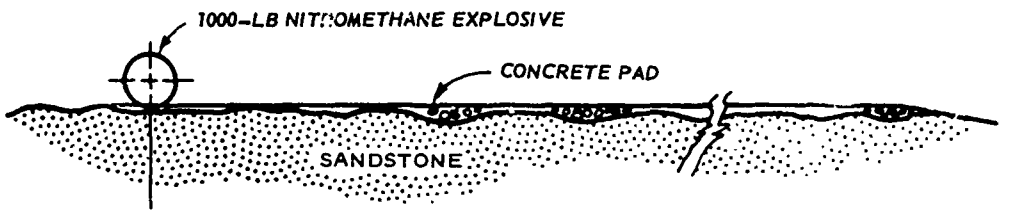

SECTION AA

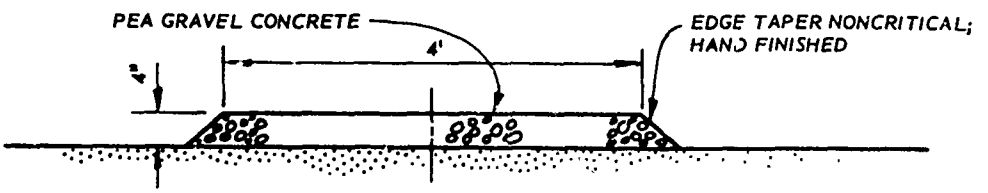

SECTION BB

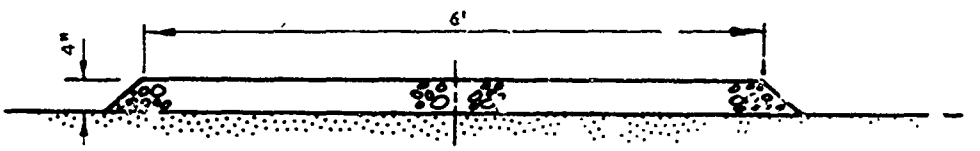

SECTION CC

Figure A.5. Airblast pad construction details.

APPENDIX B

GROUND MOTION AND SURFACE AIRBLAST-TIME HISTORIES

B.1 DATA TREATMENT

The original analog tapes were digitized and processed on the U. S. Army Engineer Waterways Experiment Station (WES) computer. Various subroutines were used as needed to make corrections for temperature effects on the velocity gage records (Reference 8),[1] filtering, and baseline shifting (References 10 and 11), especially where single and double integrations were performed. Table B.1 lists digital bandpass frequencies. Figure B.1 provides a graphical explanation of the various baseline correction techniques.

B.2 TIME HISTORY PRESENTATION

Time histories in Figures B.2 through B.23 are presented such that upward motion, outward motion (away from ground zero (GZ)), and compression are upward (positive) on the plots. Conversely, downward motion and inward motion are downward (negative) on the plots. Inset figures on the plots are uncorrected data shown in the "as recorded" condition.

Identification labeling on the plots is formatted as follows:

Location: Upper right-hand corner of plot
First Line: Experiment, event number
Second Line: Gage identifier, i.e., distance from GZ in feet, depth in feet, parameter, orientation, and analog tape number, track
Third Line: Digitizing rate, Hz
Fourth Line: Filter option
Fifth Line: Date, digital tape reel numbers

---

[1] Raised numbers refer to similarly numbered items in the list of References at the end of the main text.

EXAMPLE:

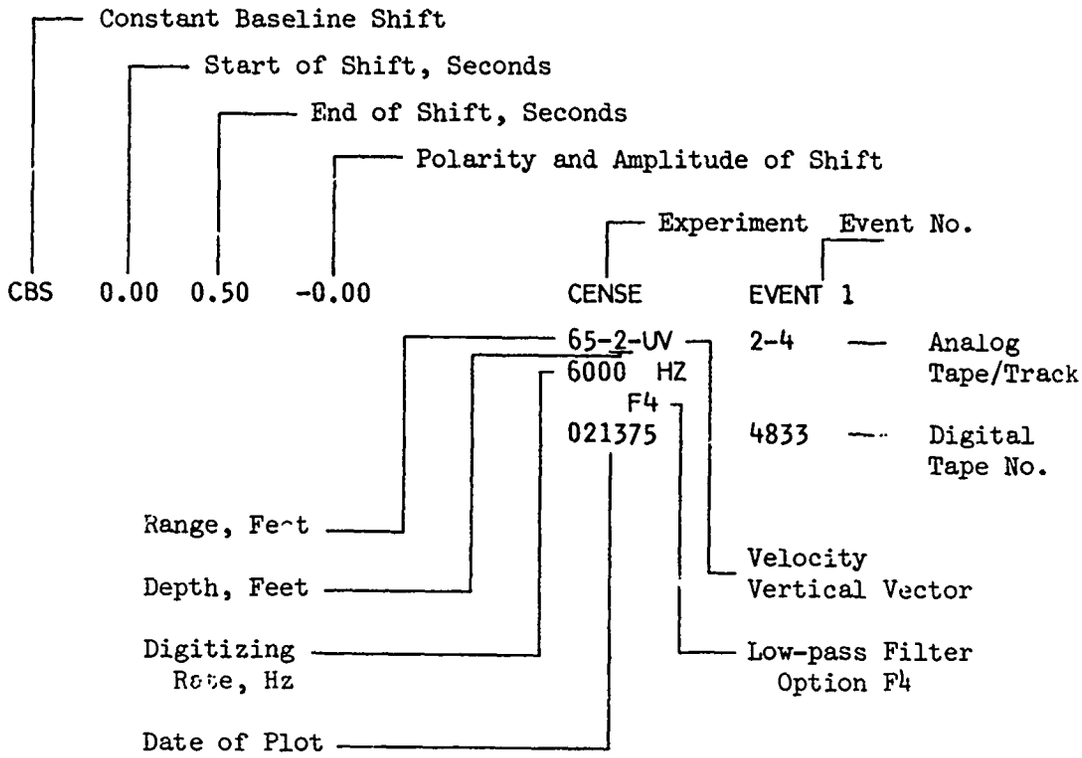
Constant Baseline Shift
Start of Shift, Seconds
End of Shift, Seconds
Polarity and Amplitude of Shift
Experiment
Event No.
CBS
0.00
0.50
-0.00
CENSE
EVENT 1
65-2-UV
6000 HZ
F4
021375
2-4
Analog Tape/Track
4833
Digital Tape No.
Range, Feet
Depth, Feet
Digitizing Rate, Hz
Date of Plot
Velocity Vertical Vector
Low-pass Filter Option F4

Table B.1. DIGITAL FILTER BANDPASS FREQUENCIES.[a]

Filter Option	Digital Filter Bandpass Frequencies, Hz, at Indicated Digital Sample Rates															
	1000		2000		4000		6000		12,000		24,000		48,000		96,000	
	All Pass	No Pass	All Pass	No Pass	All Pass	No Pass	All Pass	No Pass	All Pass	No Pass	All Pass	No Pass	All Pass	No Pass	All Pass	No Pass
F1	115	243	230	486	460	972	690	1460	1380	2920	2760	5840	5520	11,700	11,040	23,400
F2	50	120	100	240	200	480	300	720	600	1440	1200	2880	2400	5,760	4,800	11,520
F3	40	80	80	160	160	320	240	480	480	960	960	1920	1920	3,840	3,840	7,680
F4	32	60	63	120	125	240	190	360	380	720	760	1440	1520	2,880	3,040	5,760

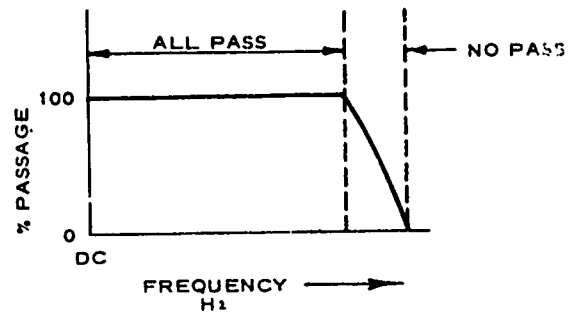

[a]References 10 and 11.

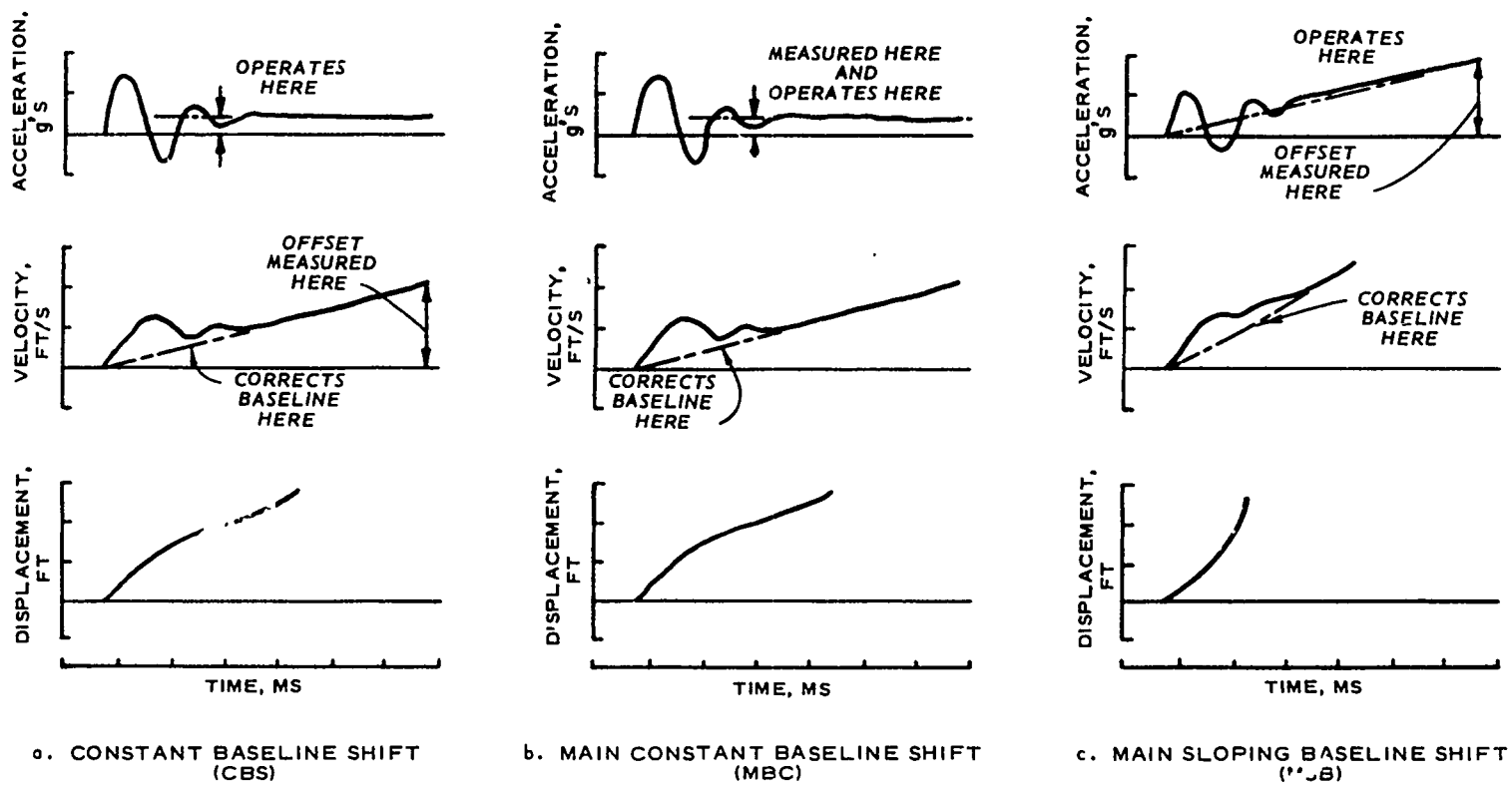

Figure B.1. Baseline correction techniques (shifts are exaggerated for illustration purposes).

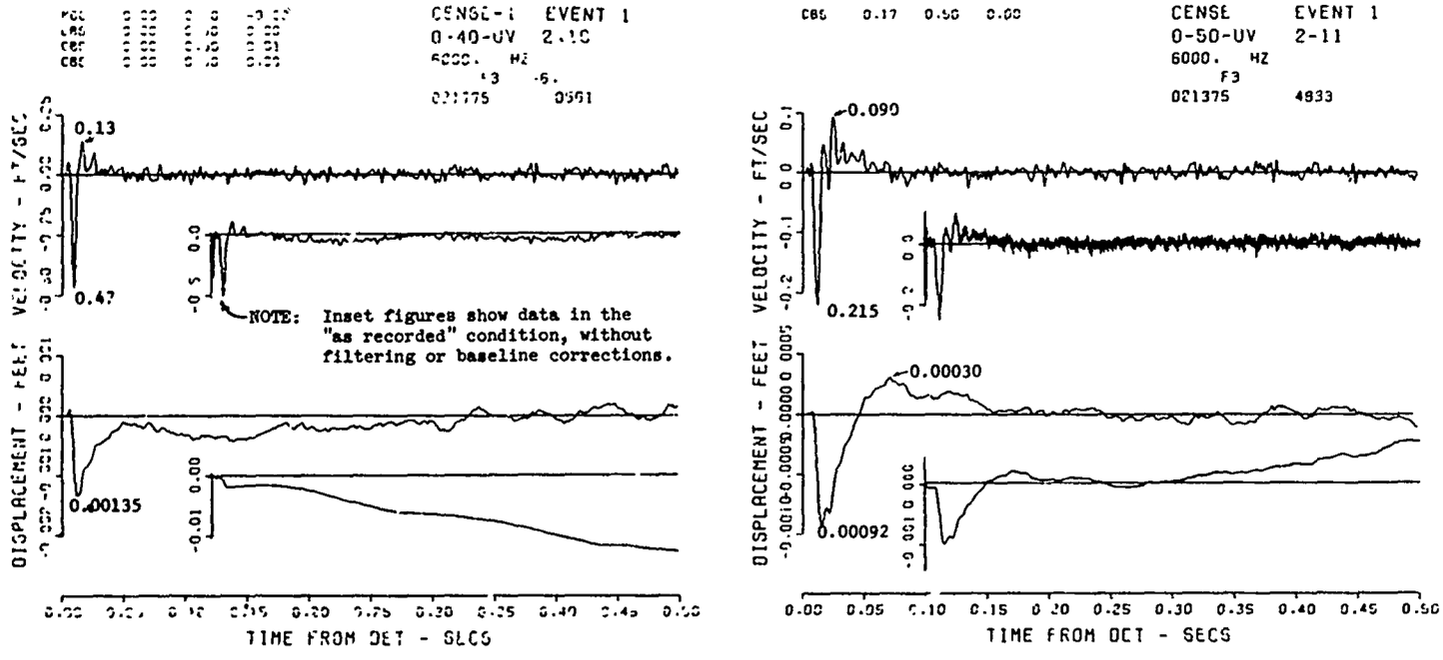

Figure B.2. Event 1, airburst, elevated $-0.57\ W^{1/3}$ (6-feet) ; motion-time histories along the vertical radial directly beneath the explosion. The signal-to-noise ratio of the records for Events 1 and 8 was degraded since gages were ranged for expected stronger motions (sheet 1 of 2).

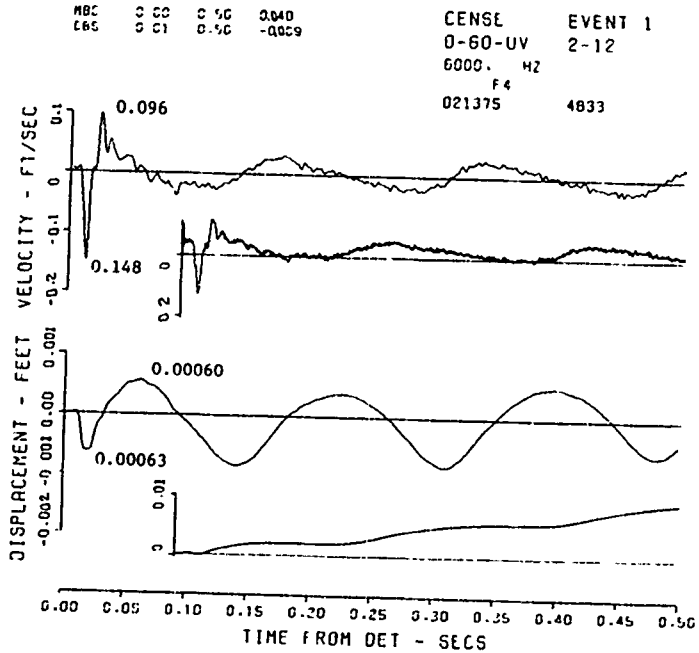

Figure B.2 (sheet 2 of 2).

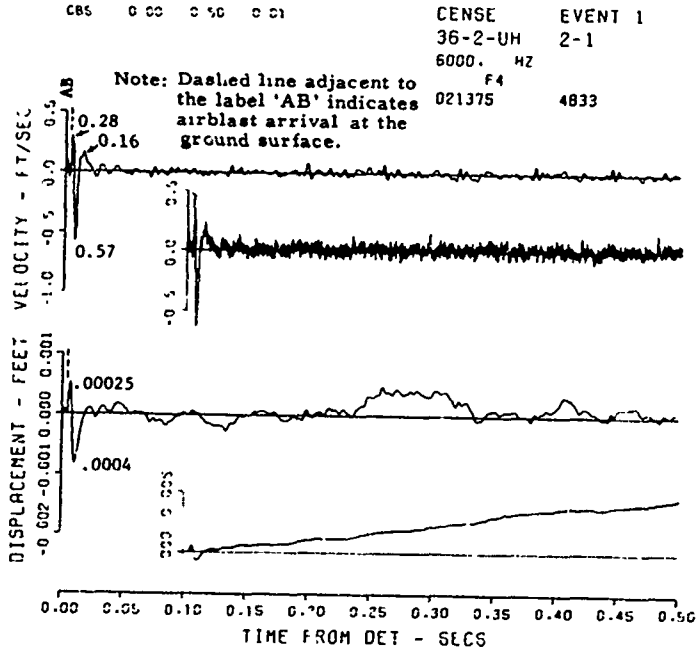

CENSE EVENT 1
36-2-UV 2-1

NO DATA RECOVERED

Figure B.3. Event 1, airblast, elevated $-0.57\ W^{1/3}$ (-6 feet) ; near-surface motion-time histories. No surface airblast-time histories were recovered for Event 1 (sheet 1 of 5).

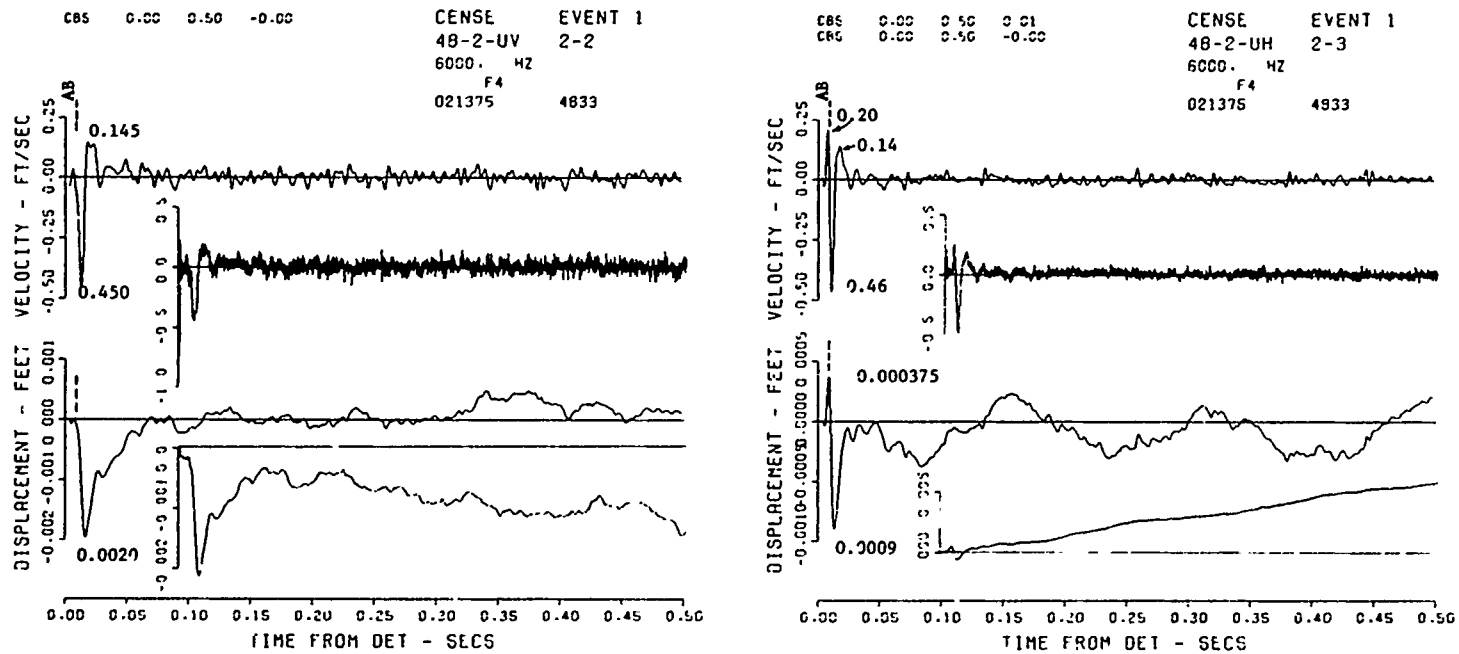

Figure B.3 (sheet 2 of 5).

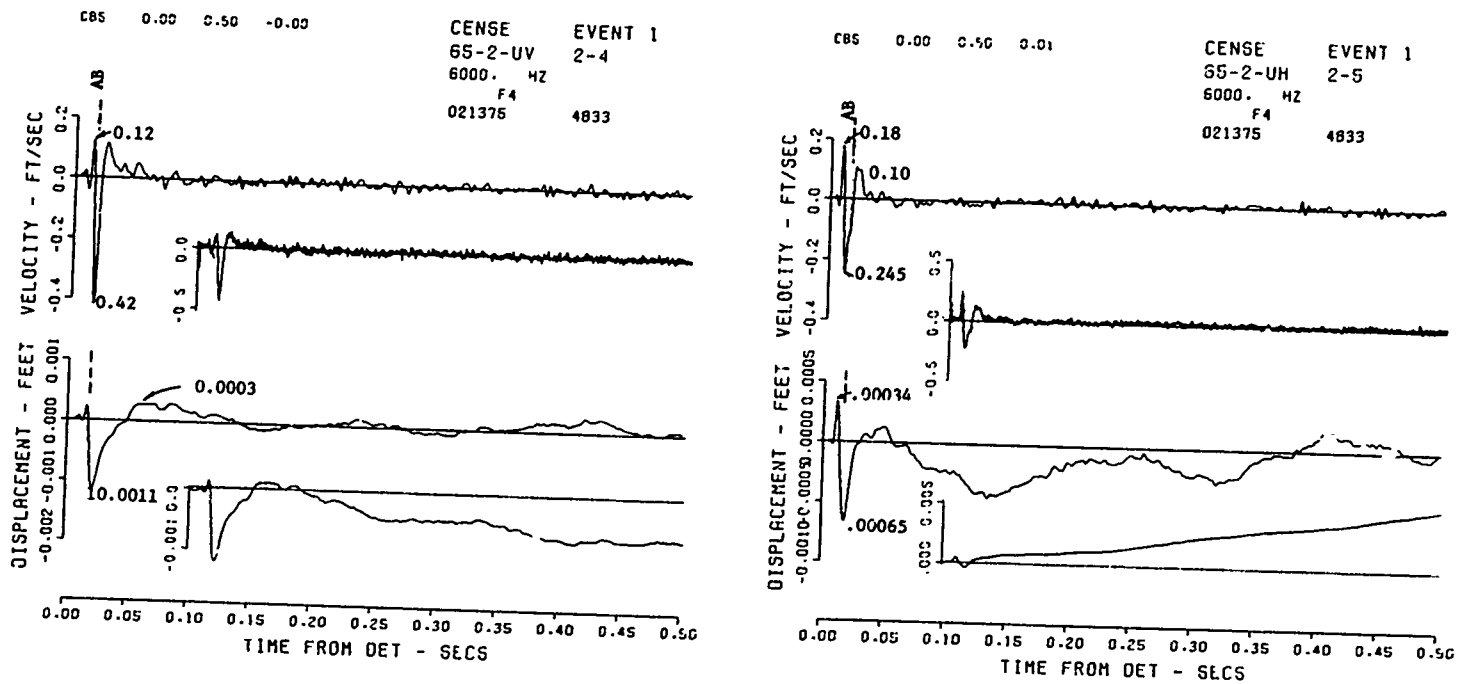

Figure B.3 (sheet 3 of 5).

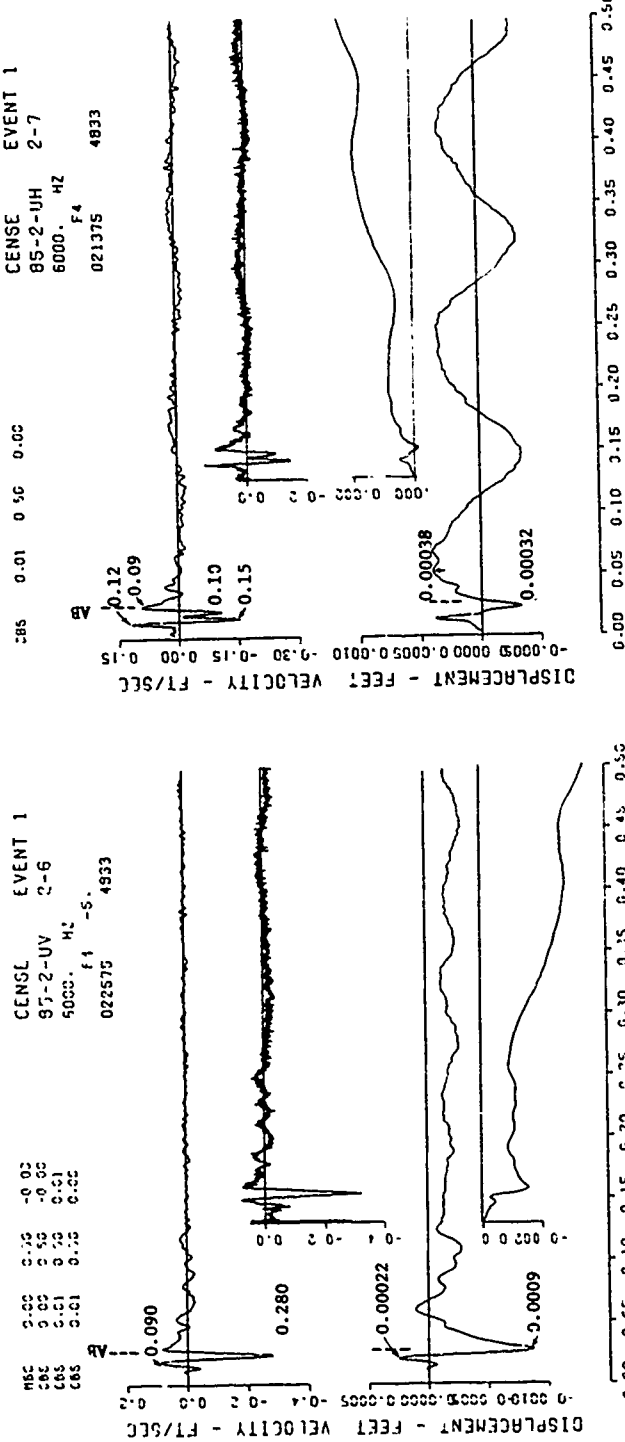

Figure B.3 (sheet 4 of 5).

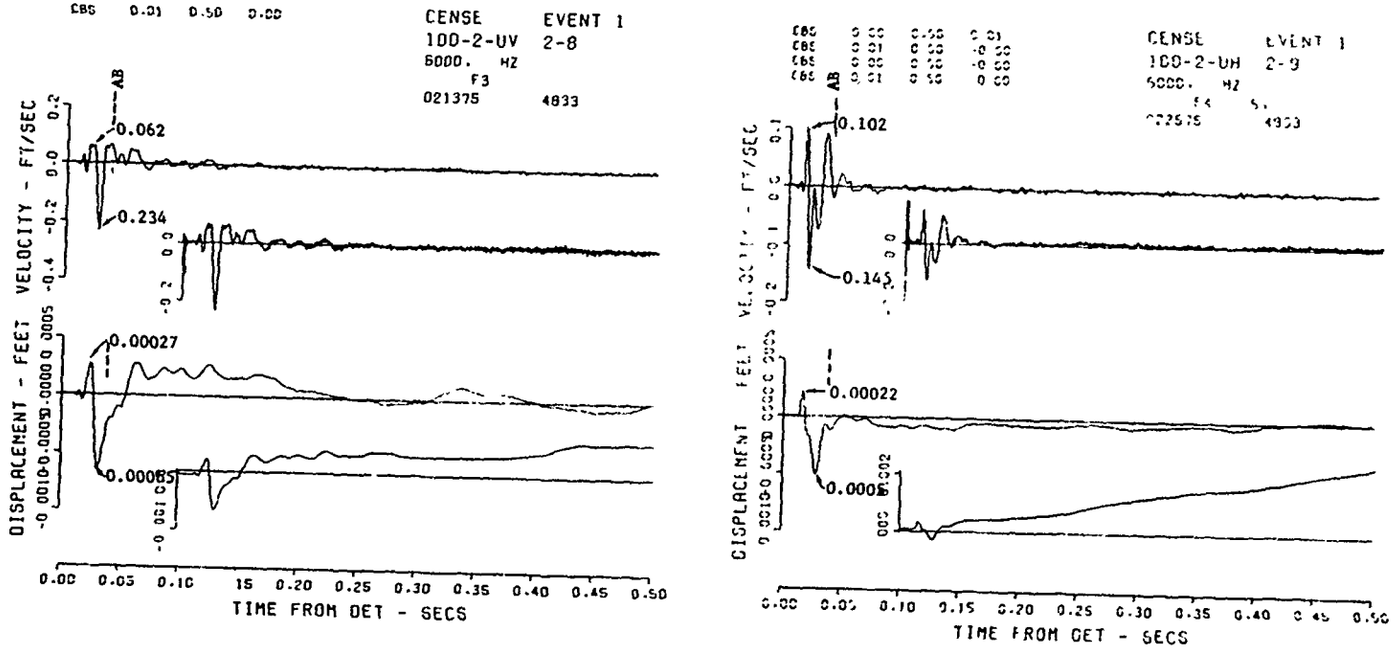

Figure B.3 (sheet 5 of 5).

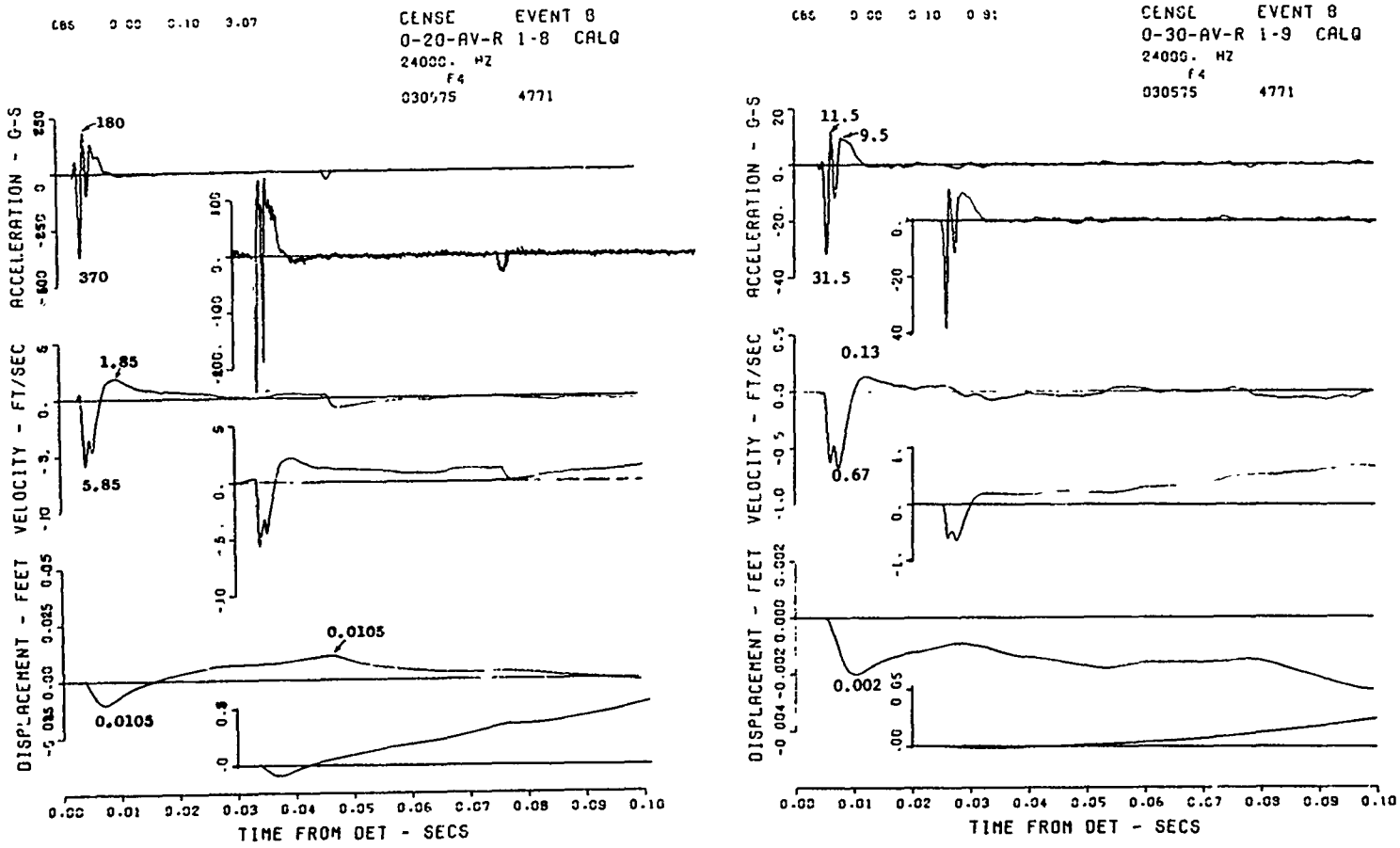

Figure B.4. Event 8, airburst, elevated $-0.57\ W^{1/3}$ (-6 feet) ; motion-time histories along the vertical radial directly beneath the explosion (sheet 1 of 3).

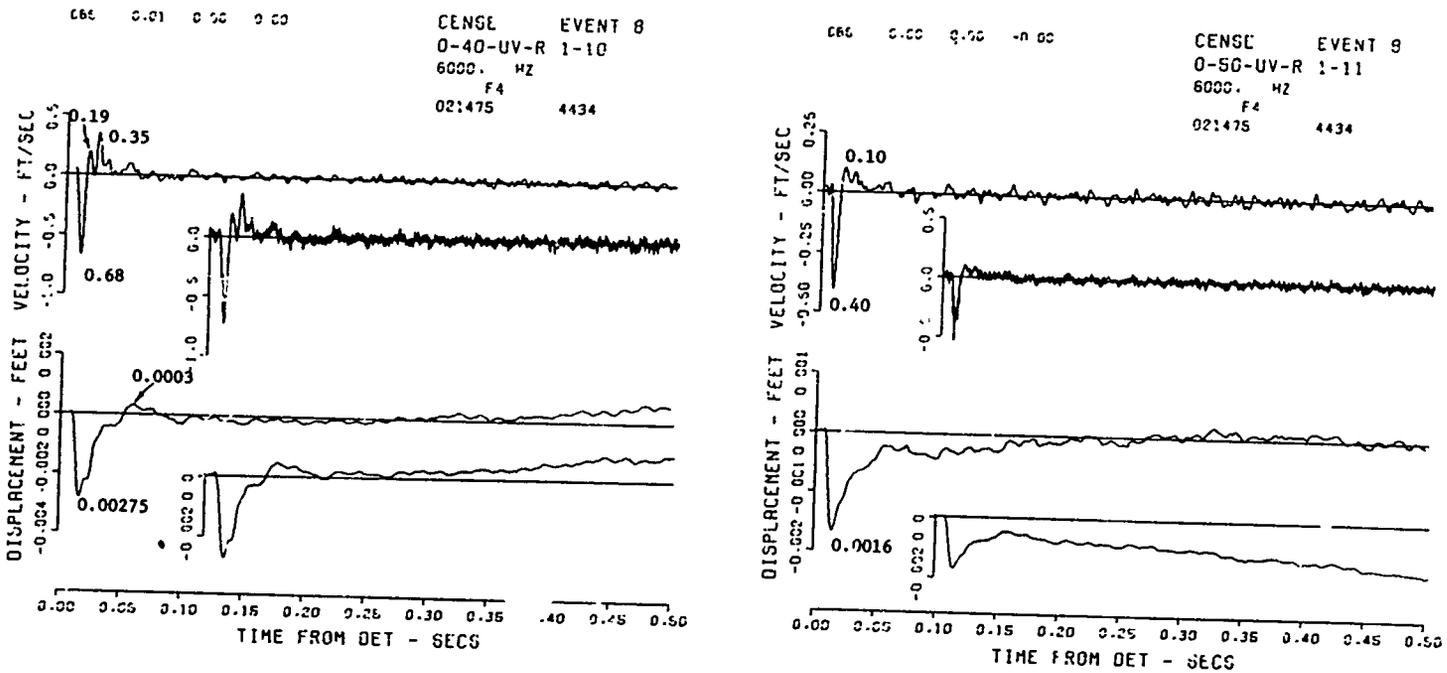

Figure B.4 (sheet 2 of 3).

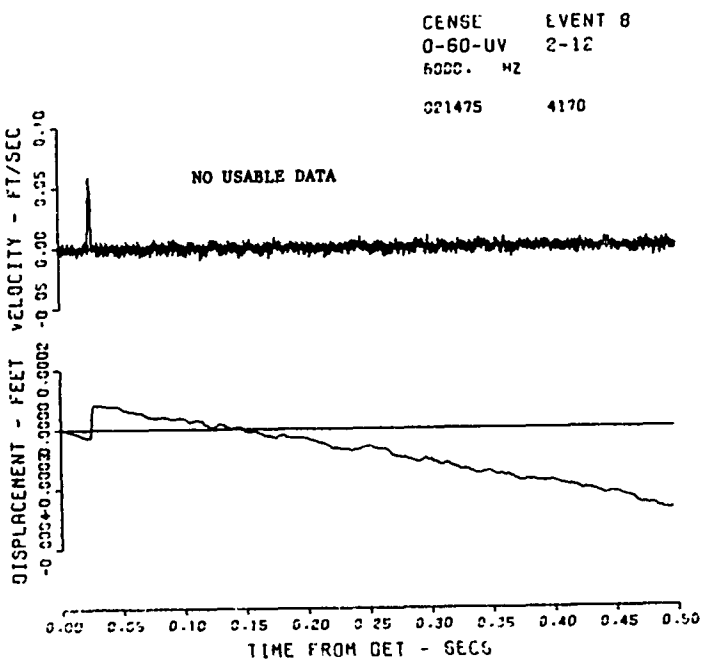

Figure B.4 (sheet 3 of 3).

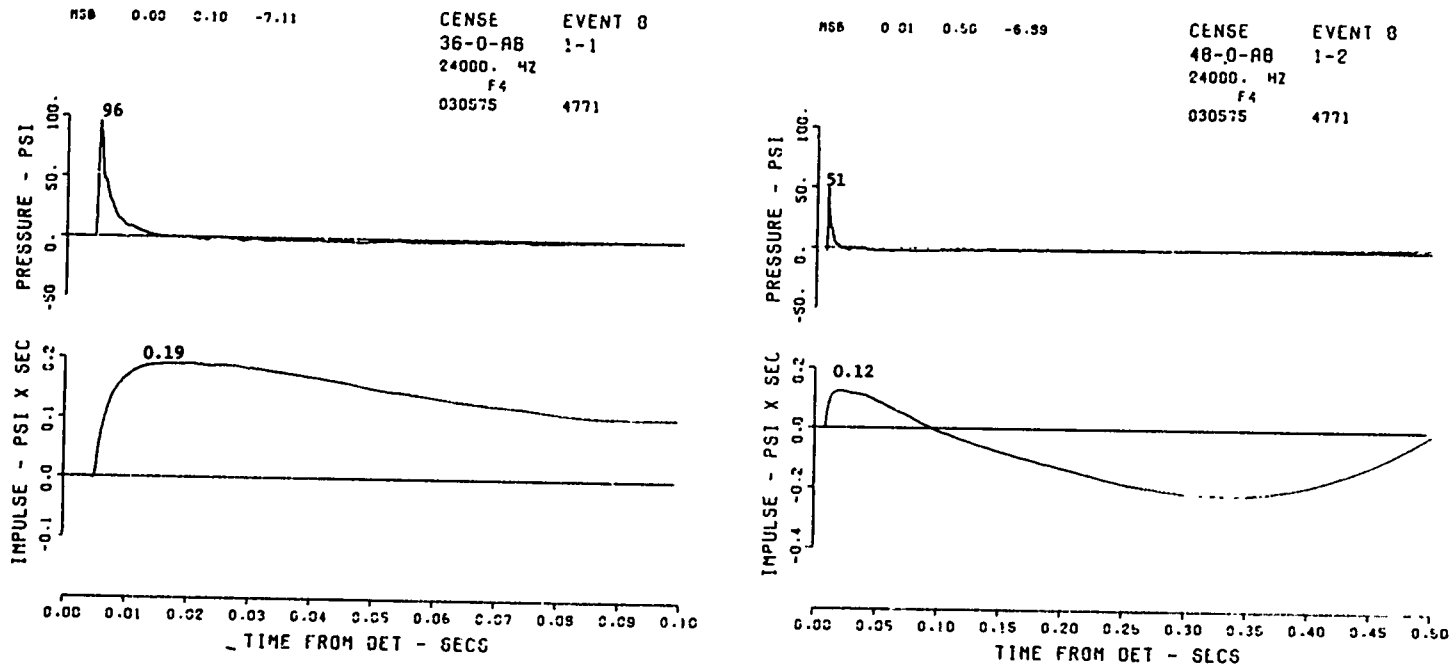

Figure B.5. Event 8, airburst, elevated $-0.57\ W^{1/3}$ (-6 feet) ; surface airblast-time histories (sheet 1 of 3).

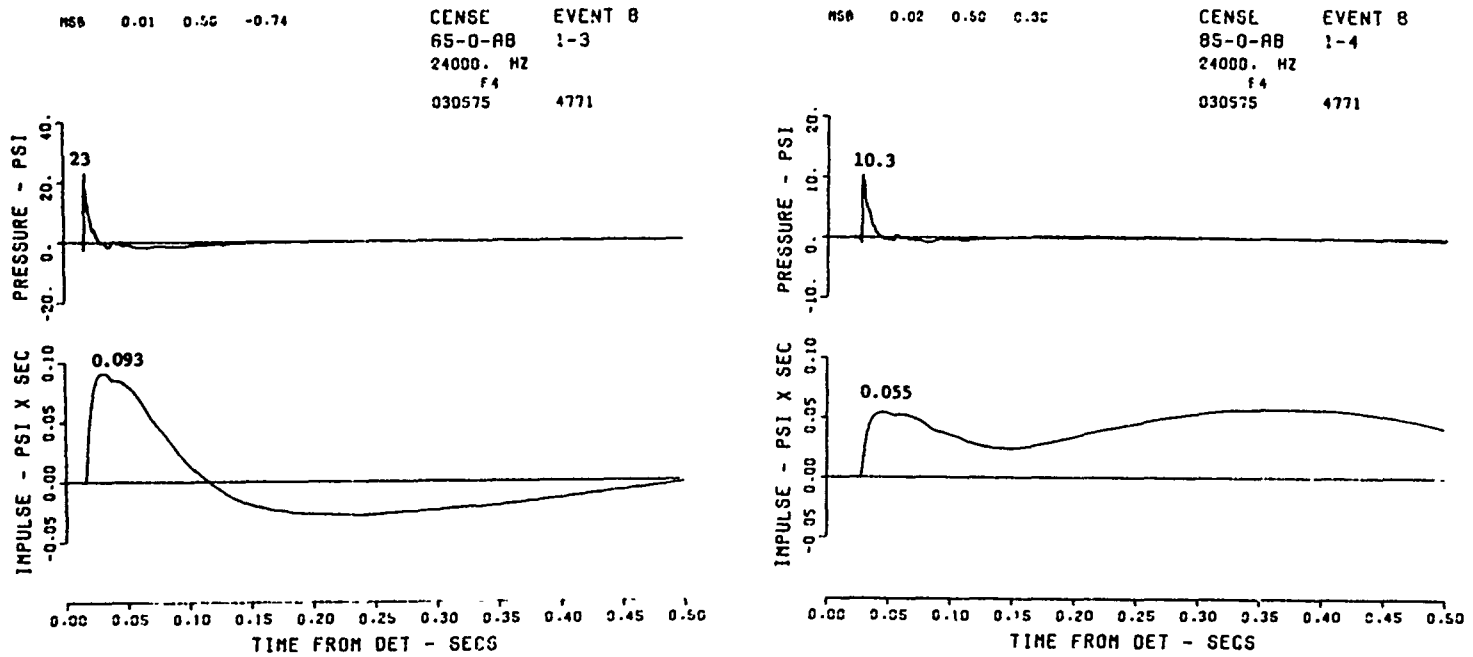

Figure B.5 (sheet 2 of 3).

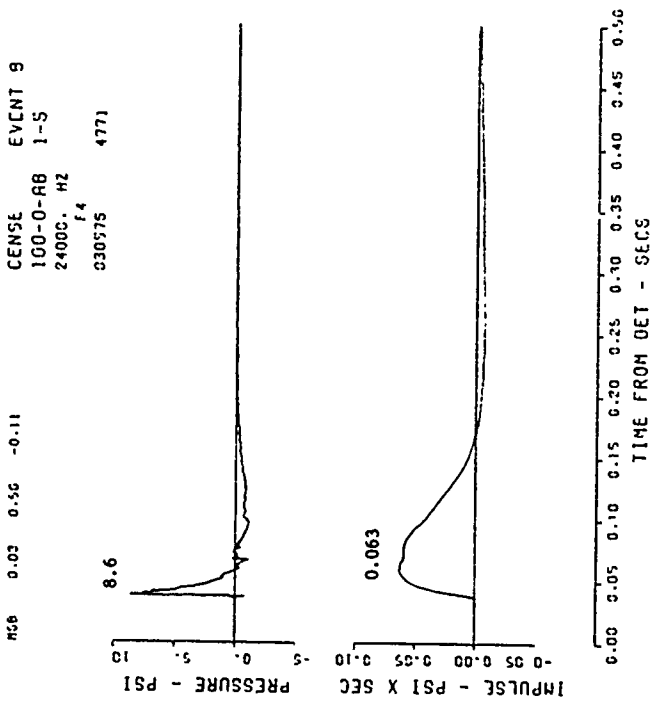

Figure B.5 (sheet 3 of 3).

CENSE 36-2-UH EVENT 8

NO DATA RECOVERED

CENSE 36-2-UV EVENT 8

NO DATA RECOVERED

CENSE 48-2-UH EVENT 8

NO DATA RECOVERED

CENSE 48-2-UH EVENT 8

NO DATA RECOVERED

CENSE 65-2-UH EVENT 8

NO DATA RECOVERED

Figure B.6. Event 8, airburst, elevated $-0.57\ W^{1/3}$ (-6 feet) ; near-surface motion-time histories (sheet 1 of 3).

CENSE EVENT 8
65-2-UV

NO DATA RECOVERED

CENSE EVENT 8
85-2-UH

NO DATA RECOVERED

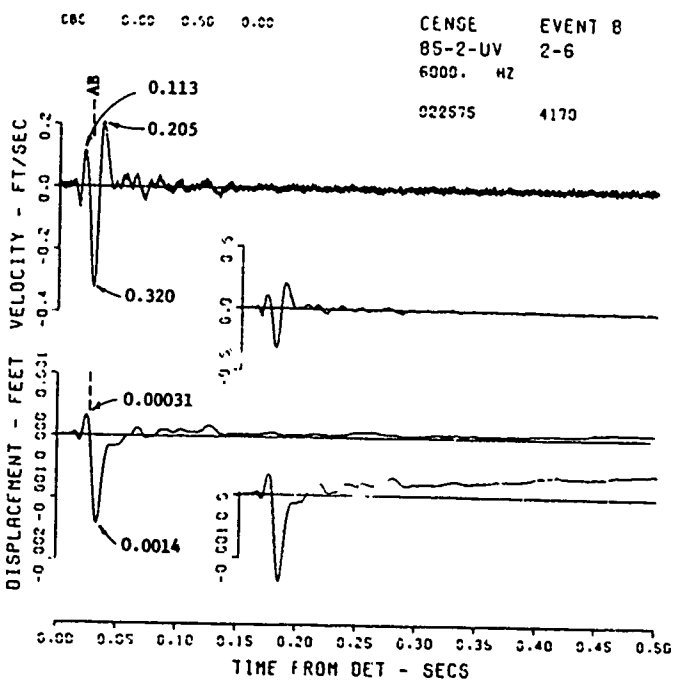

Figure B.6 (sheet 2 of 3).

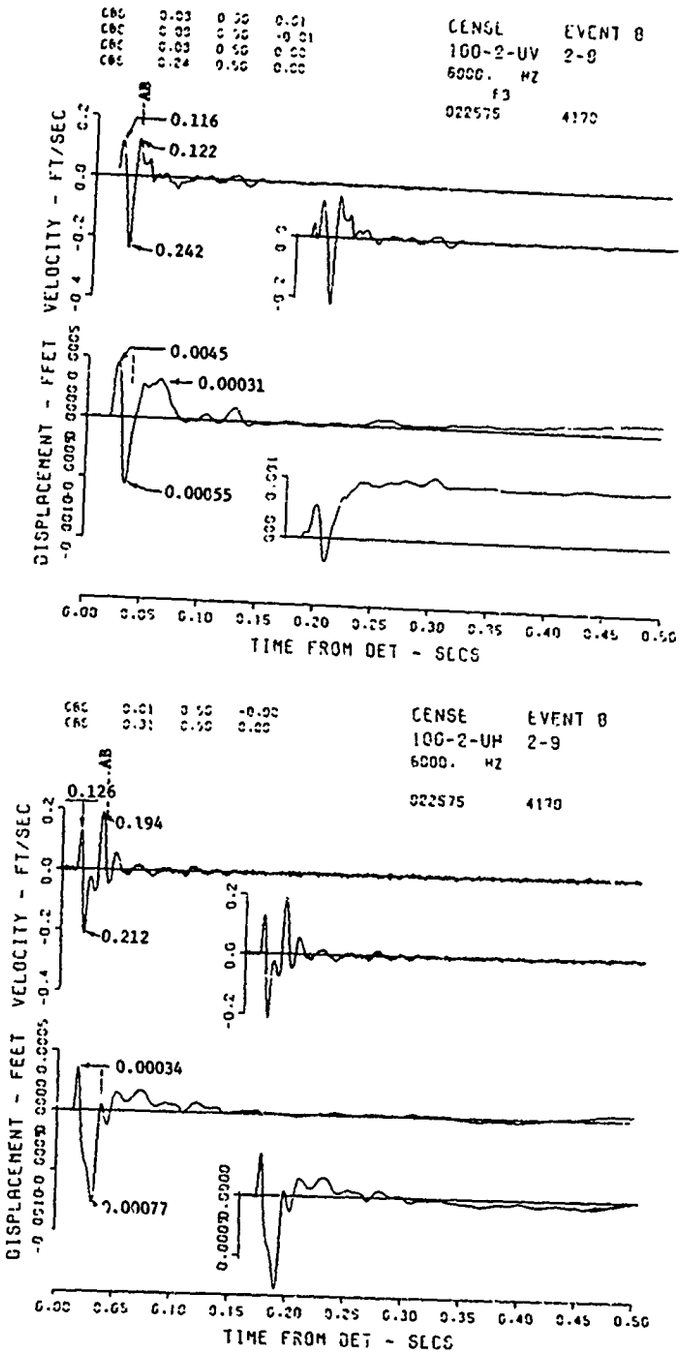

Figure B.6 (sheet 3 of 3).

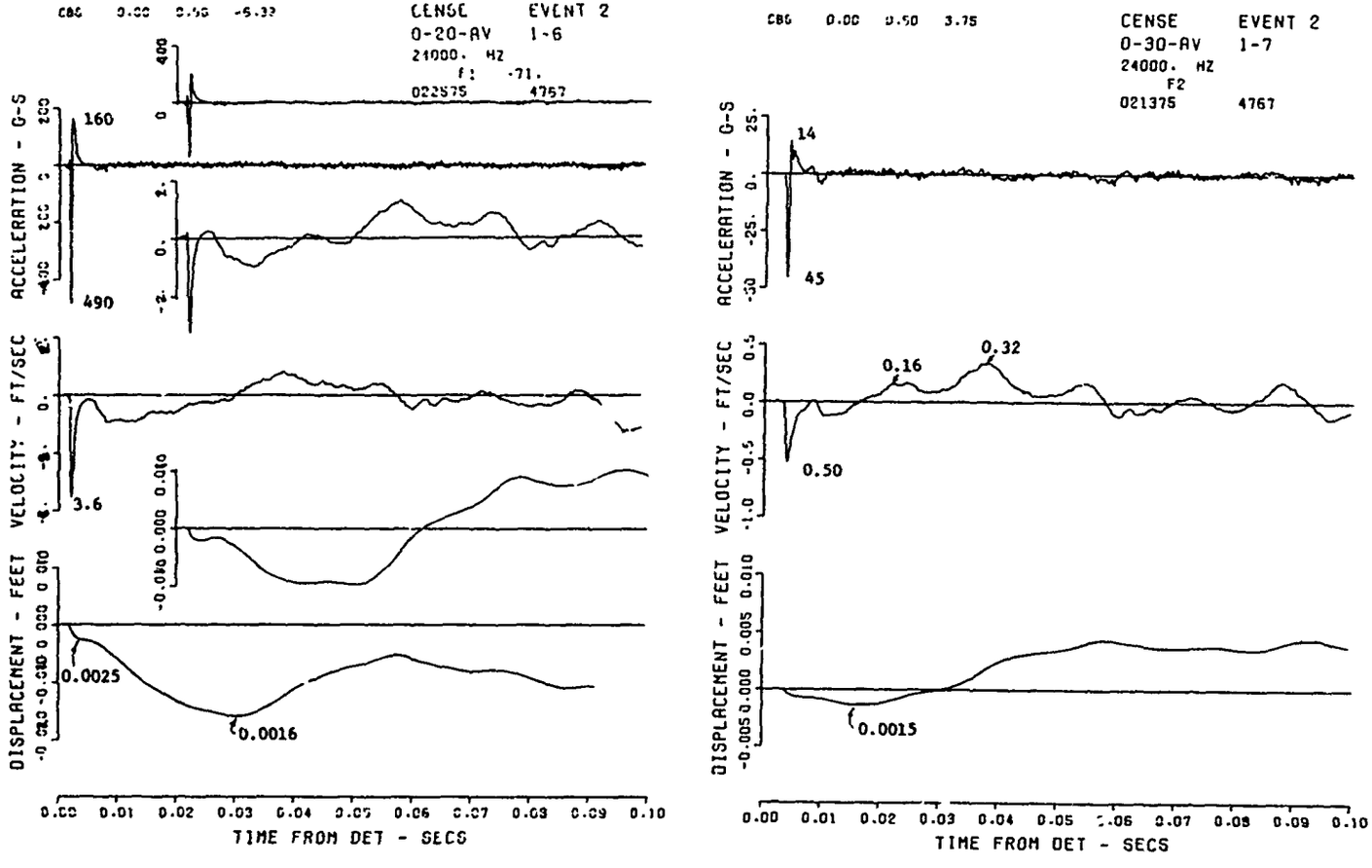

Figure B.7. Event 2, surface tangent, $-0.14\ W^{1/3}$ (-1.5 feet) ; motion-time histories along the vertical radial directly beneath the explosion (sheet 1 of 3).

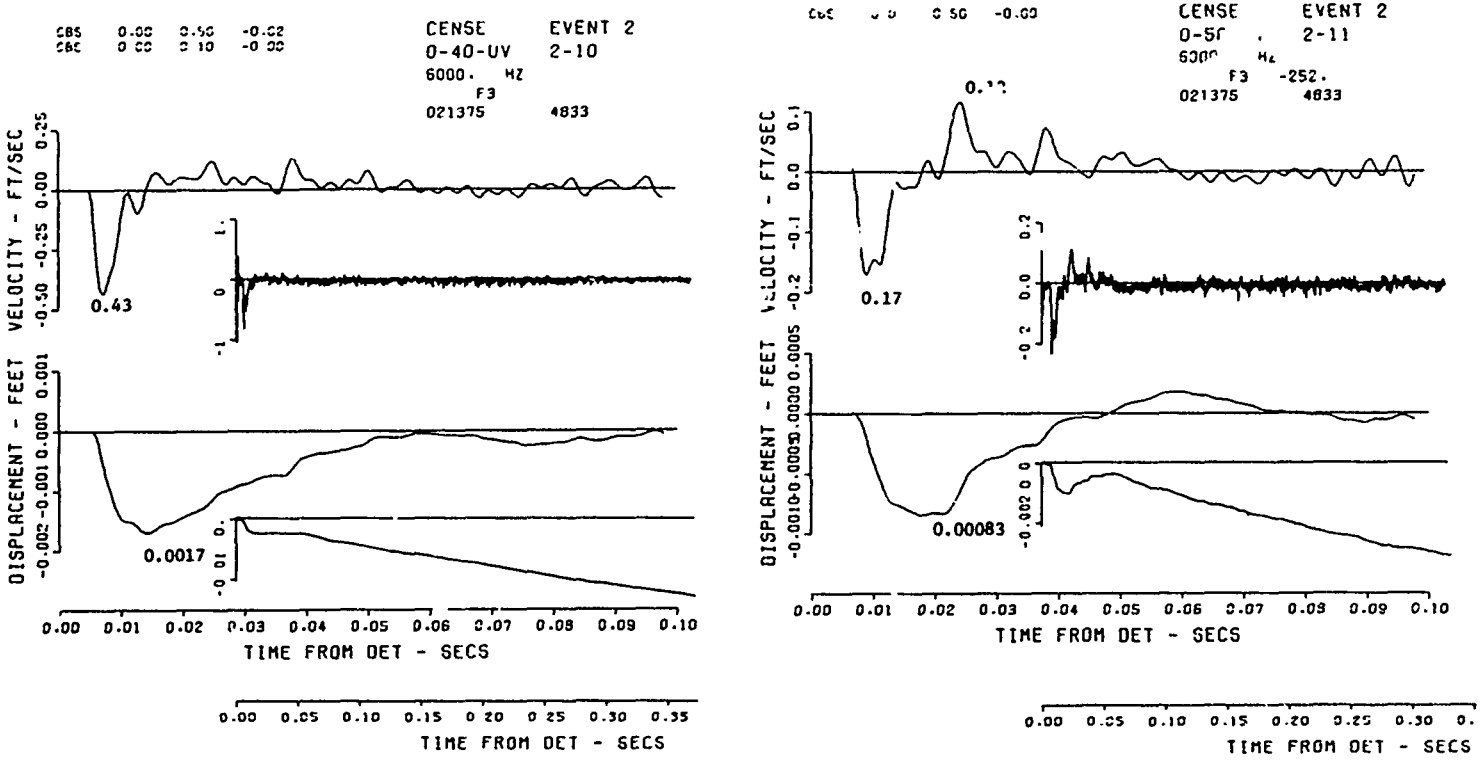

Figure B.7 (sheet 2 of 3).

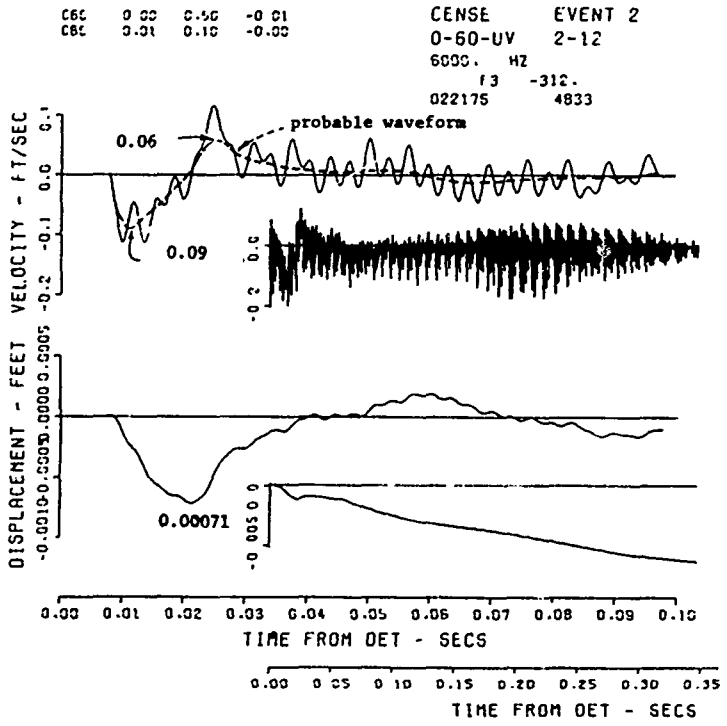

Figure B.7 (sheet 3 of 3).

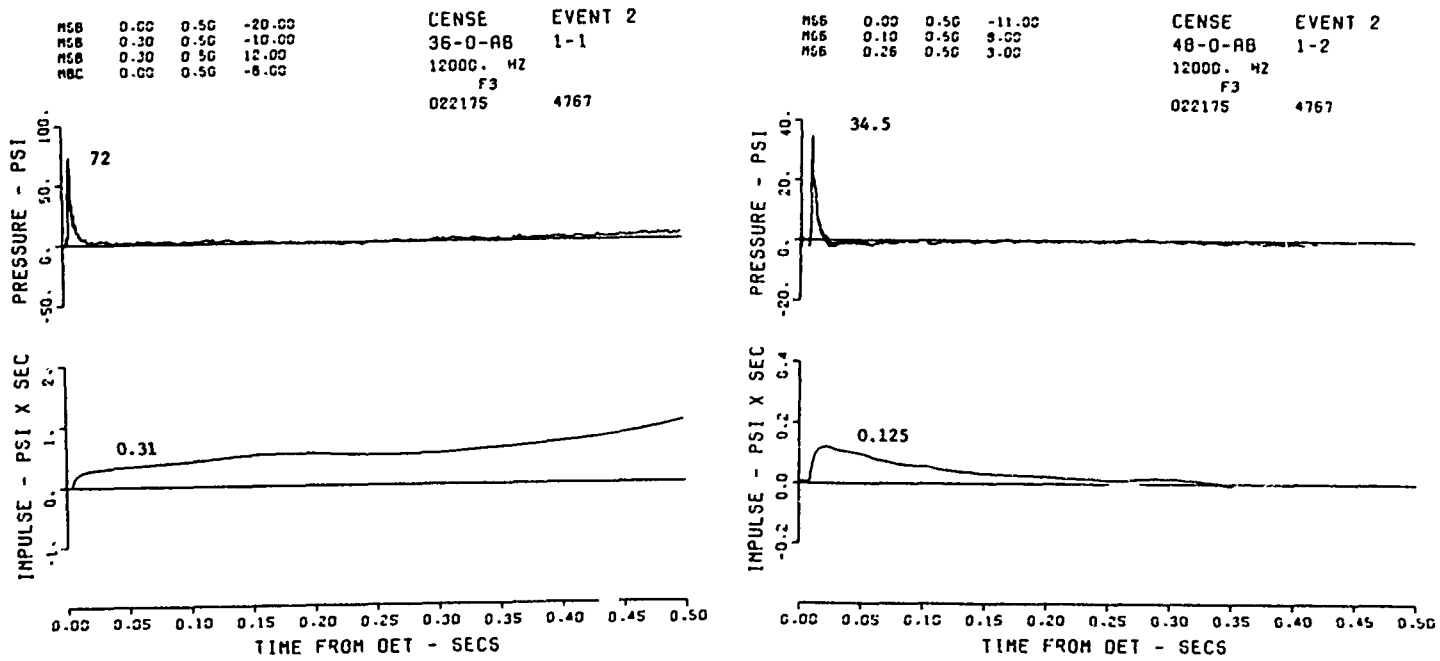

Figure B.8. Event 2, surface tangent, $-0.14\ W^{1/3}$ (-1.5 feet) ; surface airblast-time histories (sheet 1 of 3).

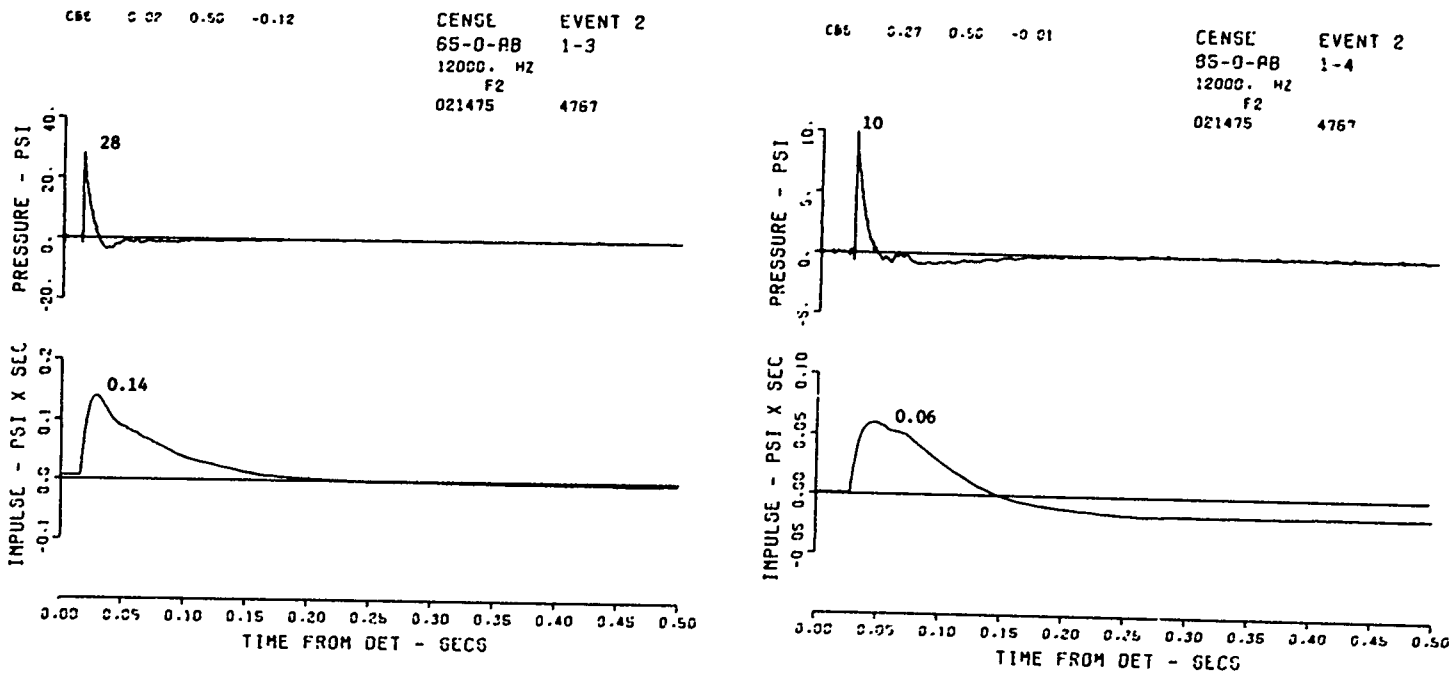

Figure B.8 (sheet 2 of 3).

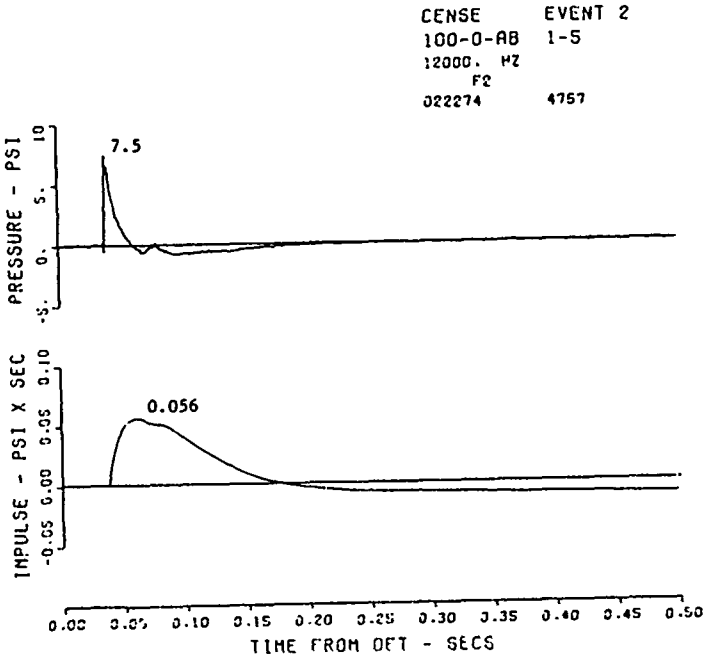

Figure B.8 (sheet 3 of 3).

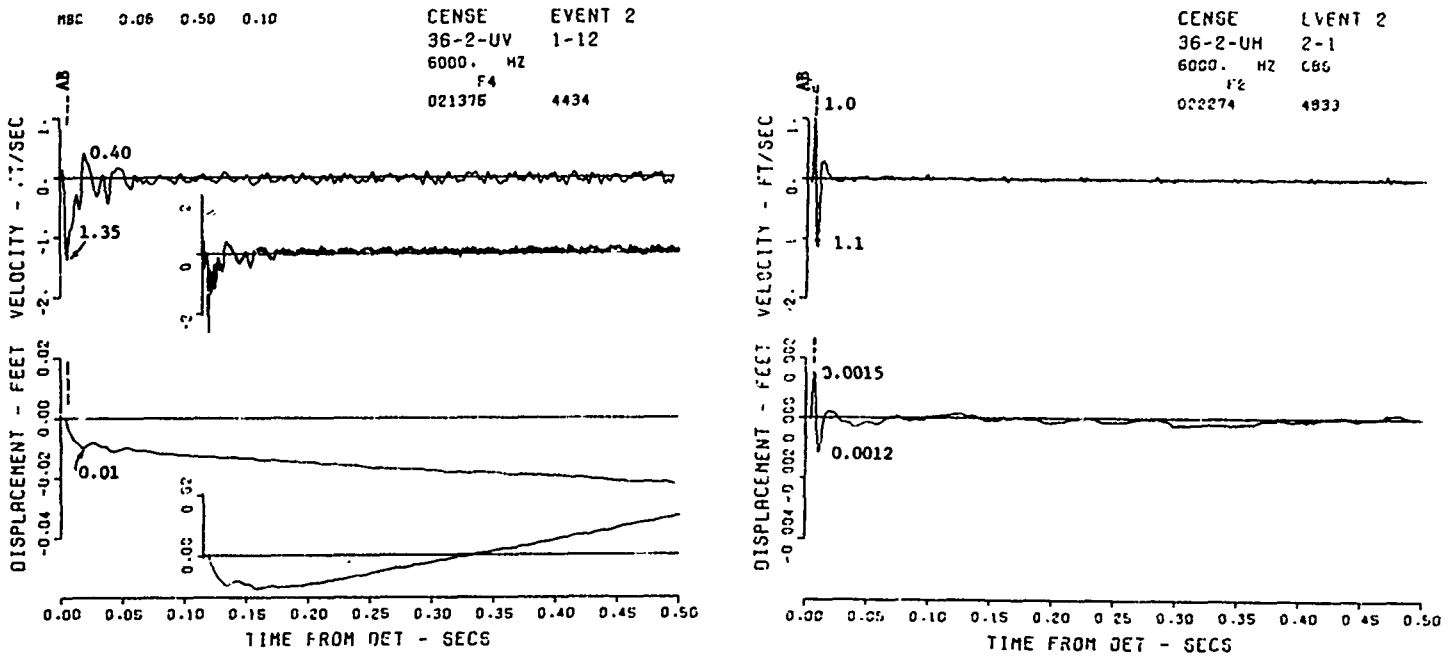

Figure B.9. Event 2, surface tangent, $-0.14\ W^{1/3}$ (-1.5 feet) ; near-surface motion-time histories (sheet 1 of 5).

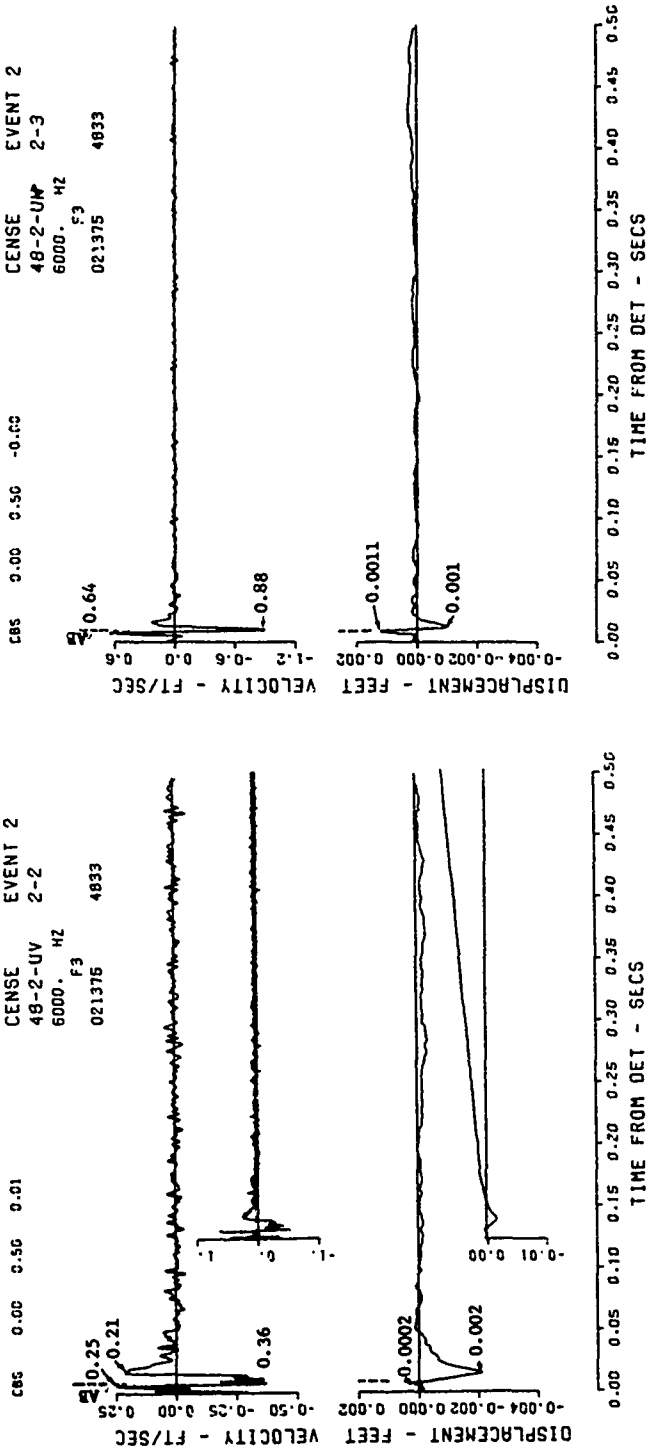

Figure B.9 (sheet 2 of 5).

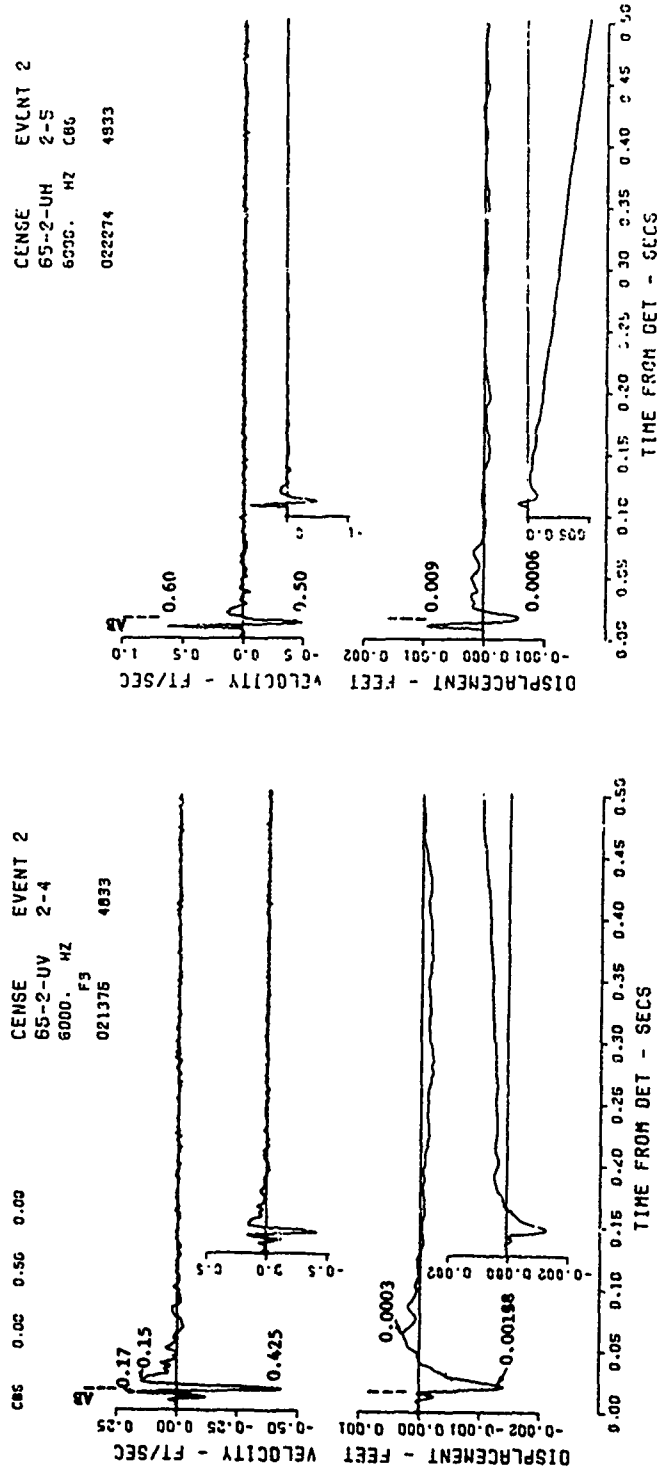

Figure B.9 (sheet 3 of 5).

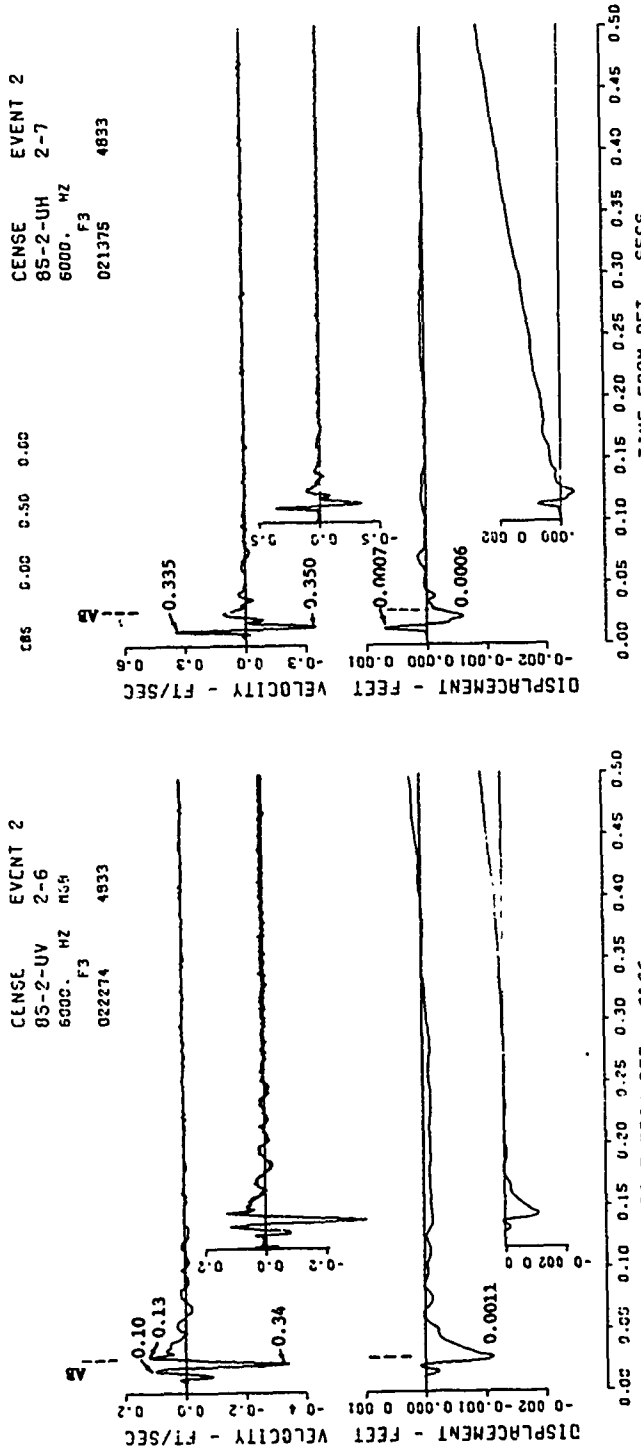

Figure B.9 (sheet 4 of 5).

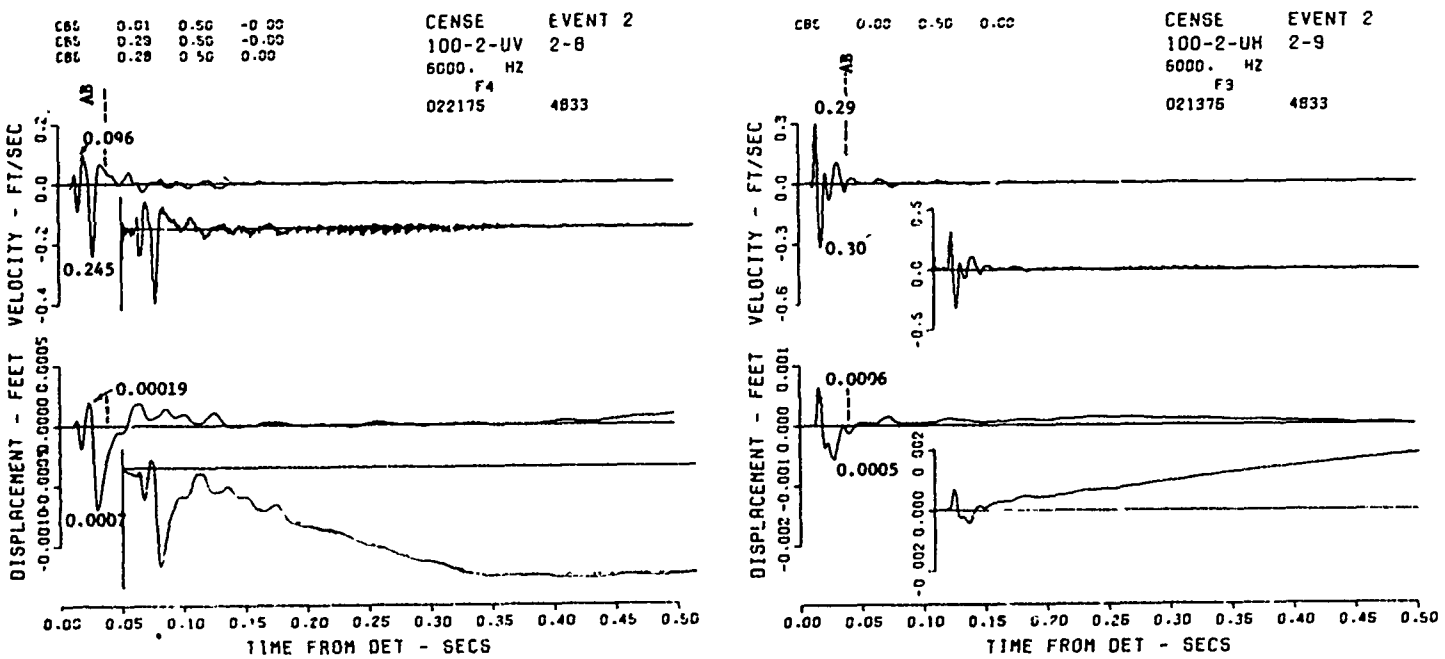

Figure B.9 (sheet 5 of 5).

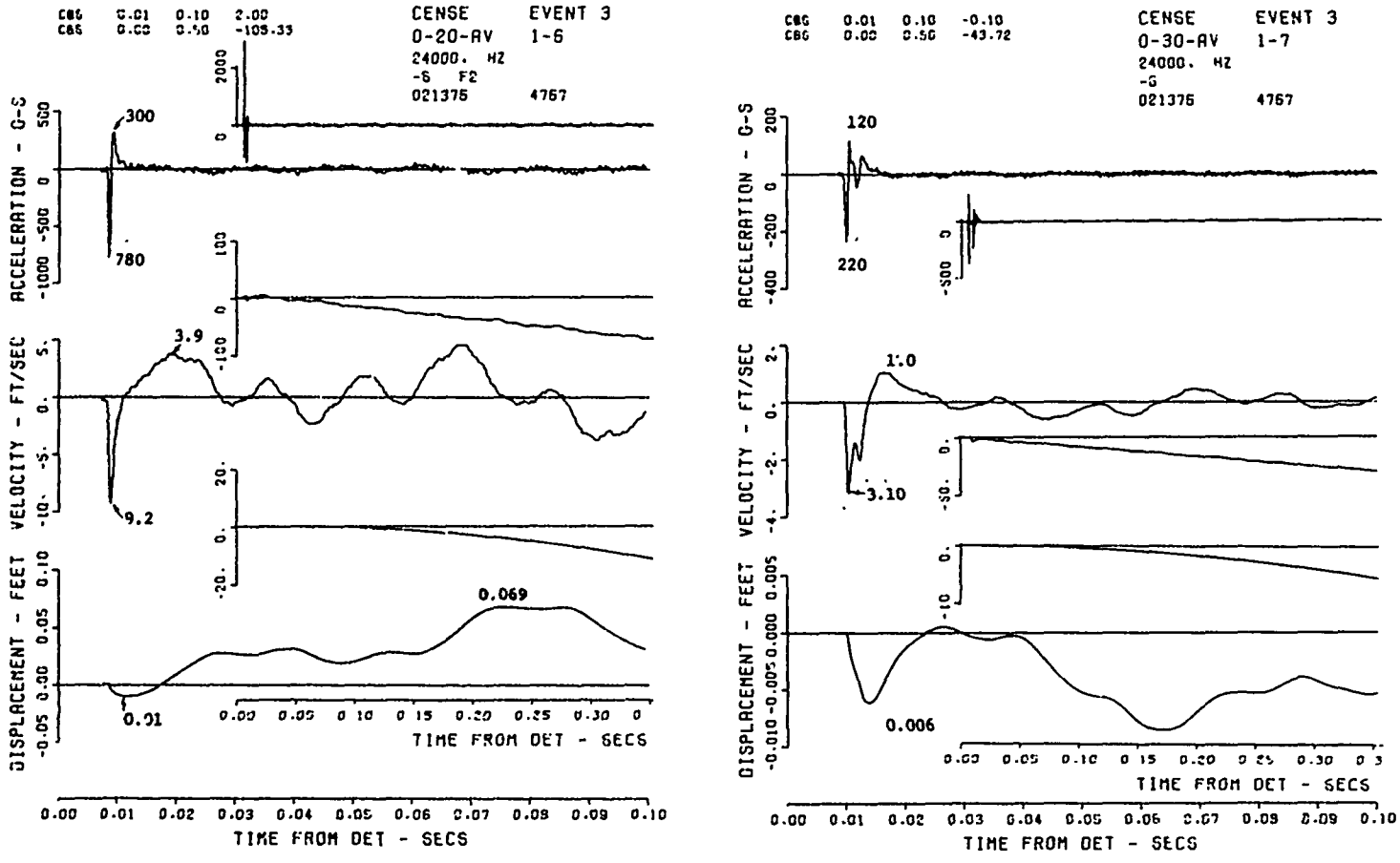

Figure B.10. Event 3, 1/4 buried, $-0.14\ W^{1/3}$ (-0.75 foot) ; motion-time histories along the vertical radial directly beneath the explosion (sheet 1 of 3).

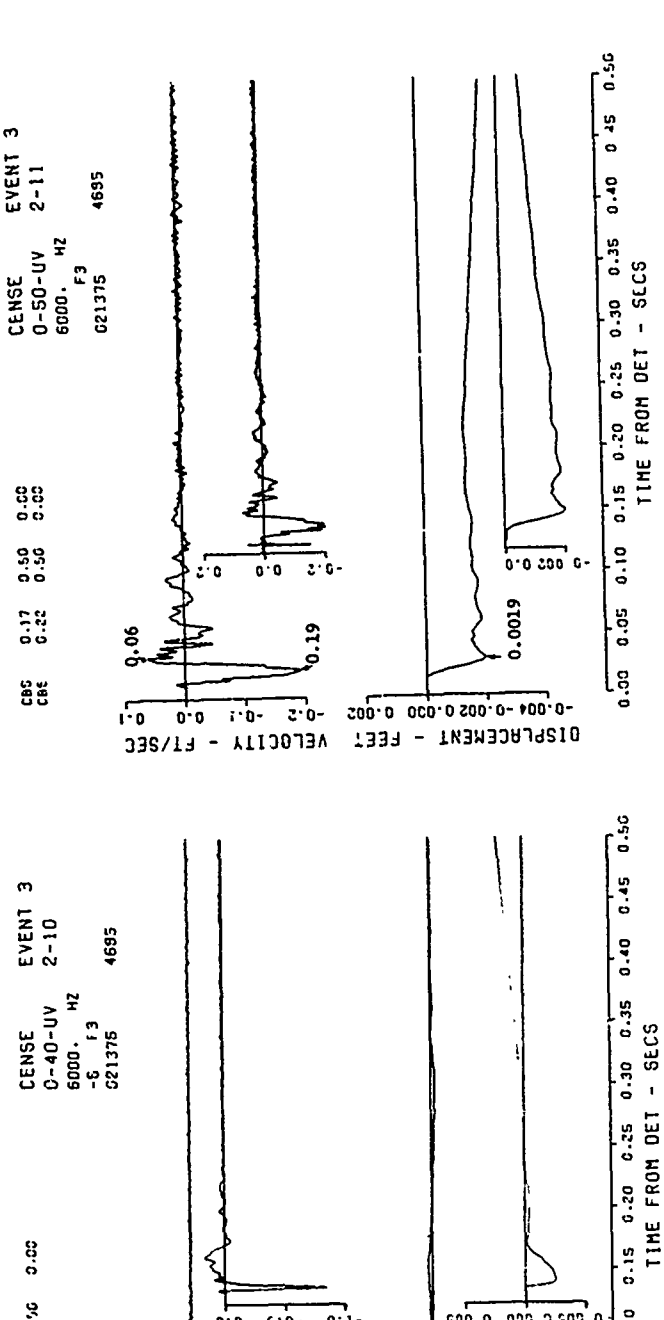

Figure B.10 (sheet 2 of 3).

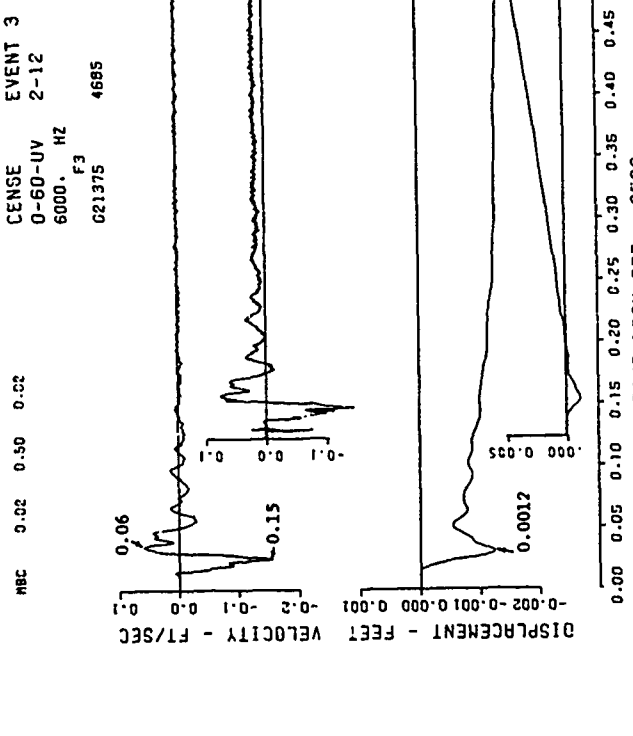

Figure B.10 (sheet 3 of 3).

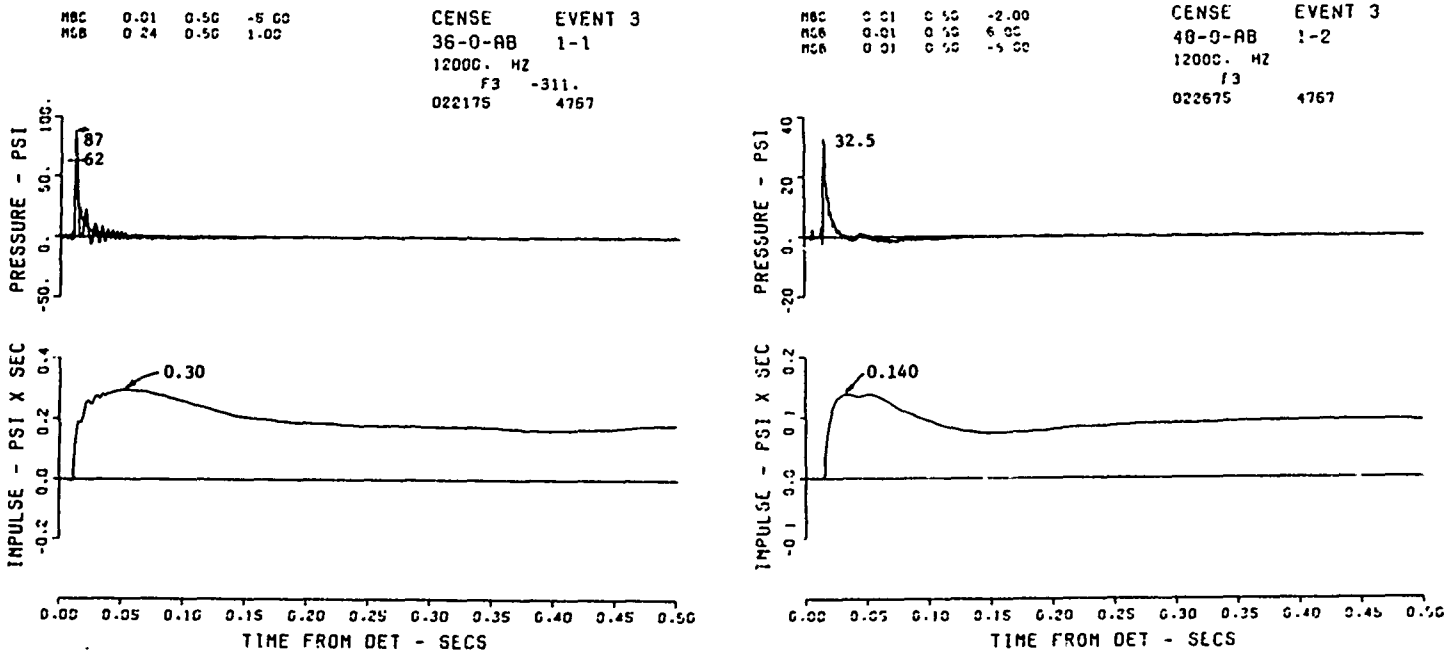

Figure B.11. Event 3, 1/4 buried, $-0.14\ W^{1/3}$ (-0.75 foot) ; surface airblast-time histories (sheet 1 of 3).

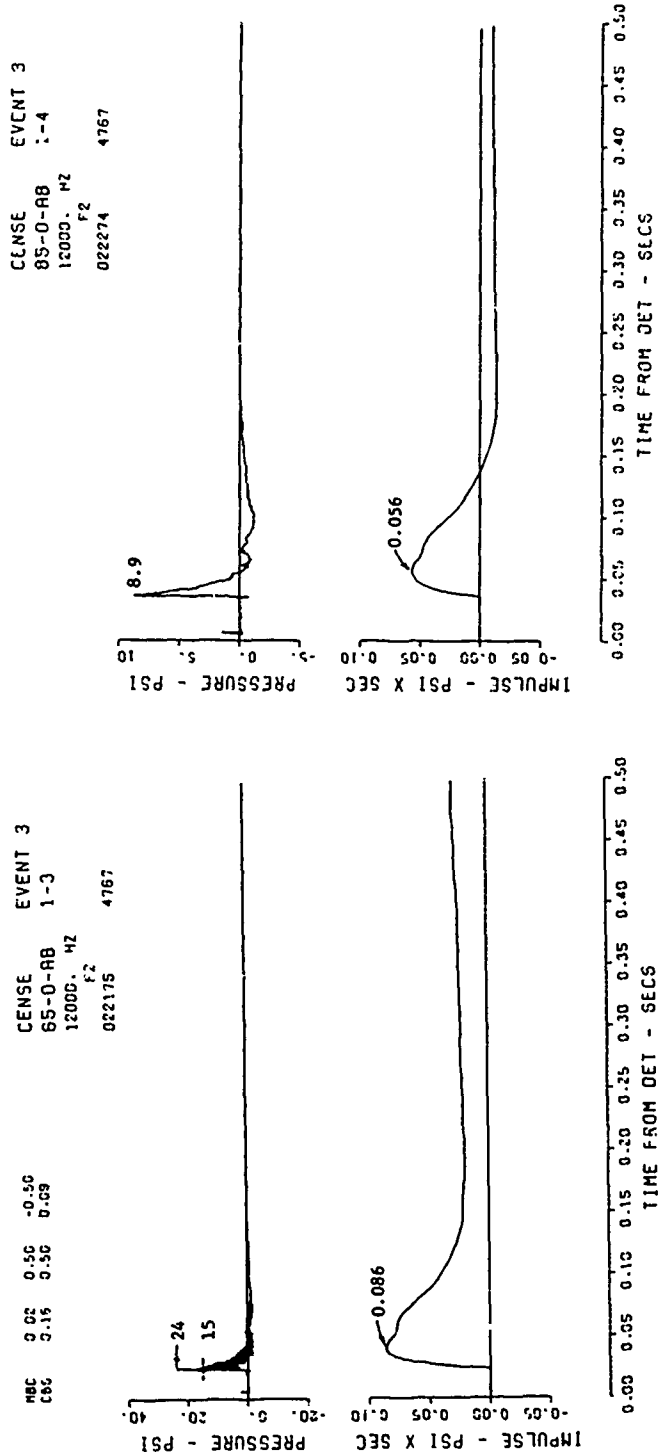

Figure B.11 (sheet 2 of 3).

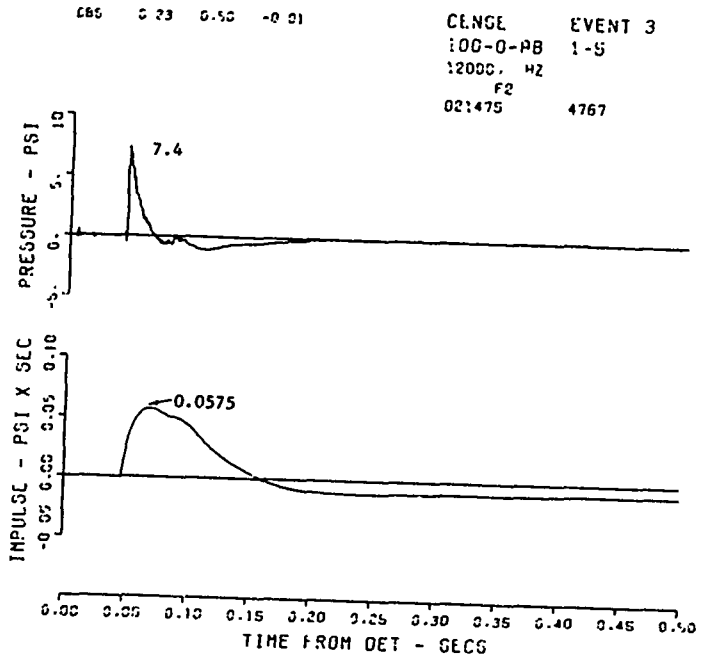

Figure B.11 (sheet 3 of 3).

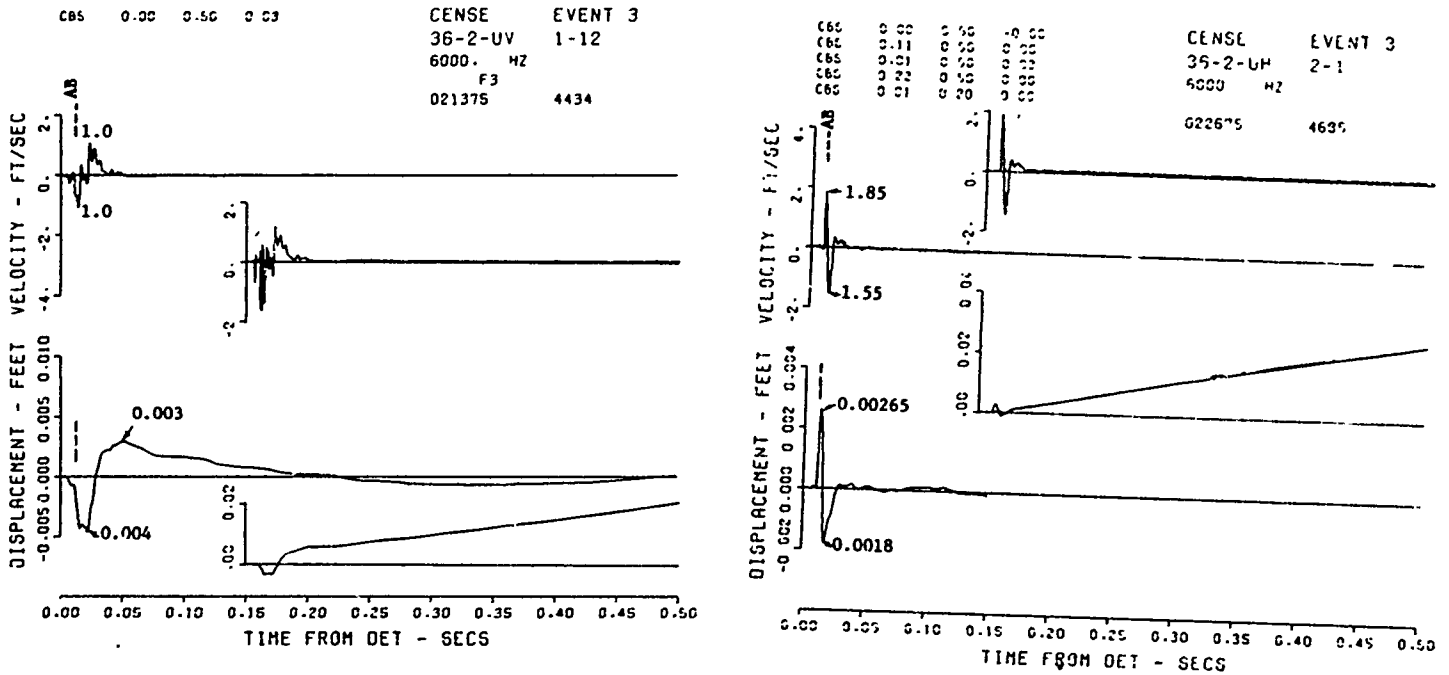

Figure B.12. Event 3, 1/4 buried, $-0.14\ W^{1/3}$ (-0.75 foot) ; near-surface motion-time histories (sheet 1 of 5).

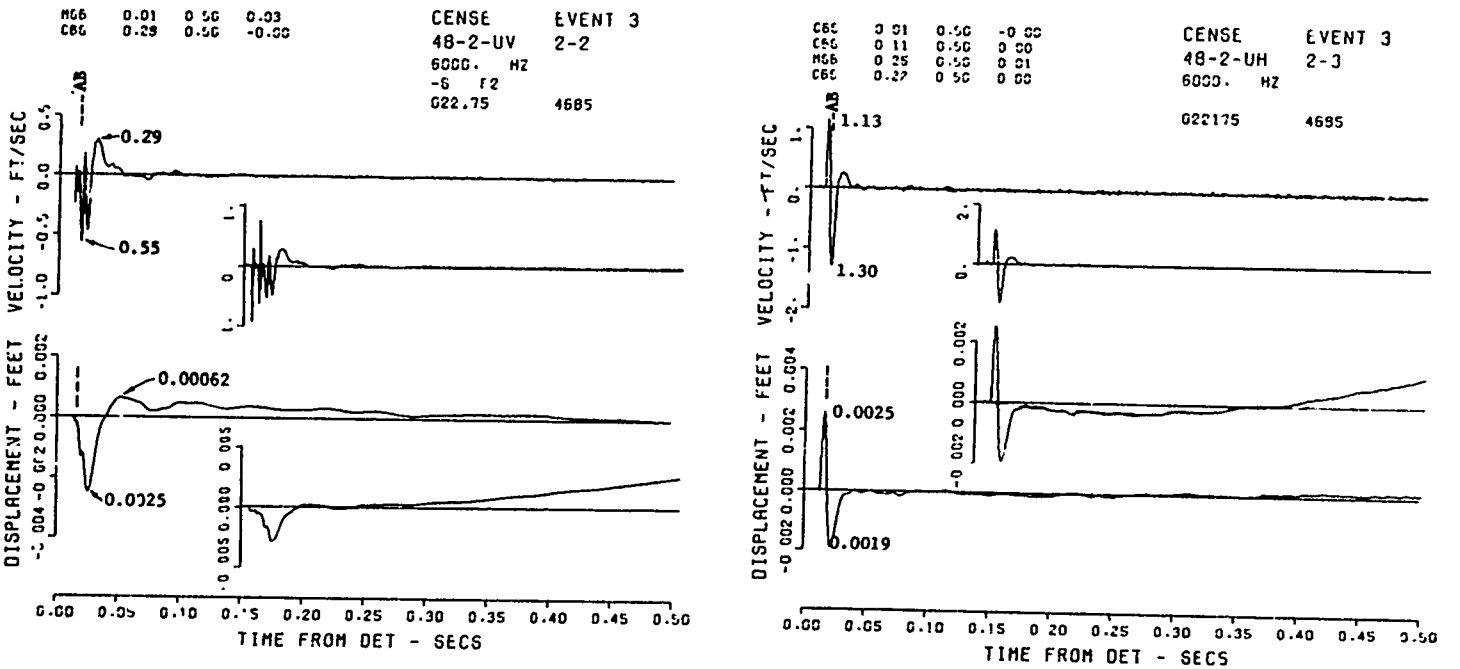

Figure B.12 (sheet 2 of 5).

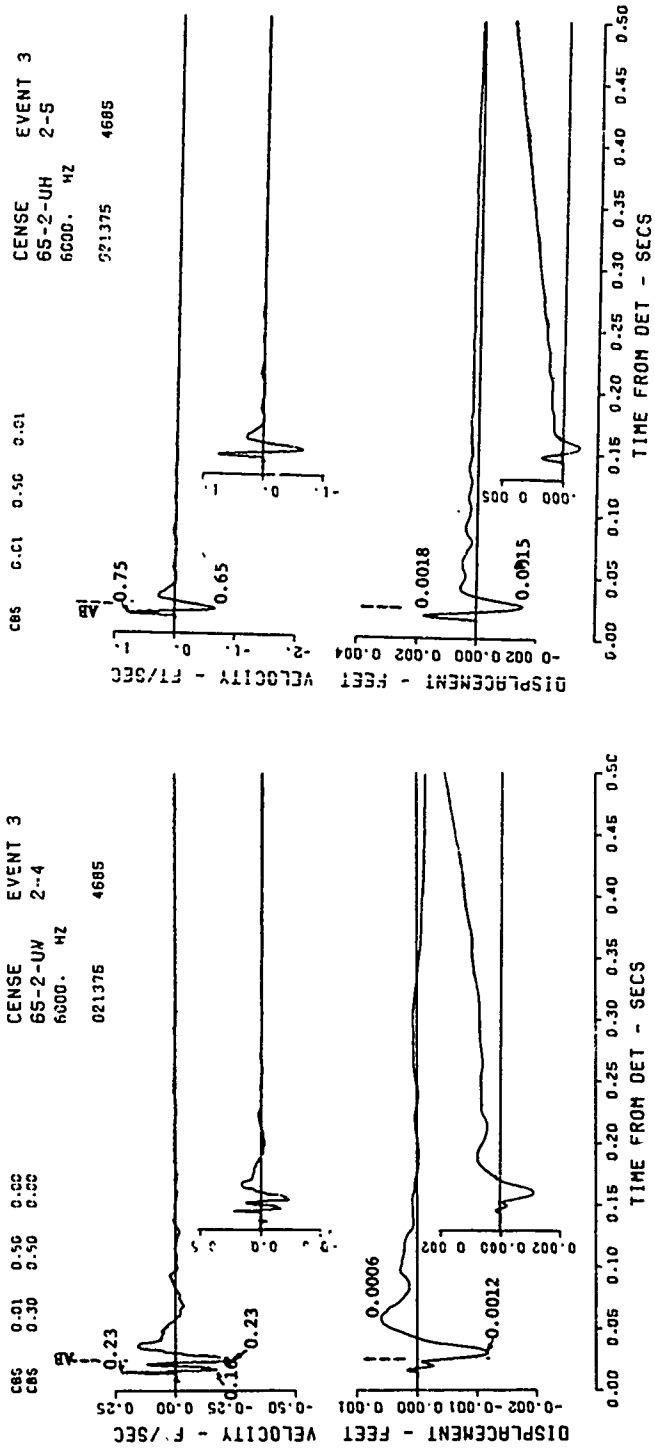

Figure B.12 (sheet 3 of 5).

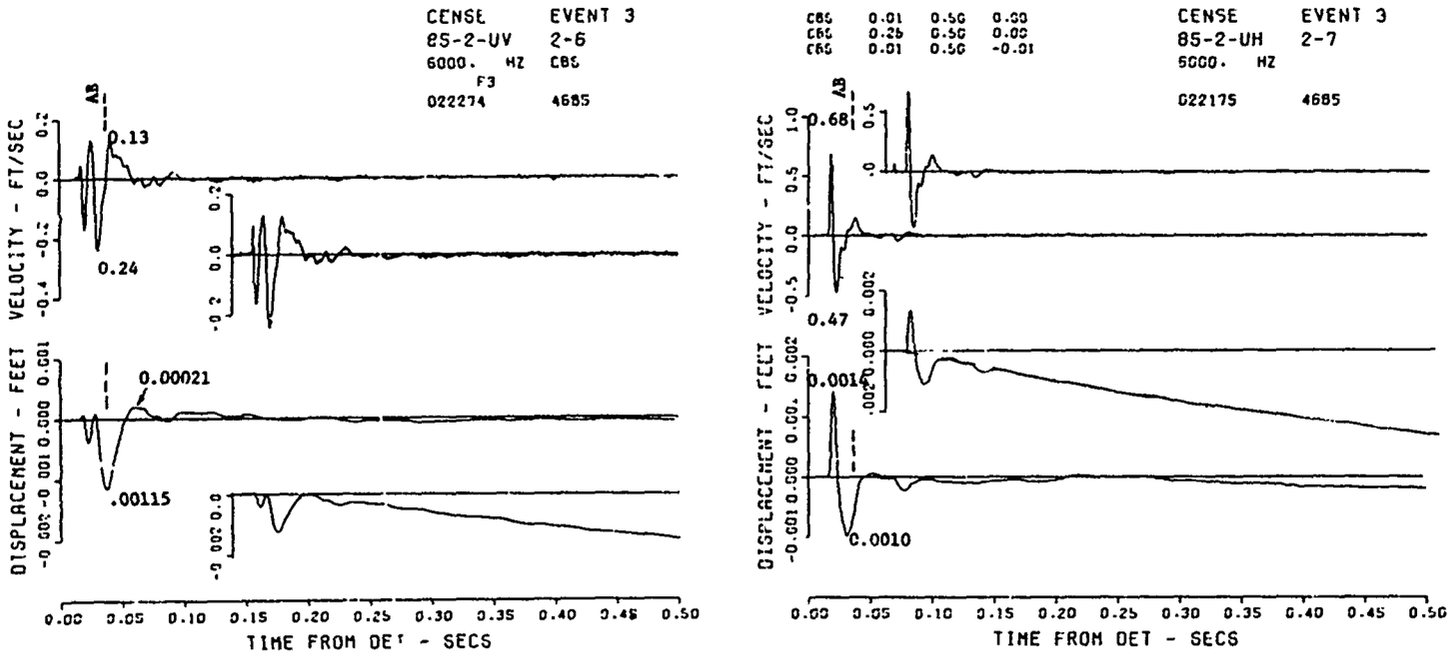

Figure B.12 (sheet 4 of 5).

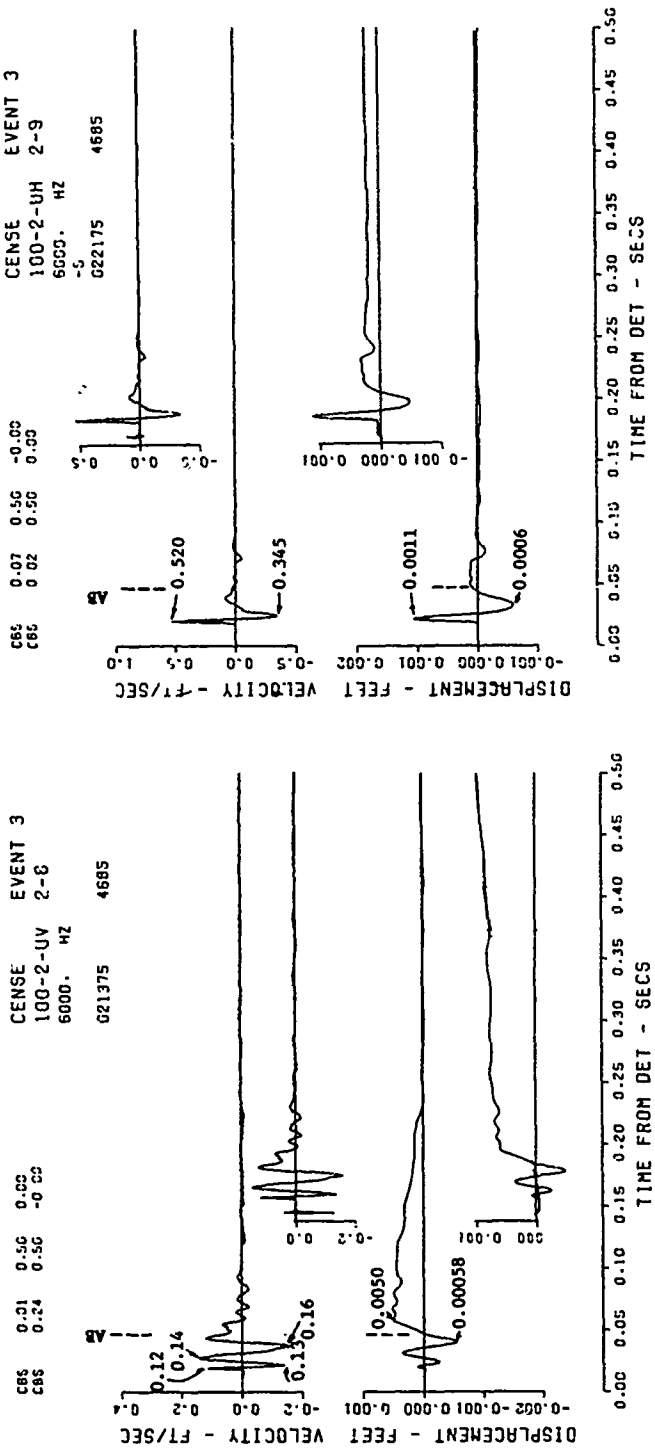

Figure B.12 (sheet 5 of 5).

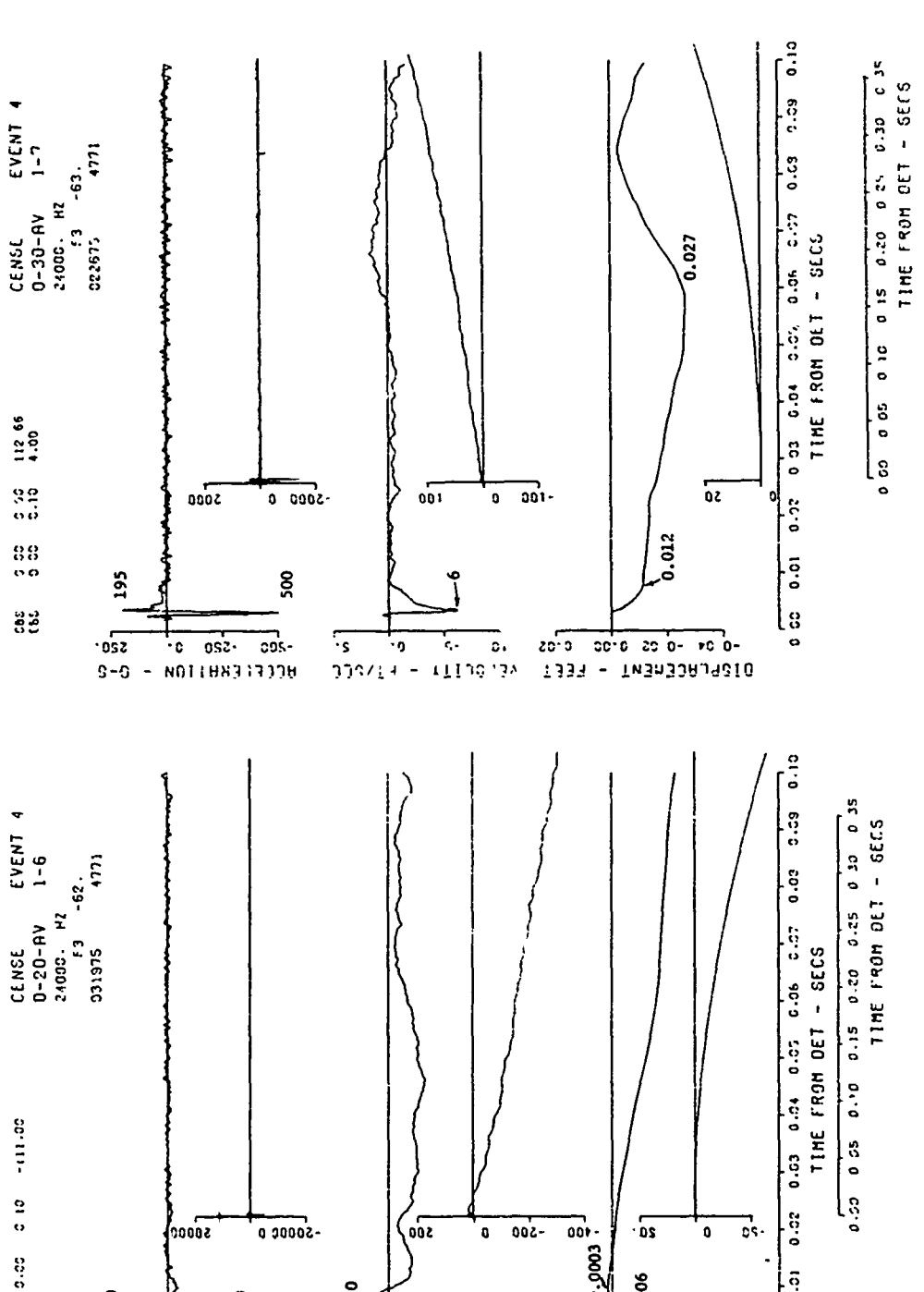

Figure B.13. Event 4, 1/2 buried, 0 $W^{1/3}$ (0 foot) ; motion-time histories along the vertical radial directly beneath the explosion (sheet 1 of 3).

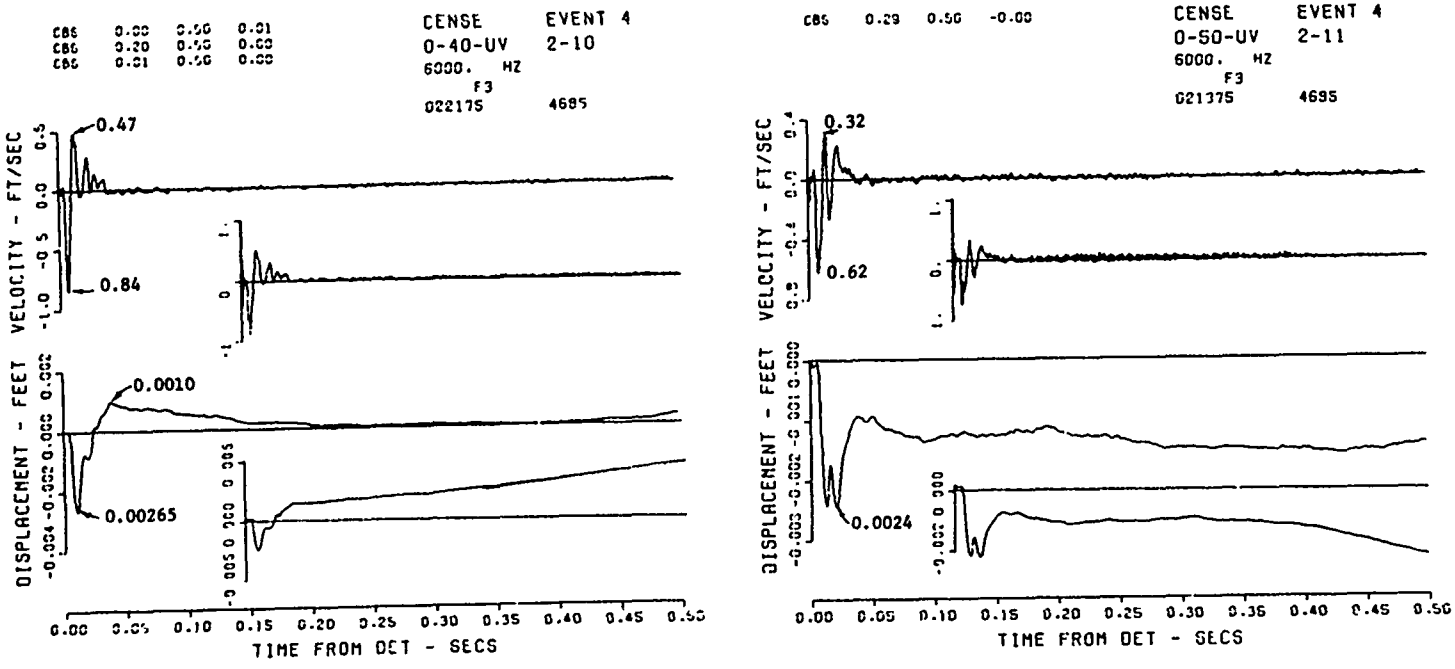

Figure B.13 (sheet 2 of 3).

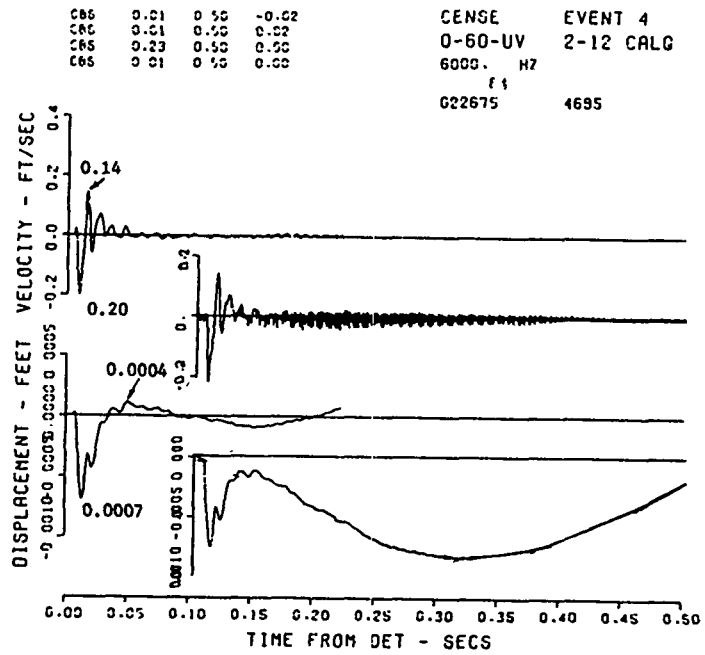

Figure B.13 (sheet 3 of 3).

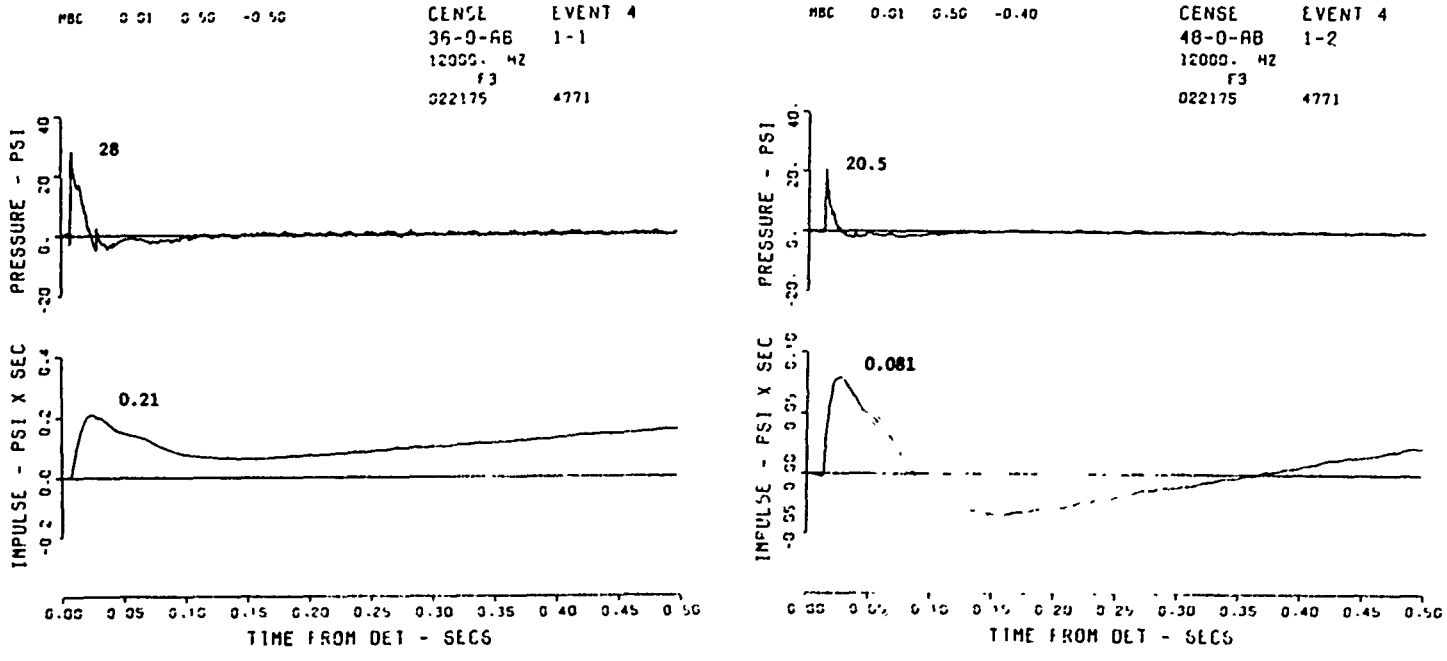

Figure B.14. Event 4, 1/2 buried, 0 $W^{1/3}$ (0 foot) ; surface airblast-time histories (sheet 1 of 3).

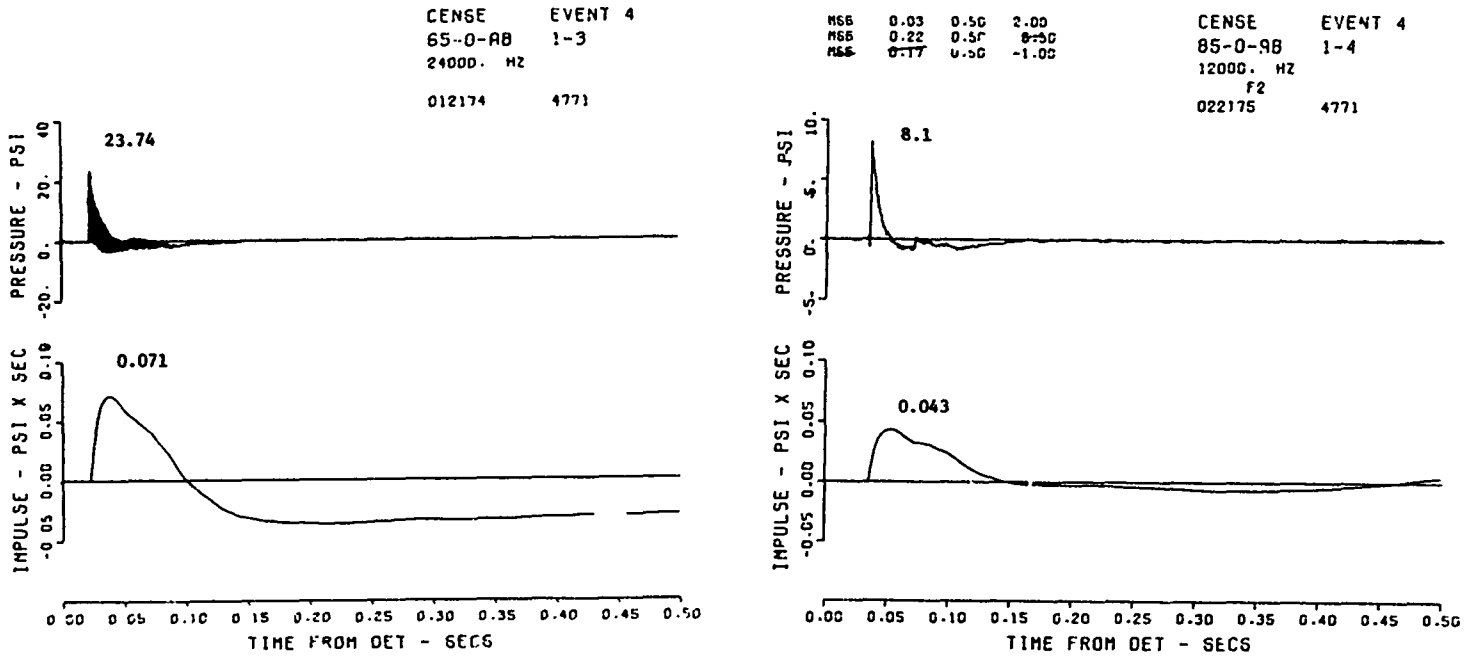

Figure B.14 (sheet 2 of 3).

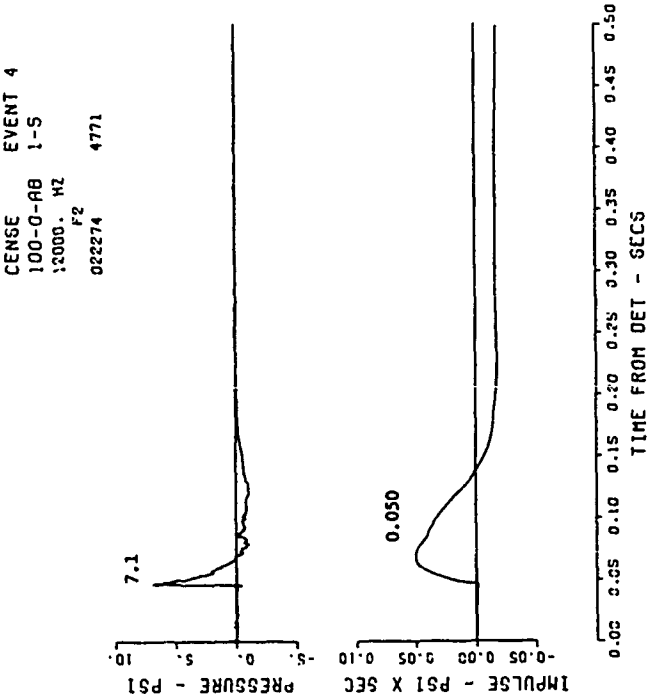

Figure B.14 (sheet 3 of 3).

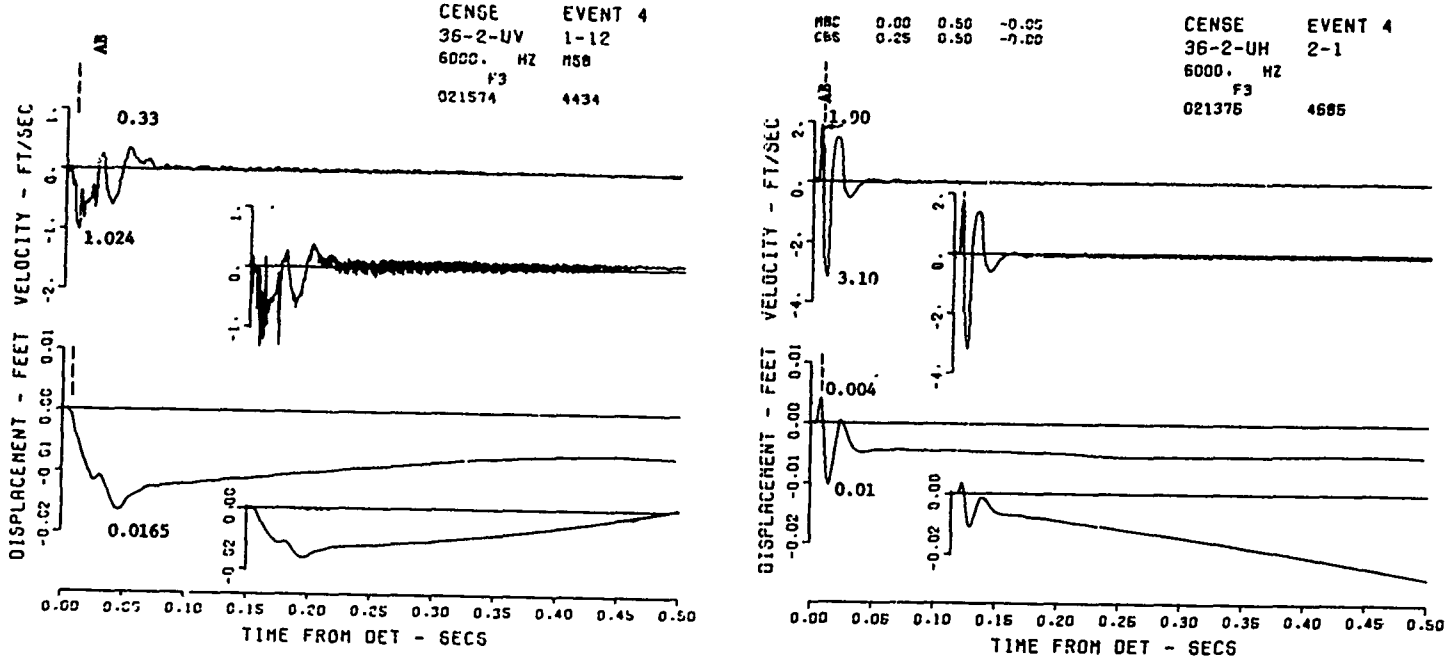

Figure B.15. Event 4, 1/2 buried, 0 $W^{1/3}$ (0 foot) ; near-surface motion-time histories (sheet 1 of 5).

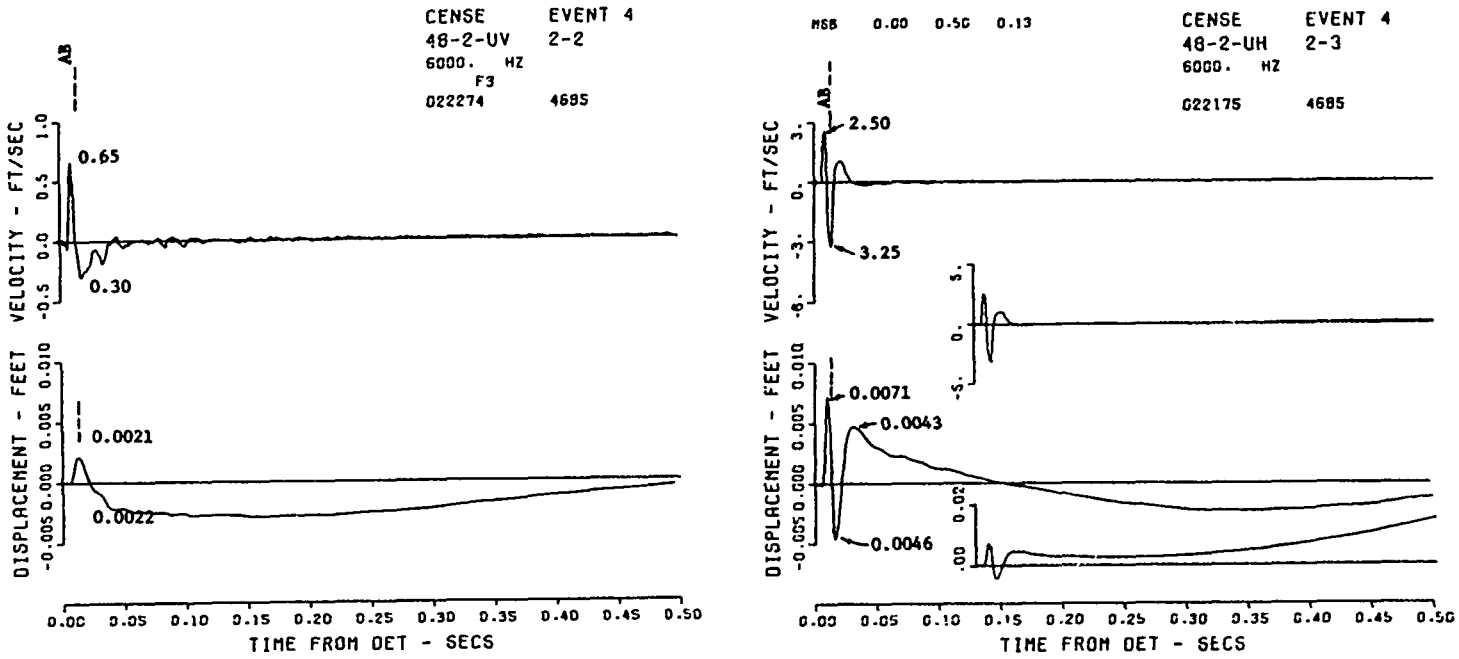

Figure B.15 (sheet 2 of 5).

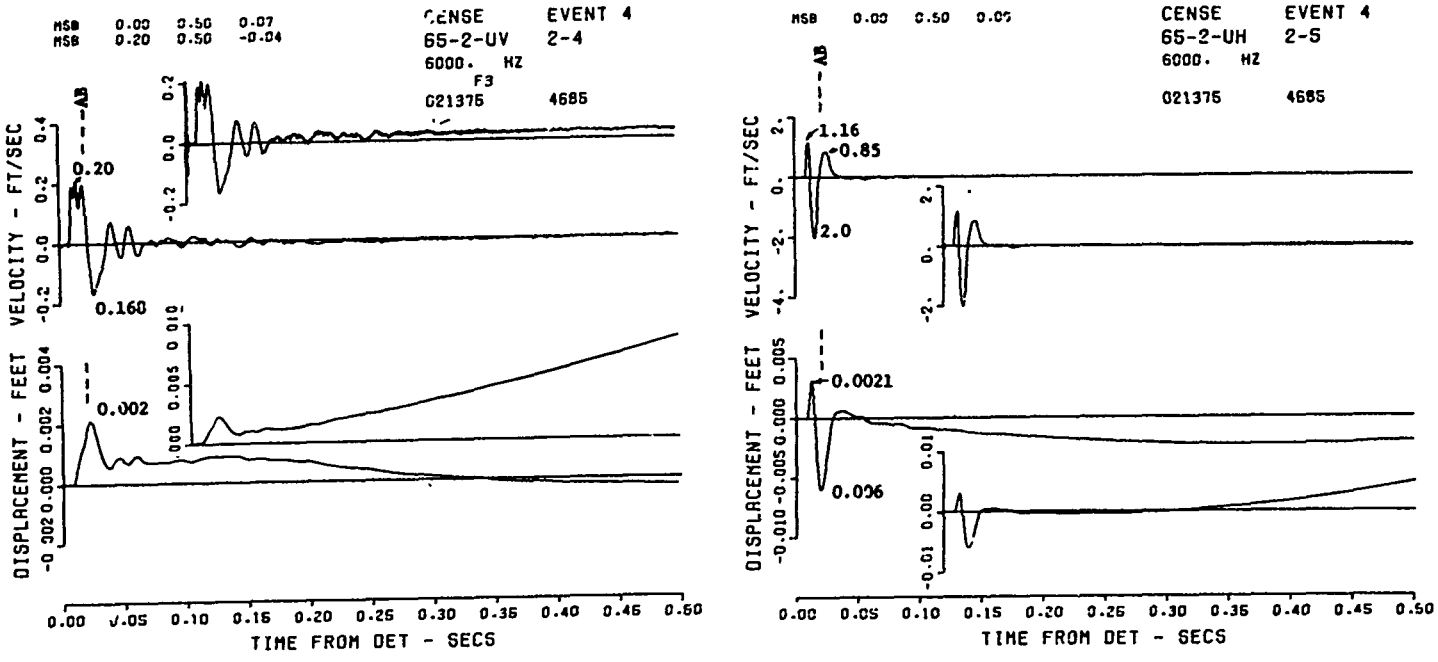

Figure B.15 (sheet 3 of 5).

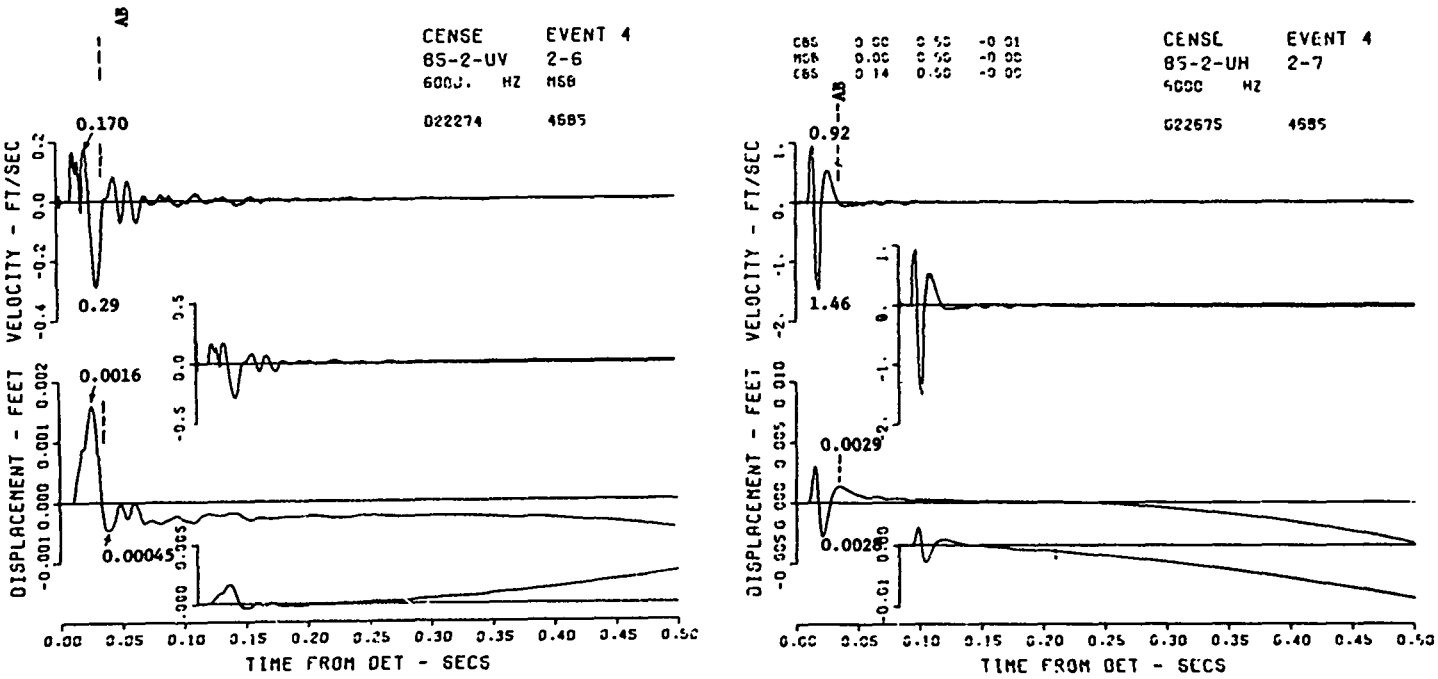

Figure B.15 (sheet 4 of 5).

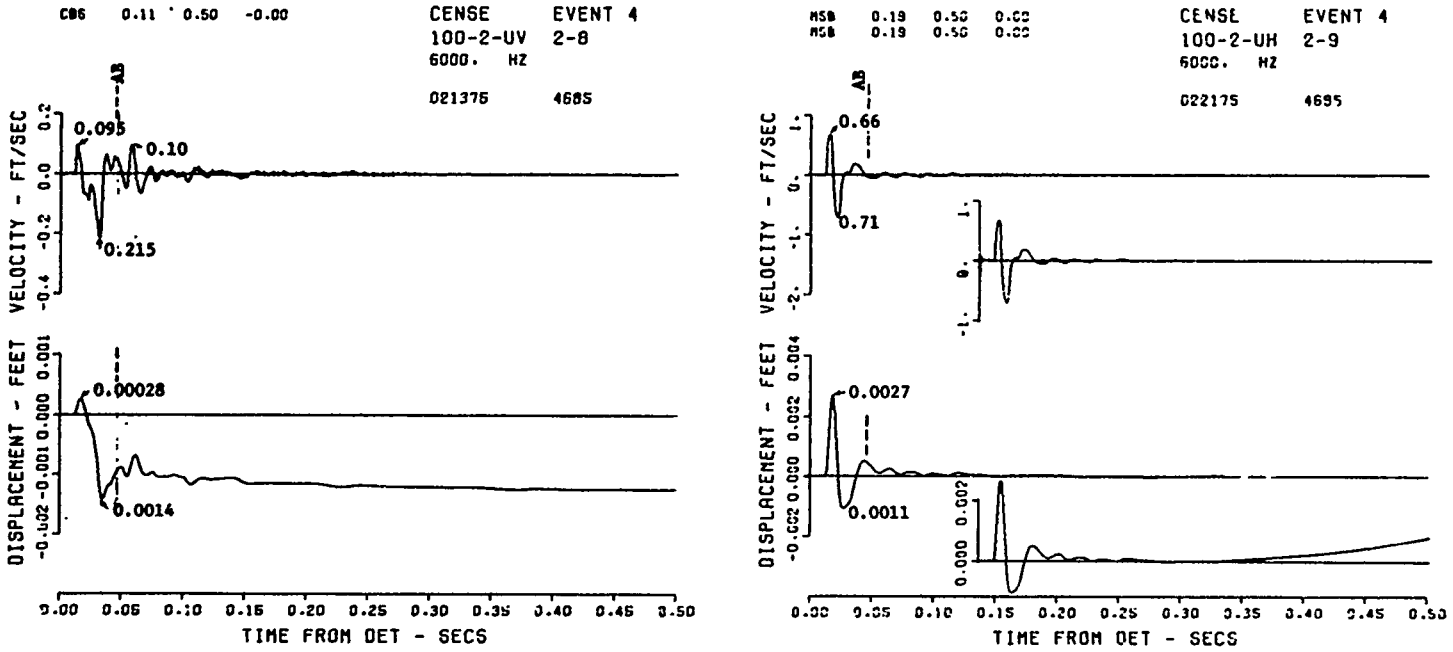

Figure B.15 (sheet 5 of 5).

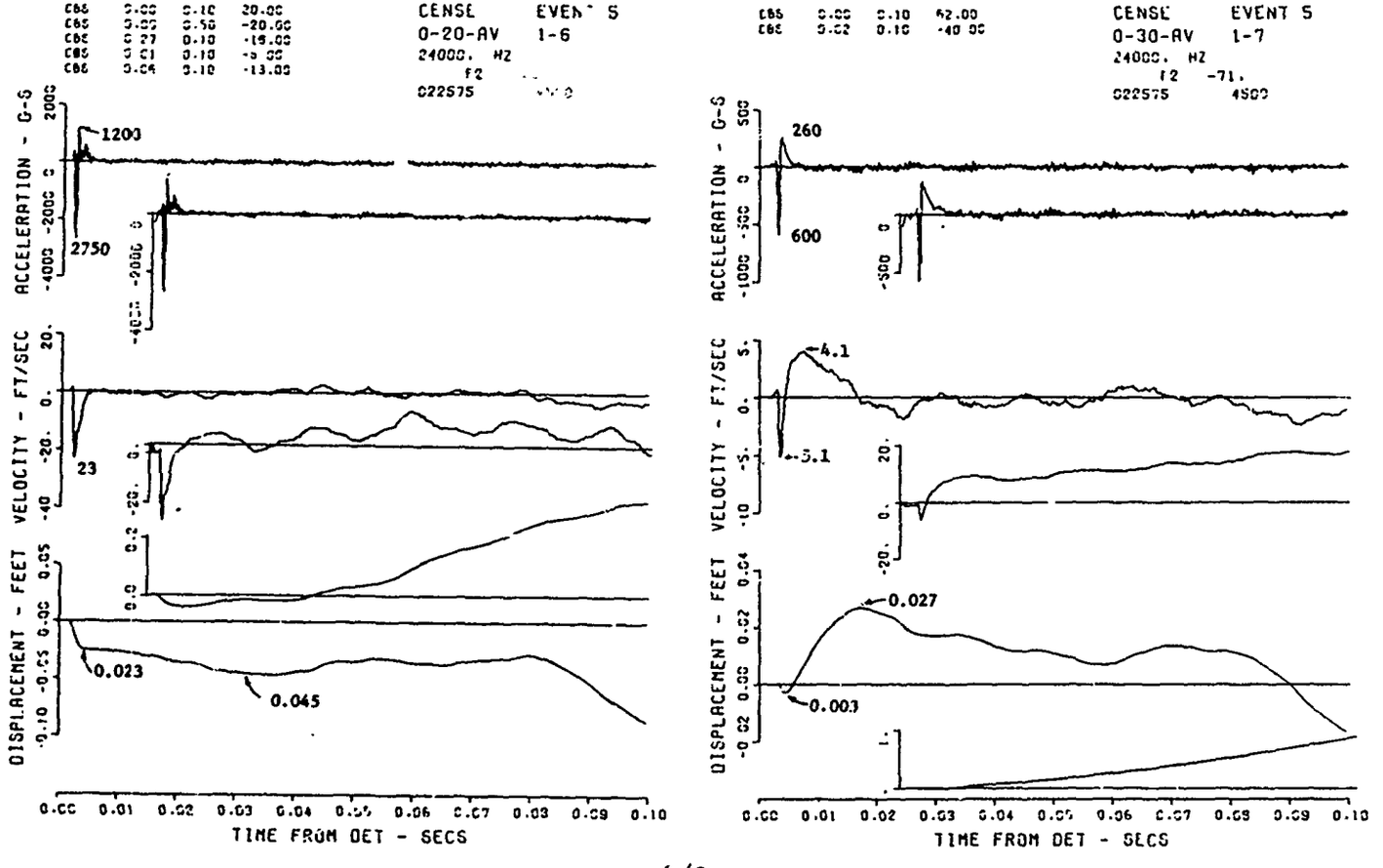

Figure B.16. Event 5, 3/4 buried, $+0.072\ W^{1/3}$ (+0.75 foot) ; motion-time histories along the vertical radial directly beneath the explosion (sheet 1 of 3).

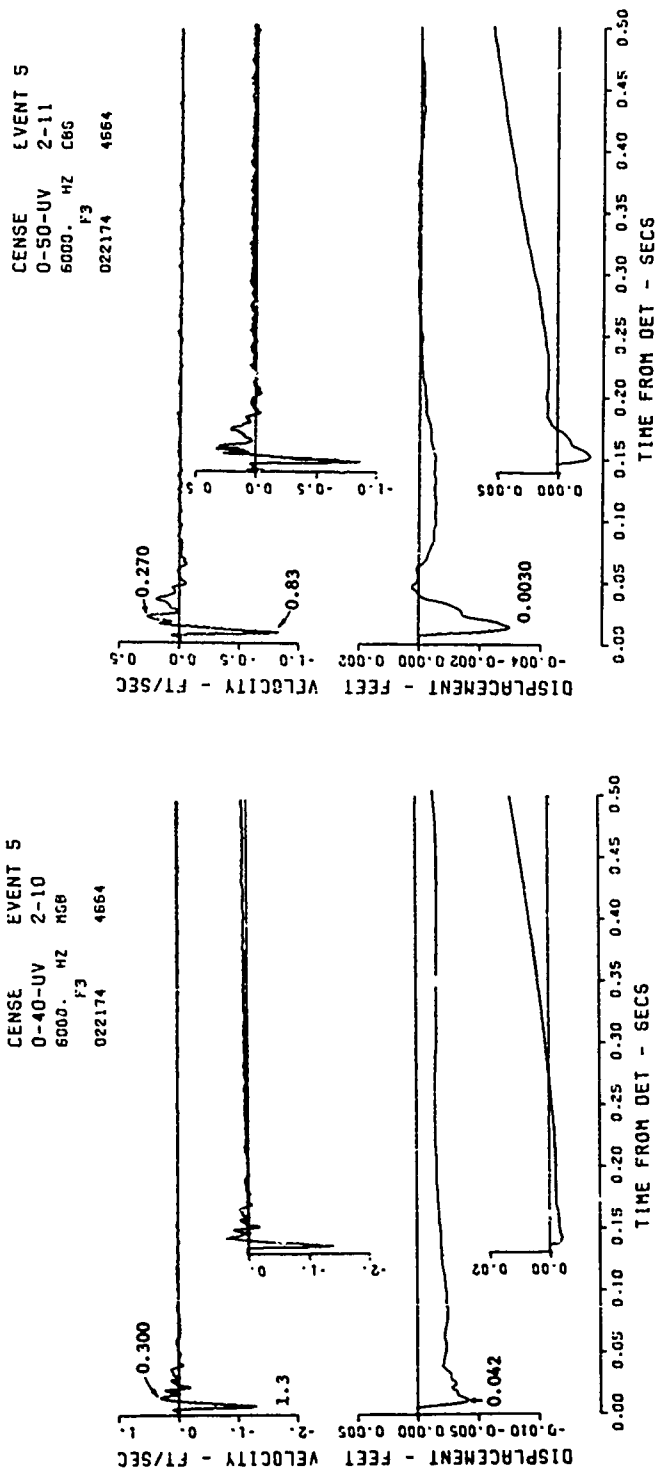

Figure B.16 (sheet 2 of 3).

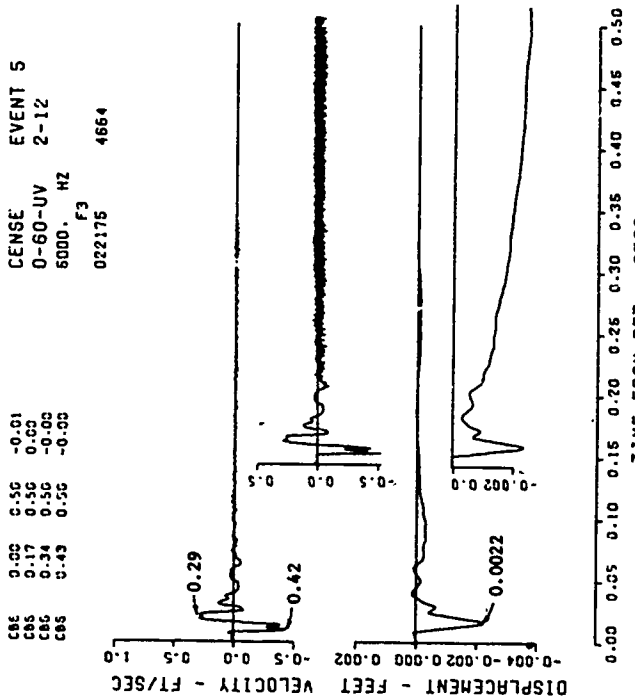

Figure B.16 (sheet 3 of 3).

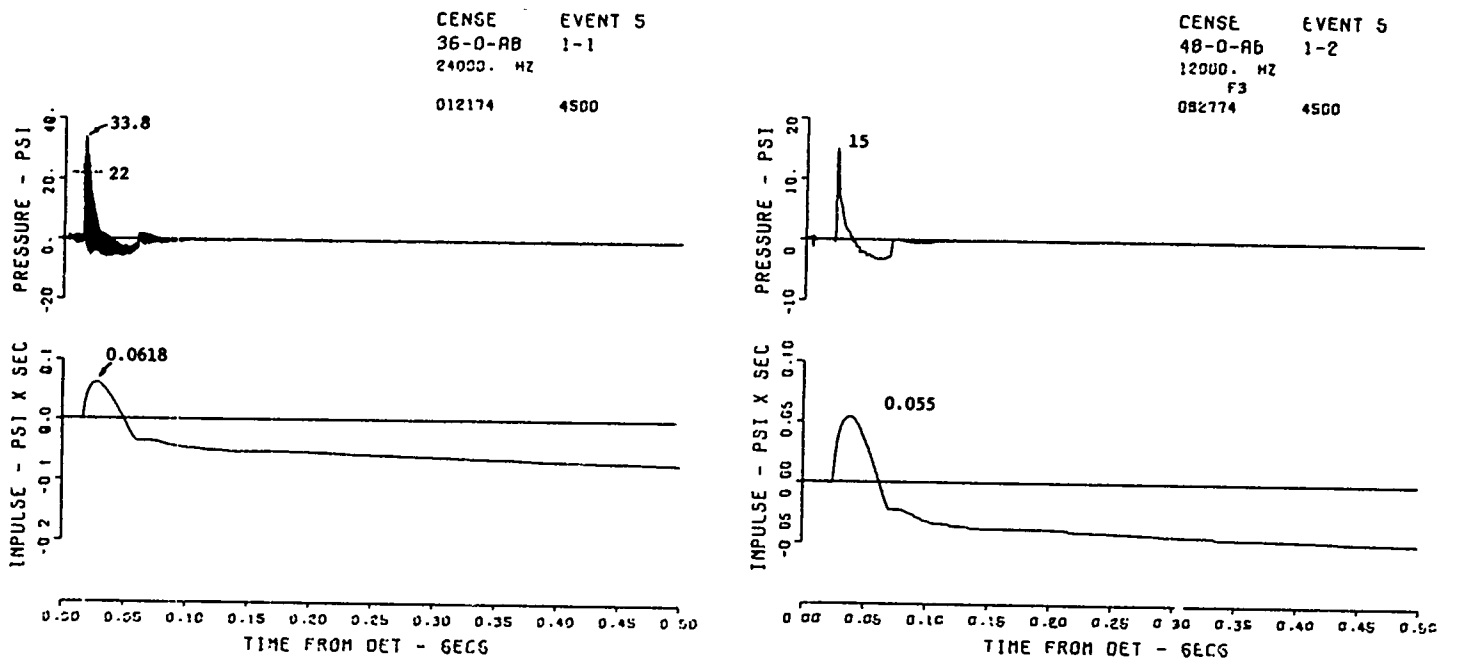

Figure B.17. Event 5, 3/4 buried, $+0.072\ W^{1/3}$ (+0.75 foot) ; surface airblast-time histories (sheet 1 of 3).

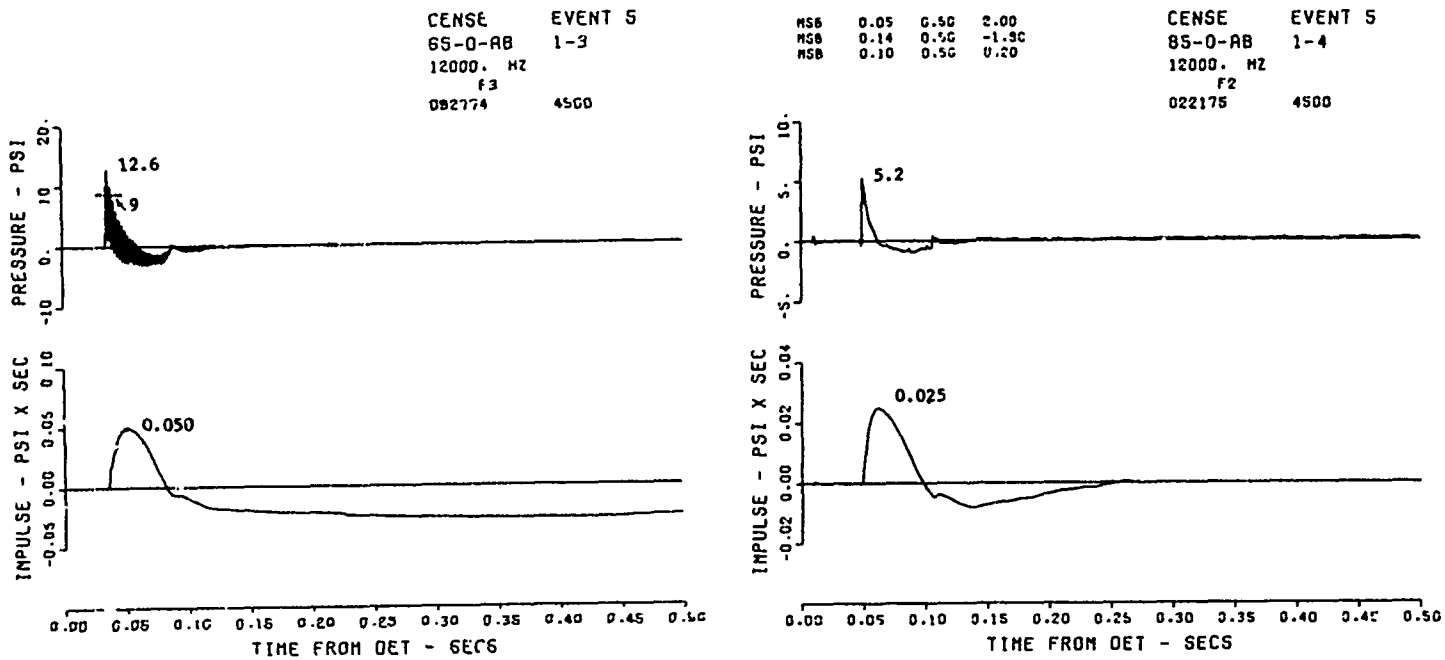

Figure B.17 (sheet 2 of 3).

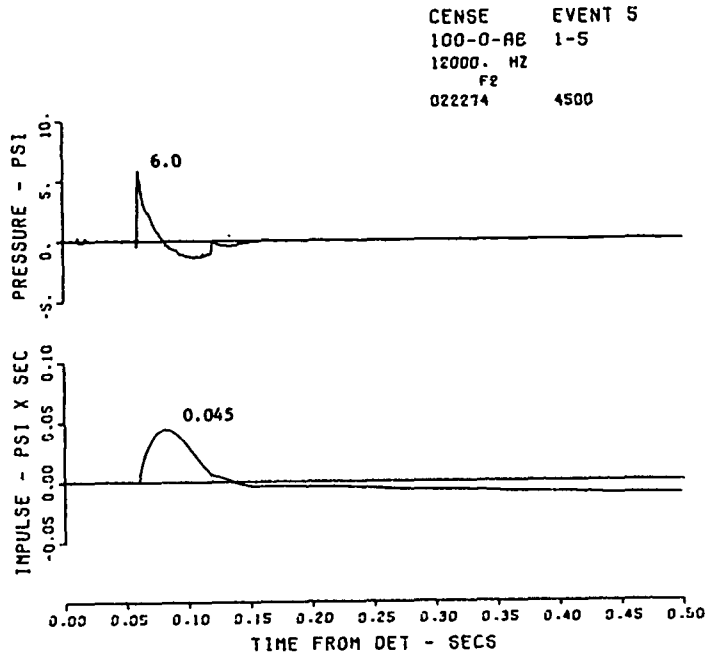

Figure B.17 (sheet 3 of 3).

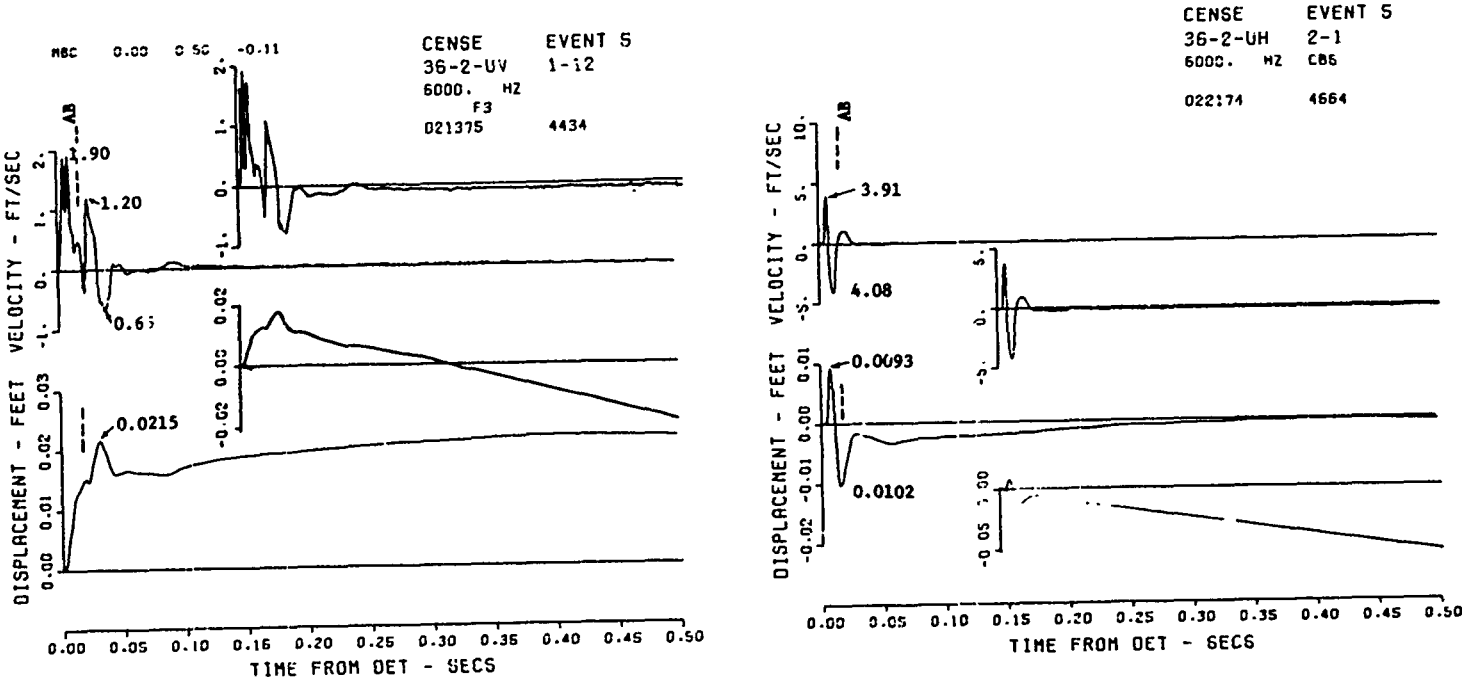

Figure B.18. Event 5, 3/4 buried, $+0.072\ W^{1/3}$ (+0.75 foot) ; near-surface motion-time histories (sheet 1 of 5).

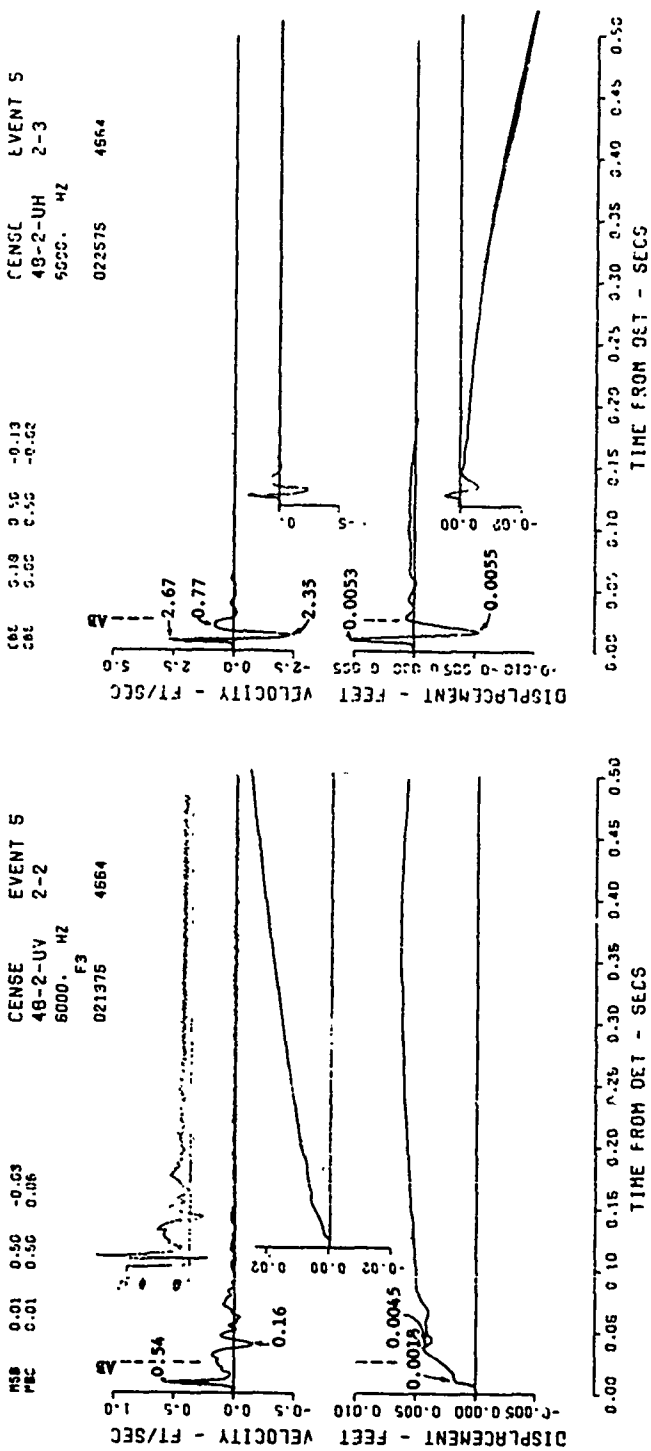

Figure B.18 (sheet 2 of 5).

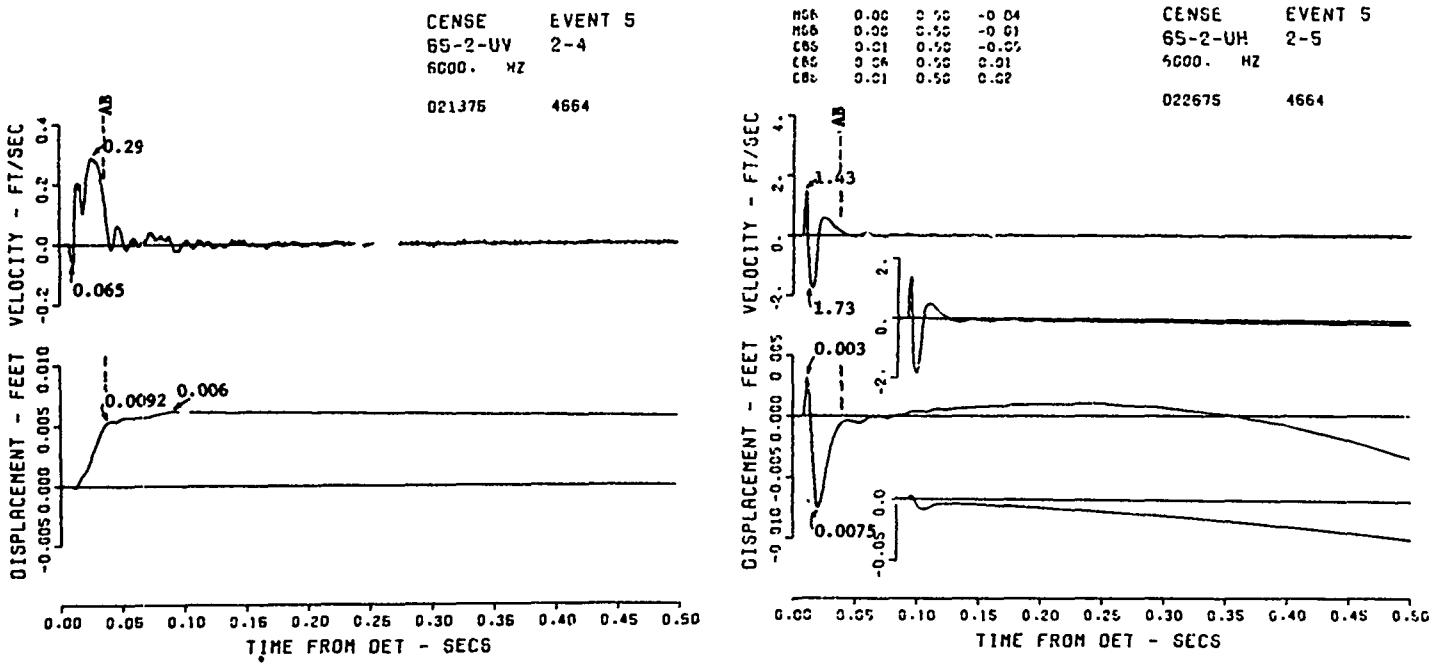

Figure B.18 (sheet 3 of 5).

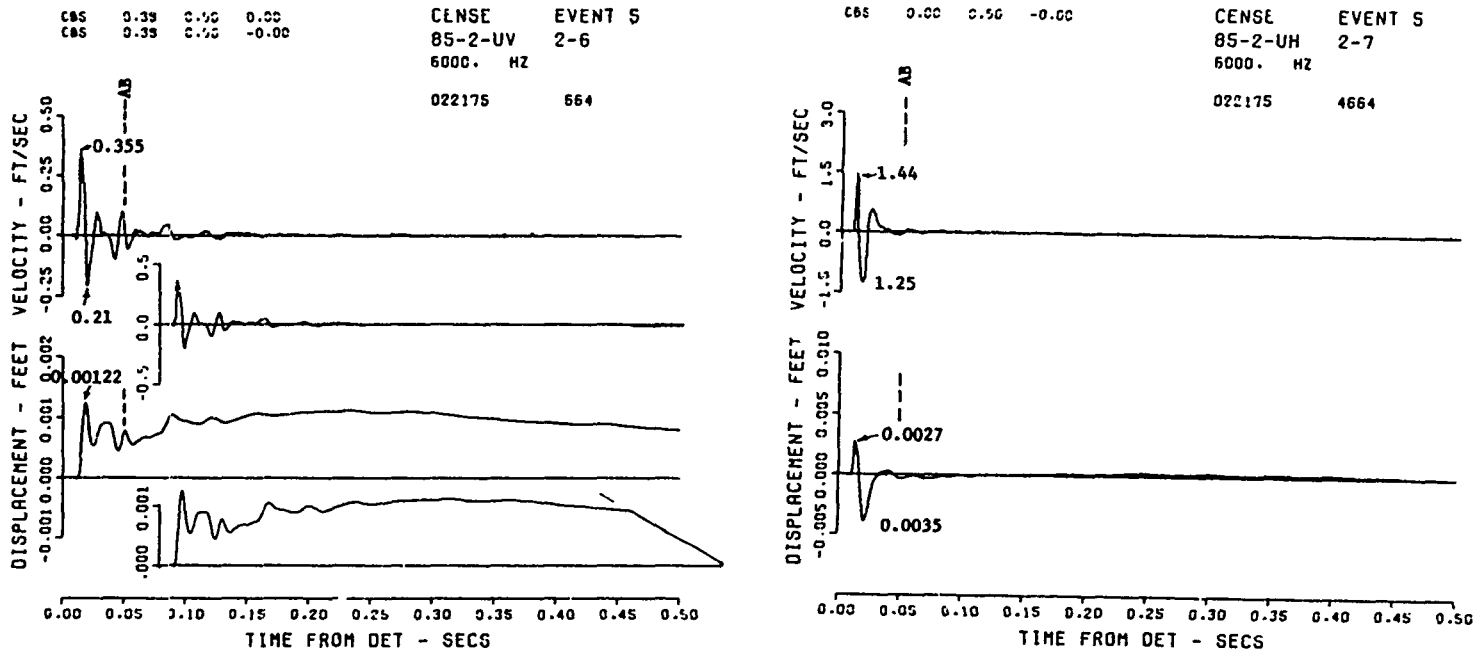

Figure B.18 (sheet 4 of 5).

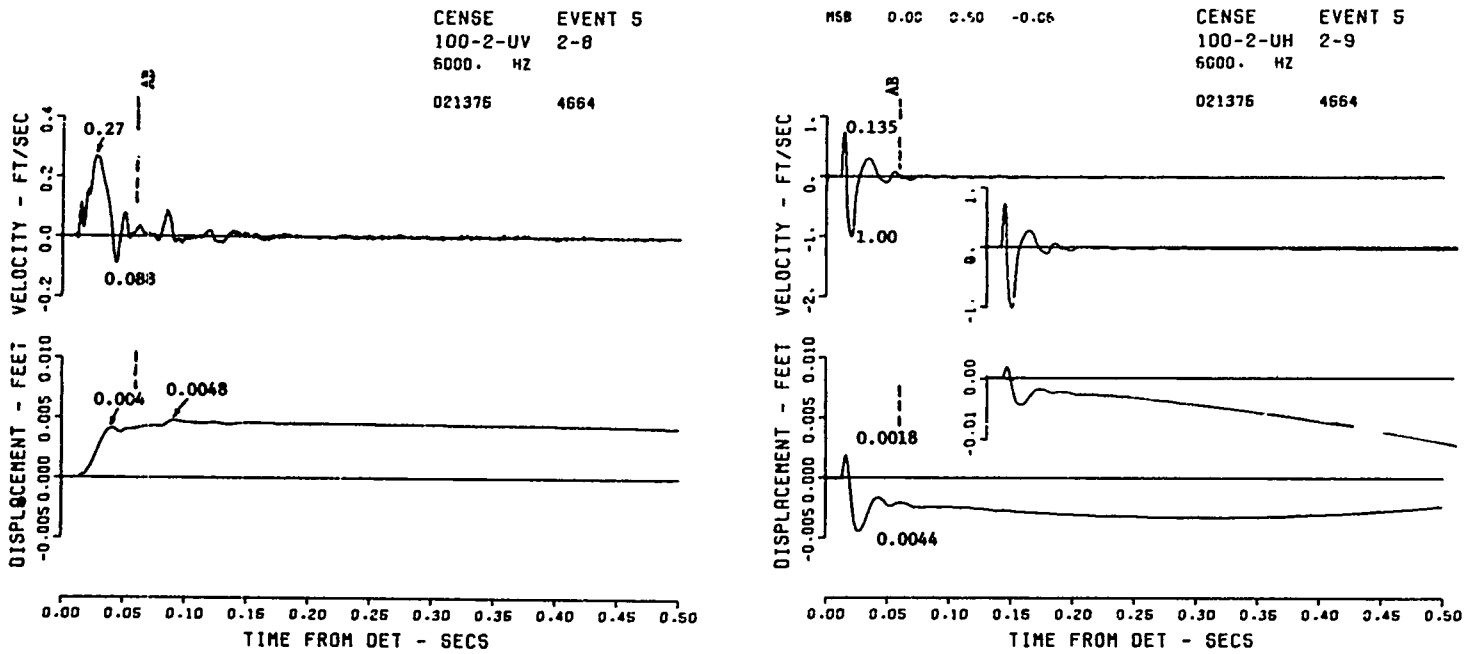

Figure B.18 (sheet 5 of 5).

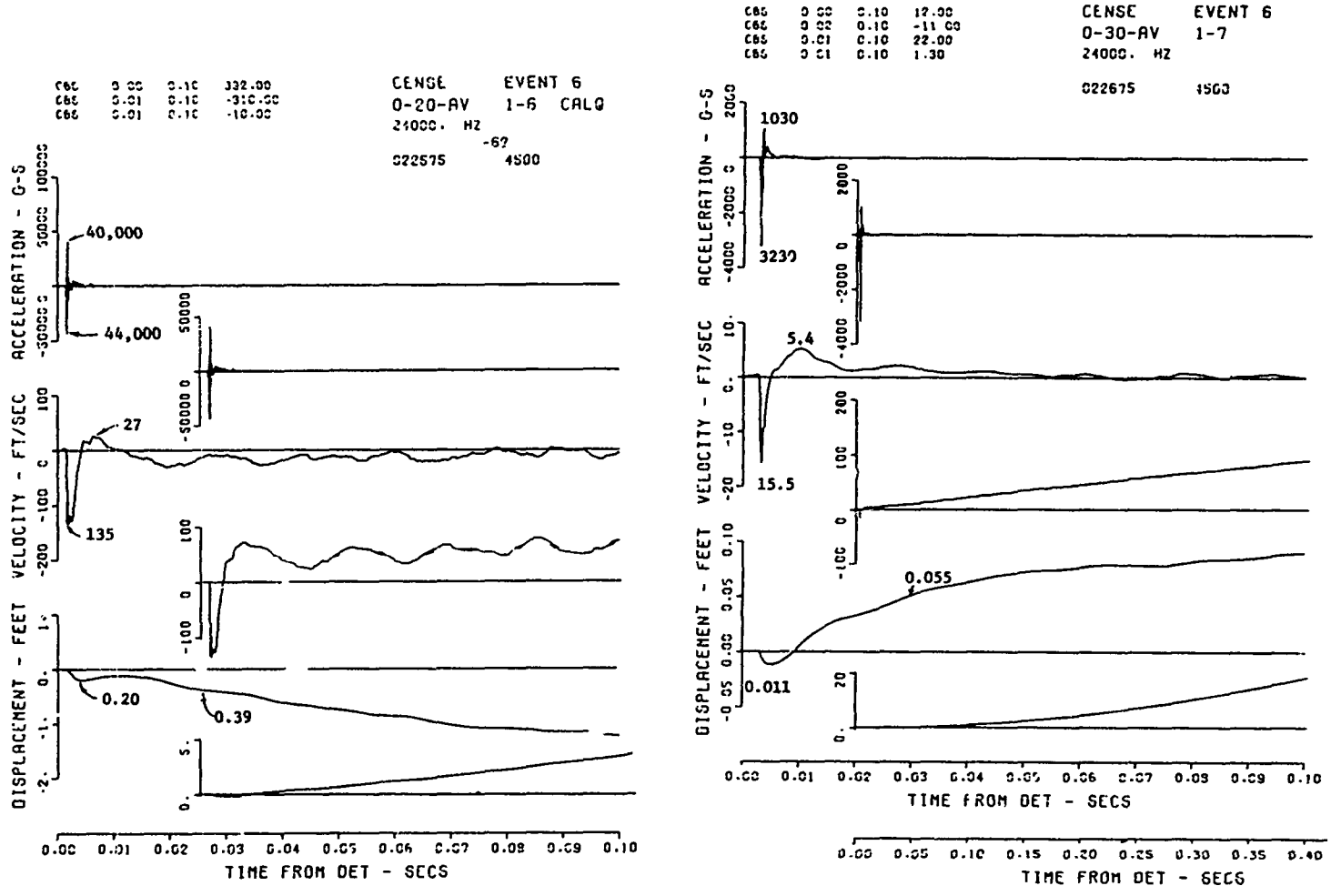

Figure B.19. Event 6, buried tangent, $+0.14\ W^{1/3}$ (+1.5 feet) ; motion-time histories along the vertical radial directly beneath the explosion (sheet 1 of 3).

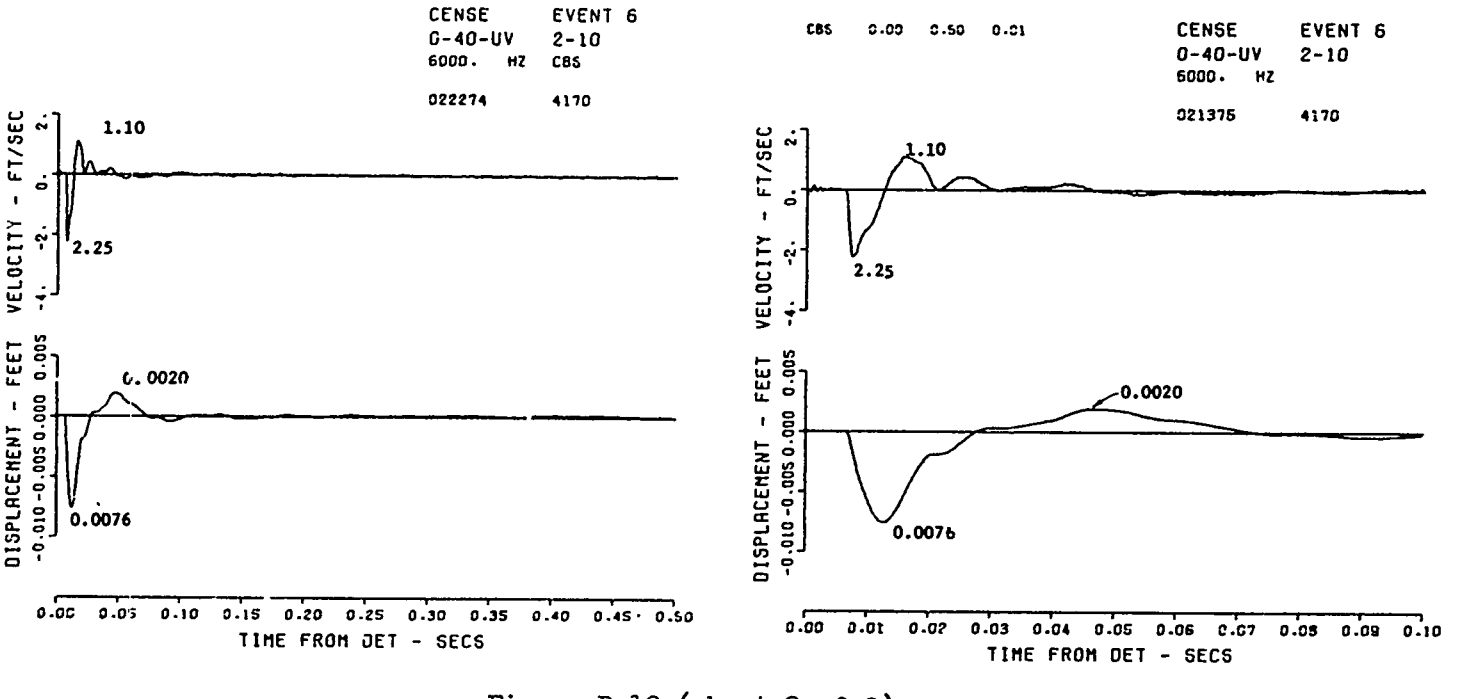

Figure B.19 (sheet 2 of 3).

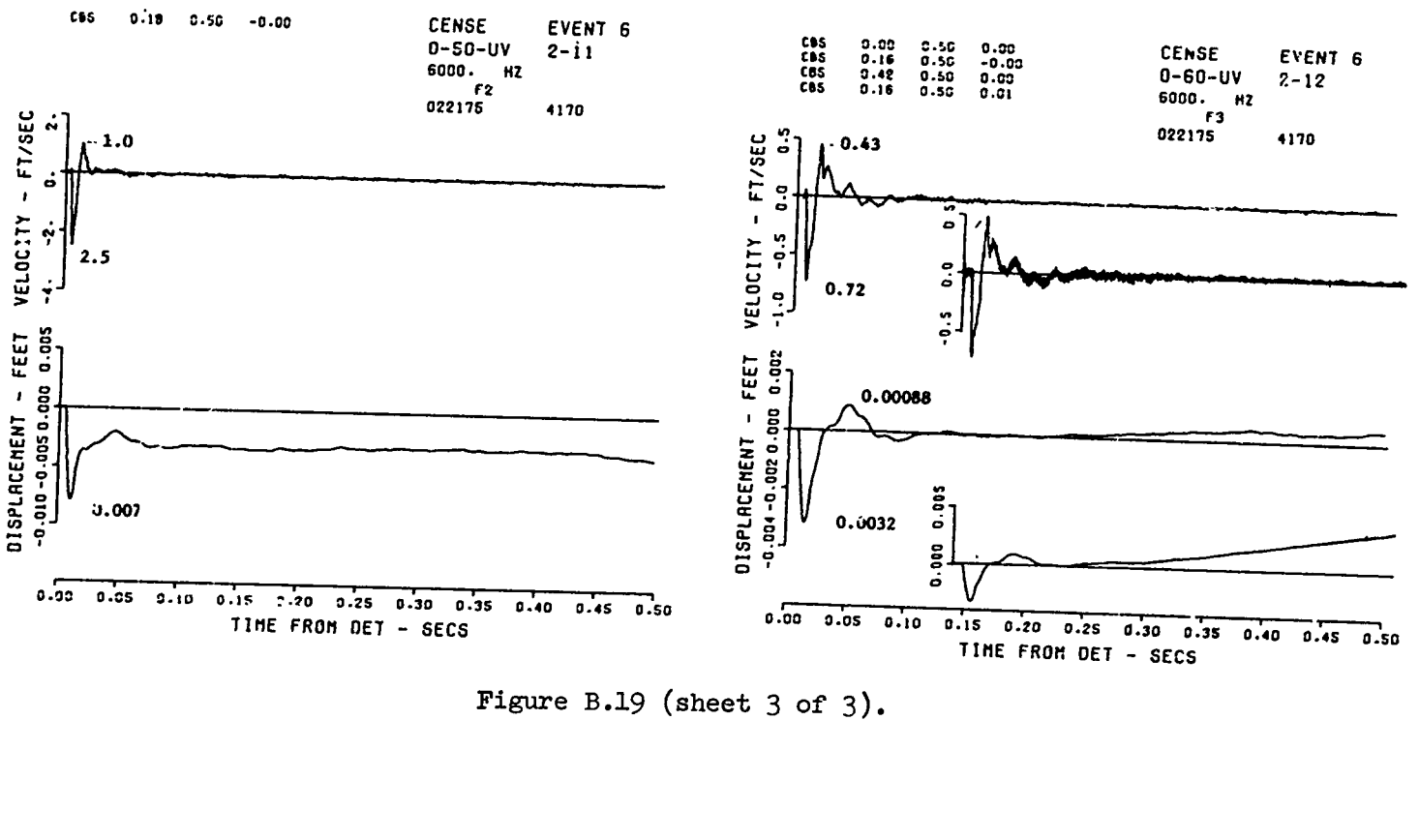

Figure B.19 (sheet 3 of 3).

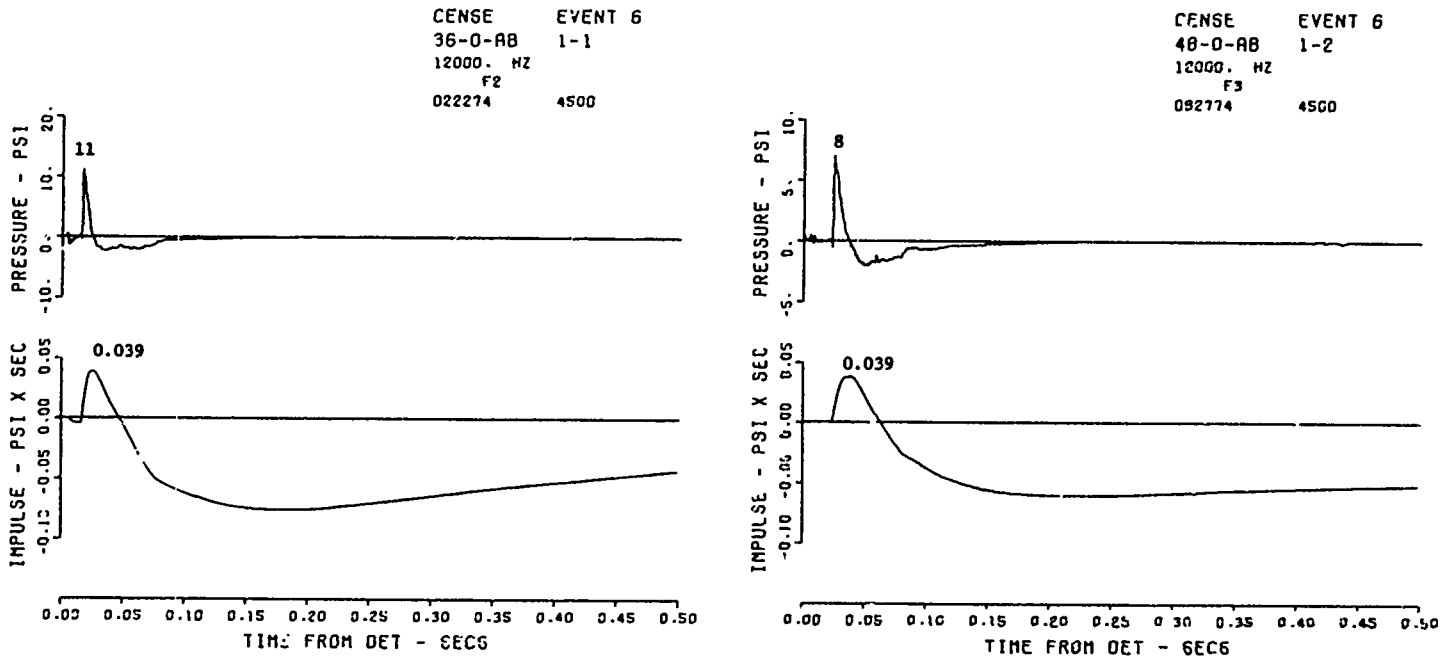

Figure B.20. Event 6, buried tangent, $+0.1^{b}$ $W^{1/3}$ (+1.5 feet) ; surface airblast-time histories (sheet 1 of 3).

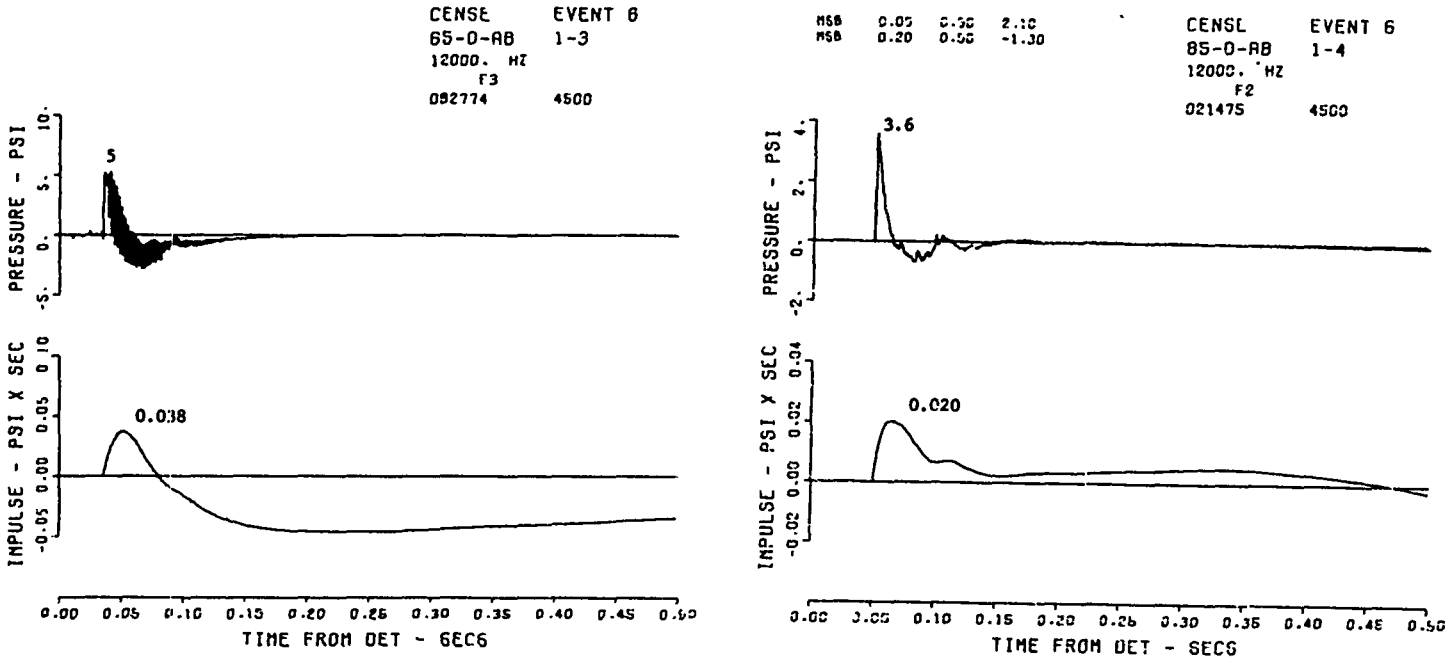

Figure B.20 (sheet 2 of 3).

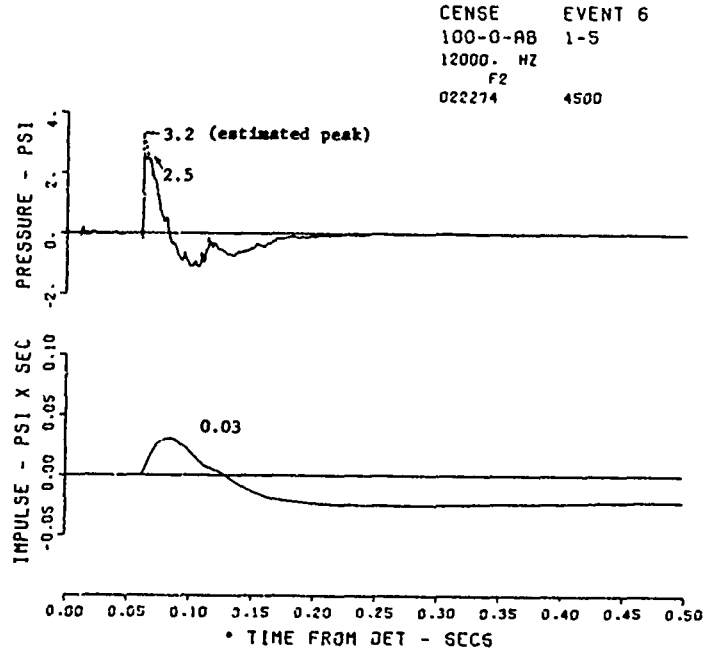

Figure B.20 (sheet 3 of 3).

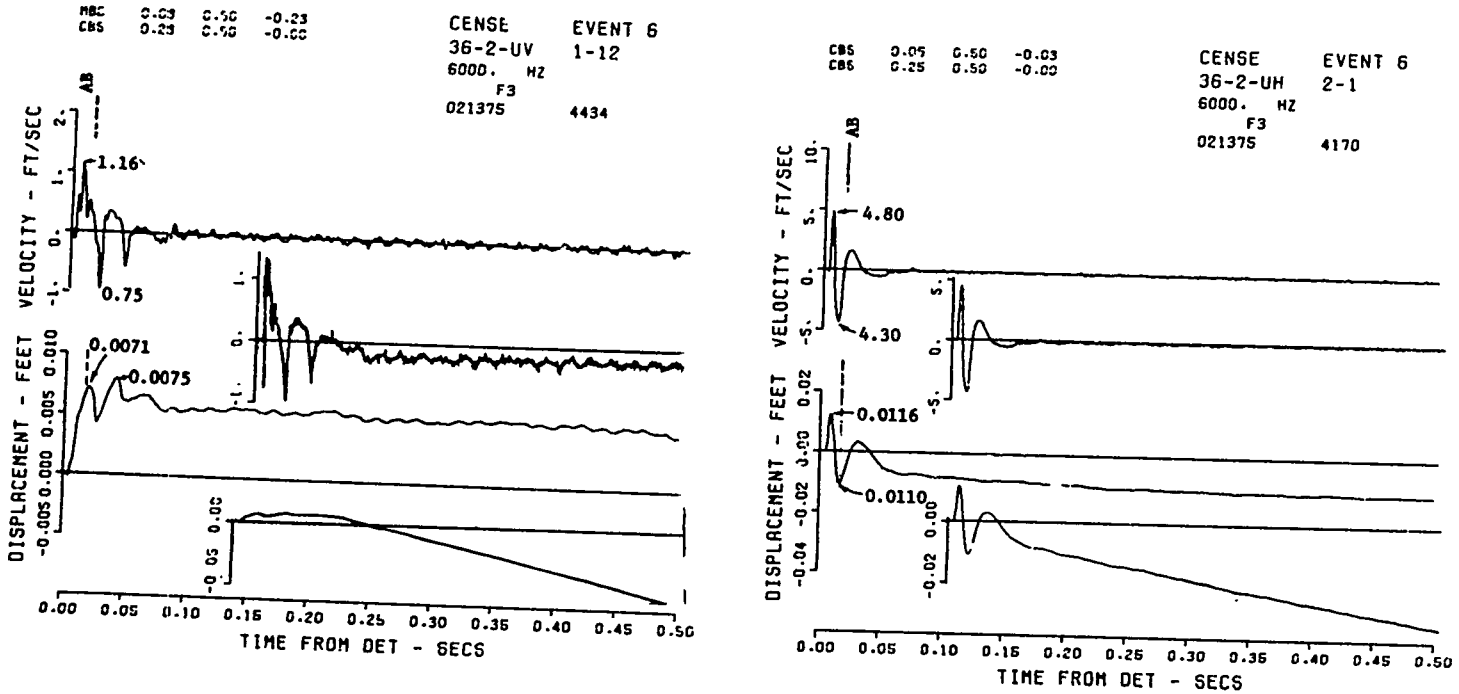

Figure B.21. Event 6, buried tangent, $+0.14\ W^{1/3}$ (+1.5 feet) ; near-surface horizontal motion-time histories (sheet 1 of 5).

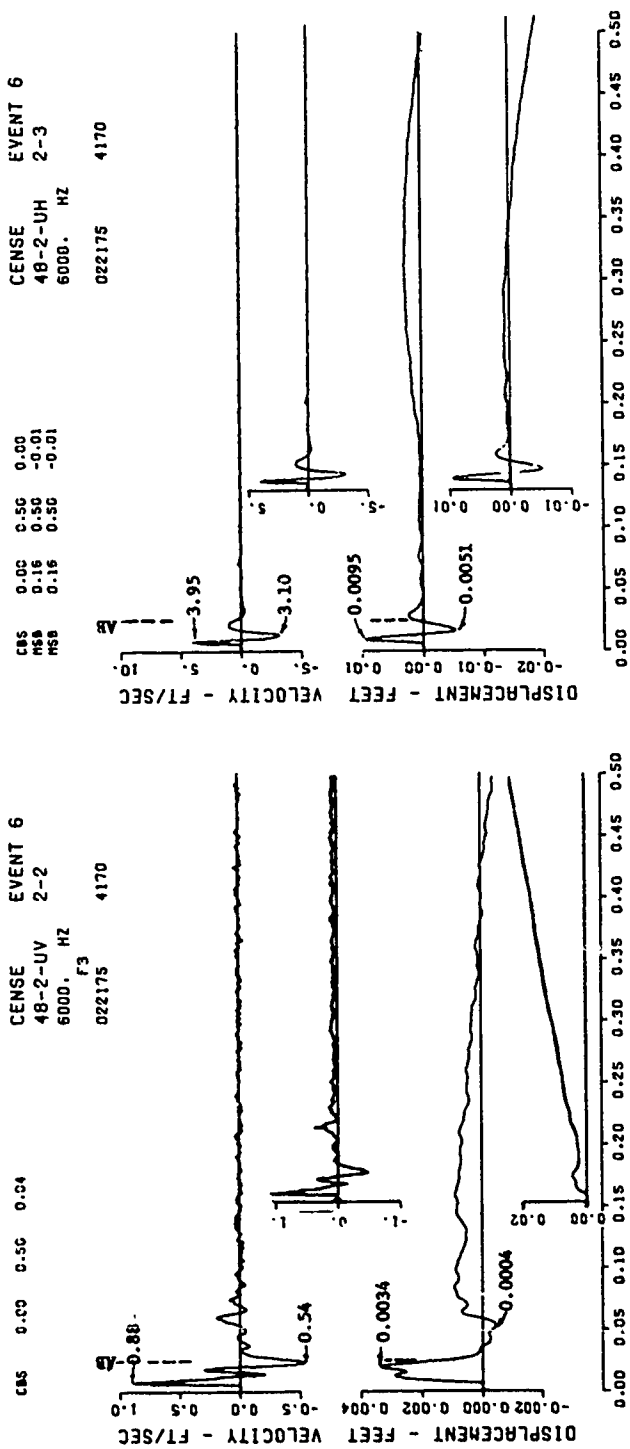

Figure B.21 (sheet 2 of 5).

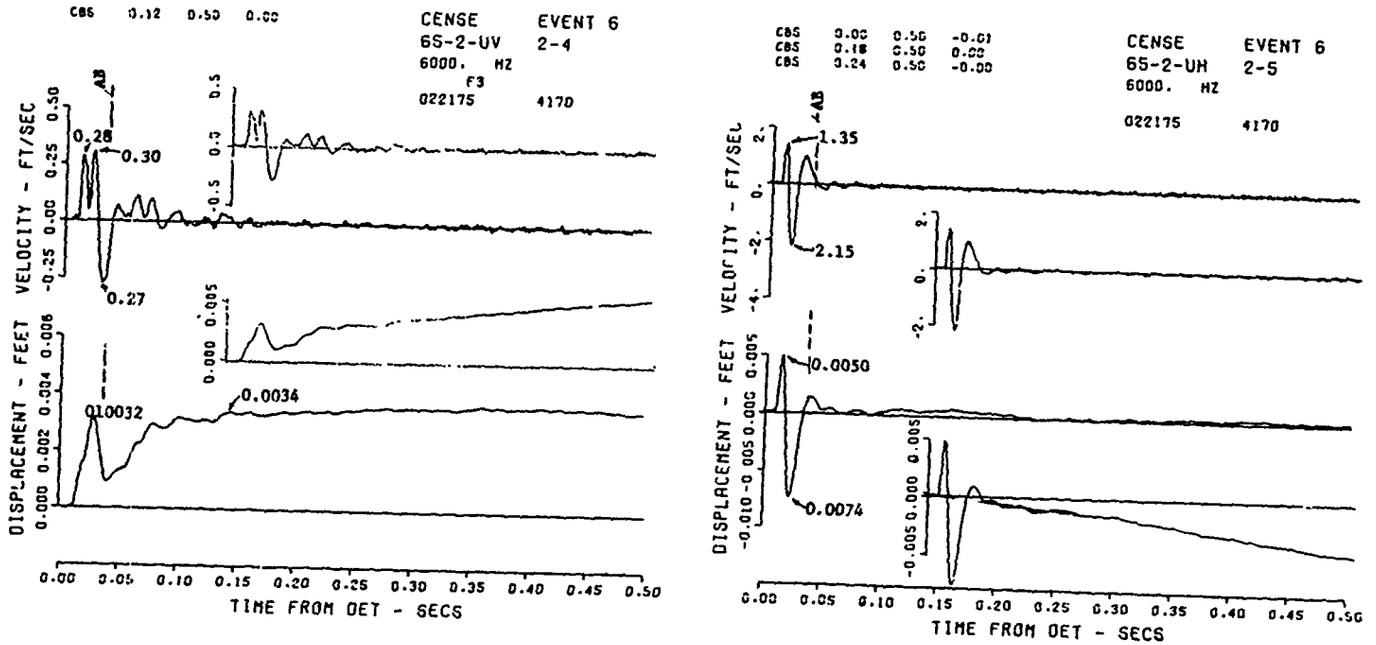

Figure B.21 (sheet 3 of 5).

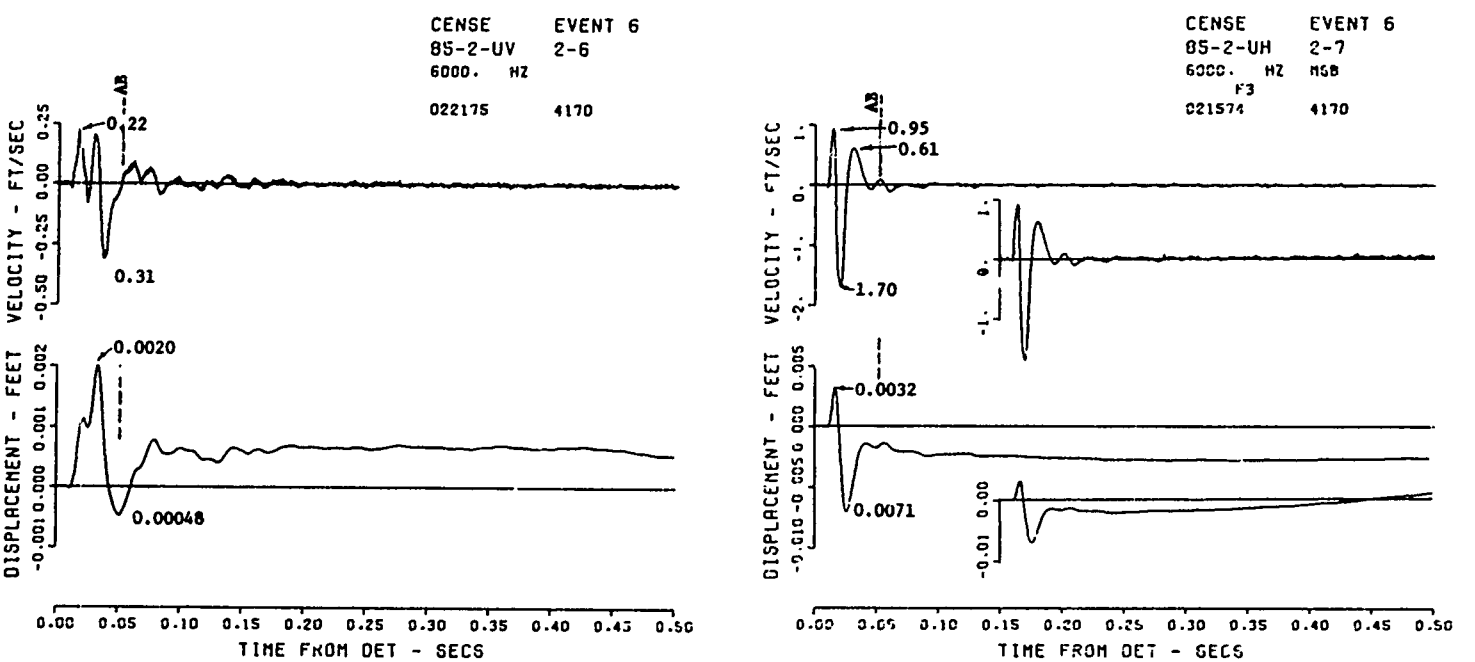

Figure B.21 (sheet 4 of 5).

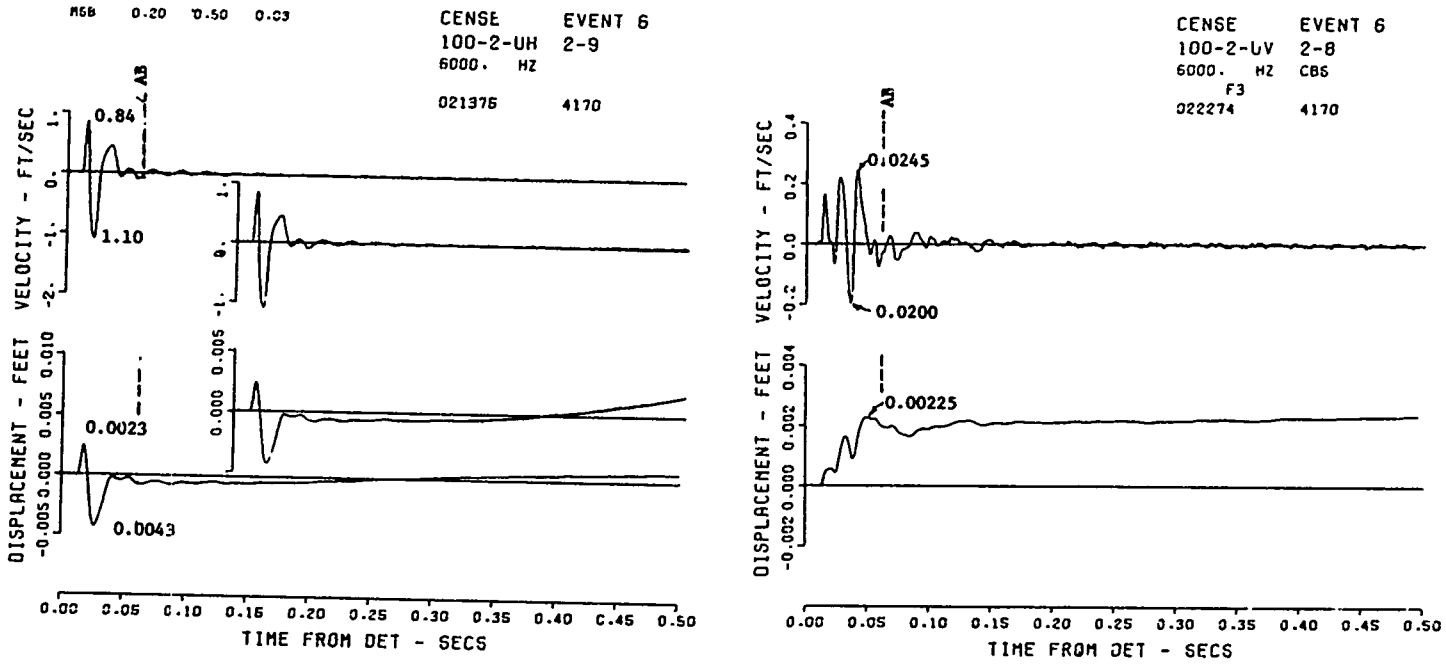

Figure B.21 (sheet 5 of 5).

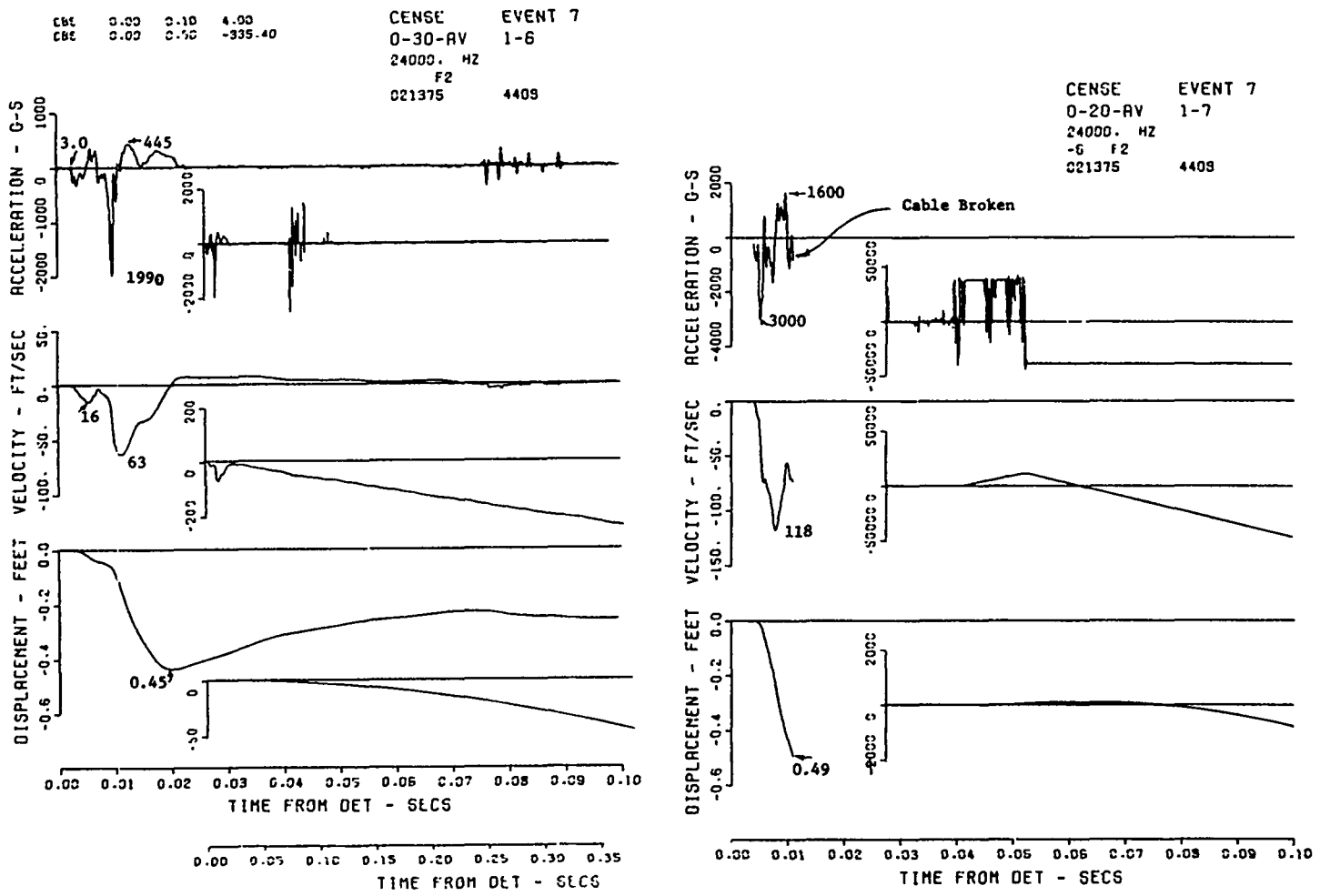

Figure B.22. Event 7, buried, +1 $W^{1/3}$ (10.5 feet) ; motion-time histories along the vertical radial directly beneath the explosion (sheet 1 of 5).

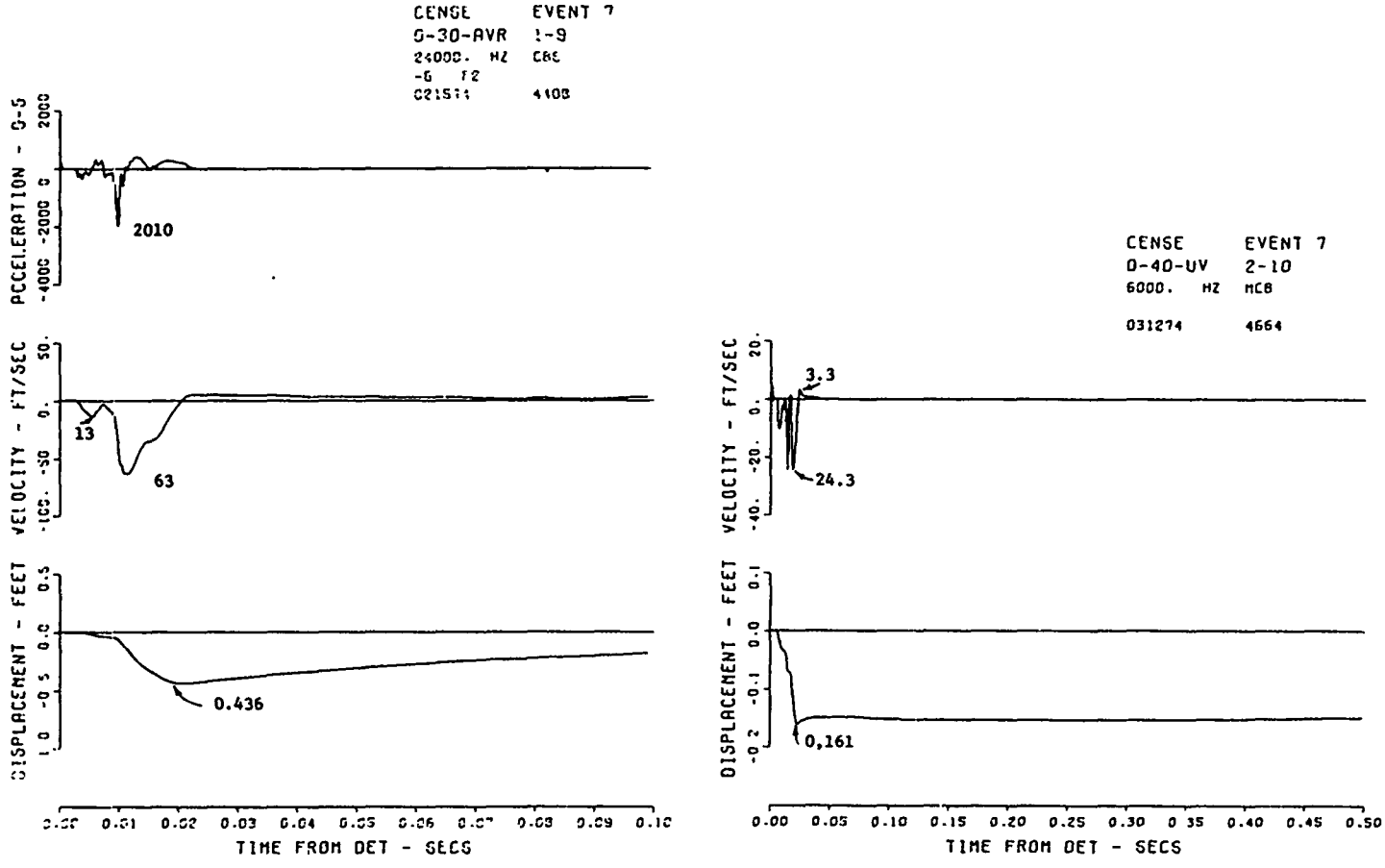

Figure B.22 (sheet 2 of 5).

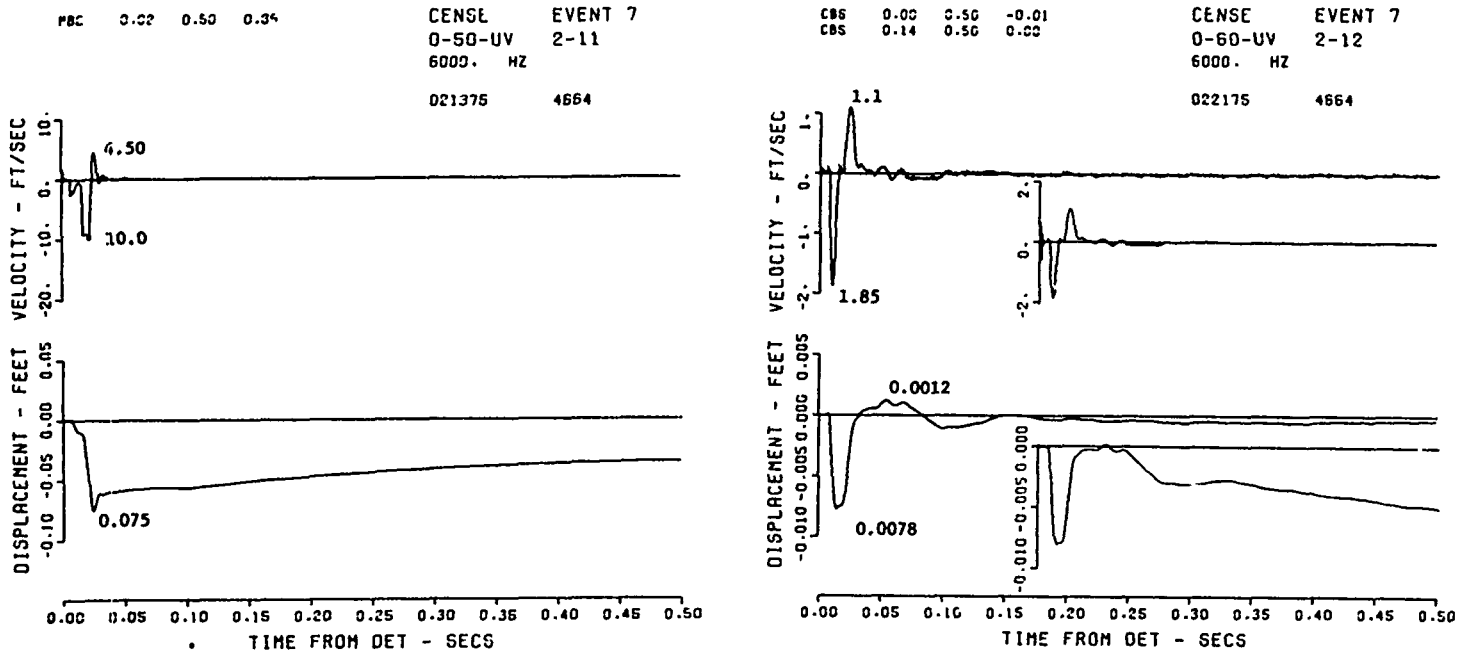

Figure B.22 (sheet 3 of 5).

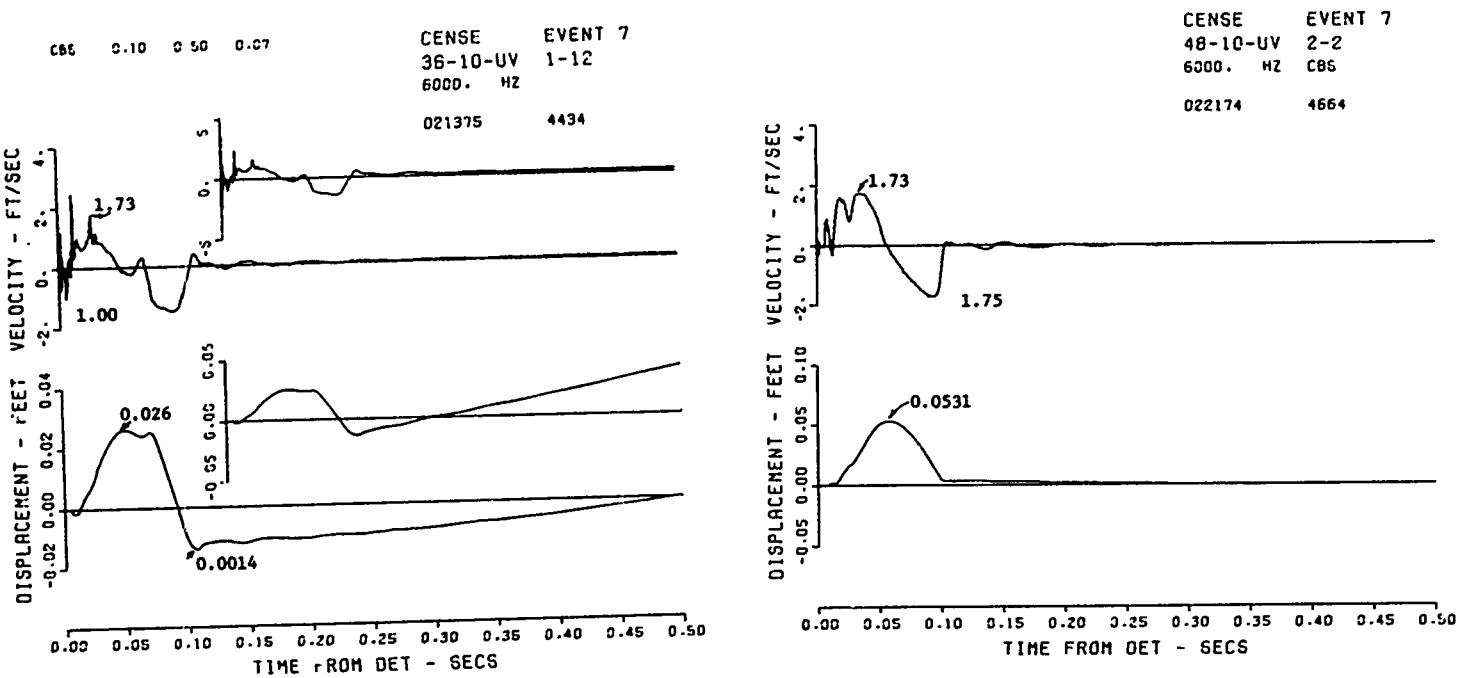

Figure B.22 (sheet 4 of 5).

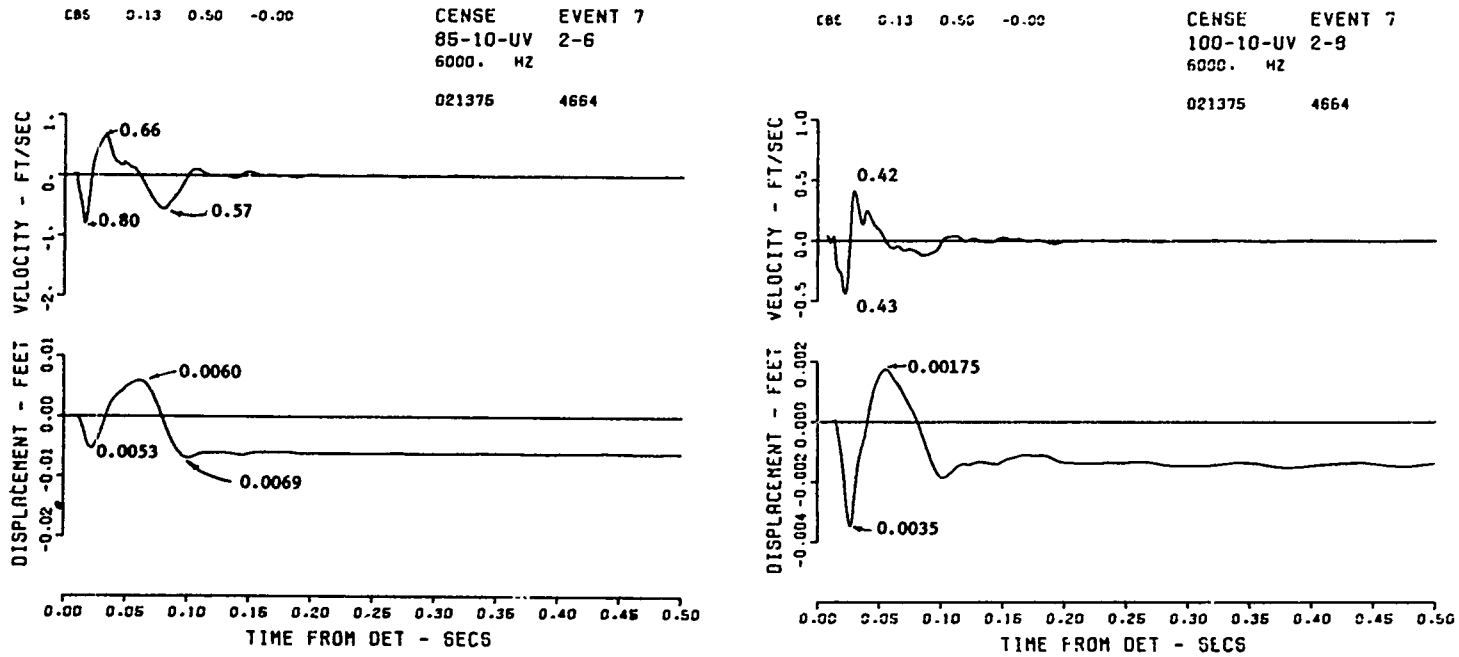

Figure B.22 (sheet 5 of 5).

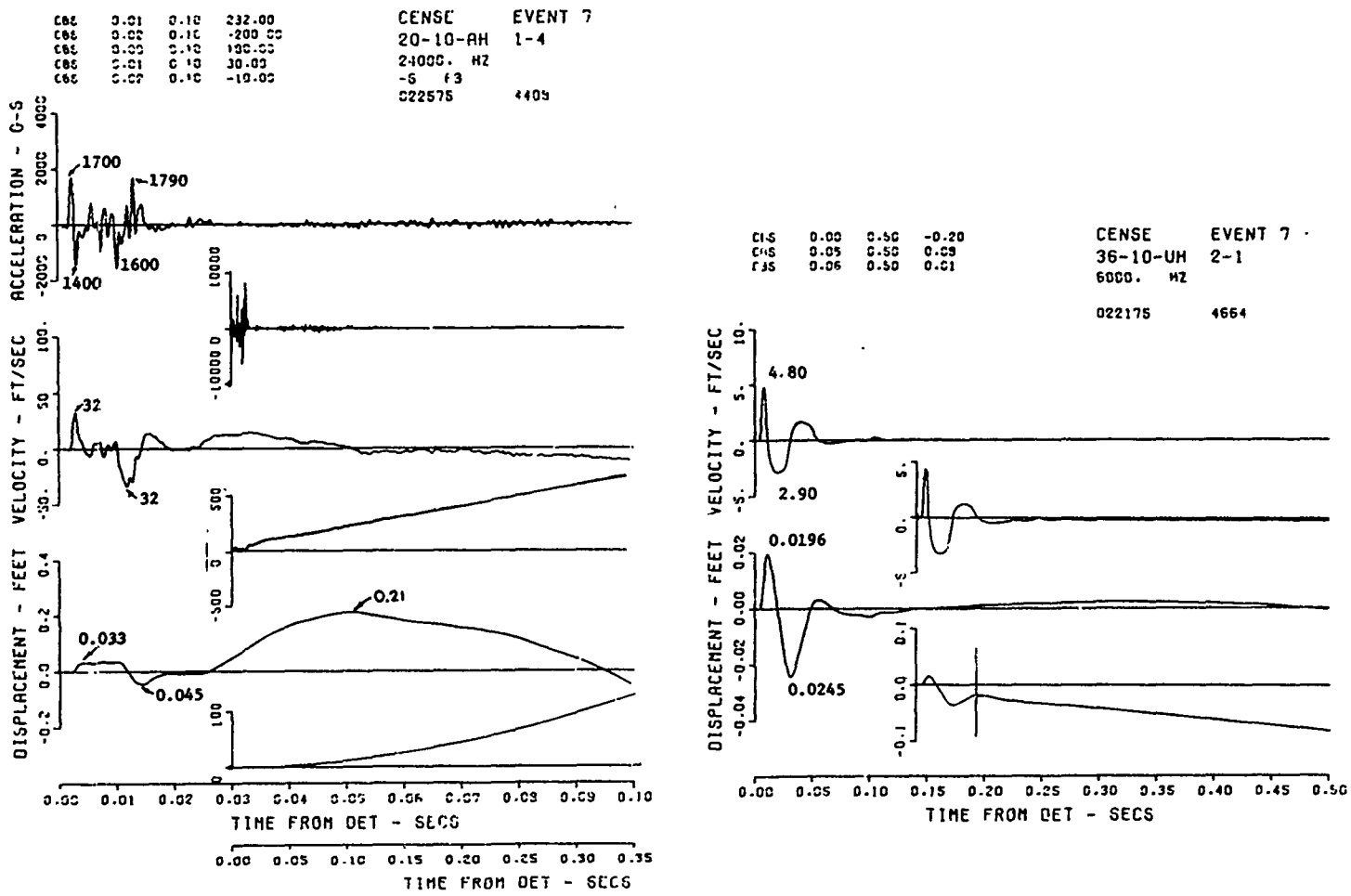

Figure B.23. Event 7, buried, +1 $W^{1/3}$ (10.5 feet) ; motion-time histories along the horizontal radial at charge depth (sheet 1 of 3).

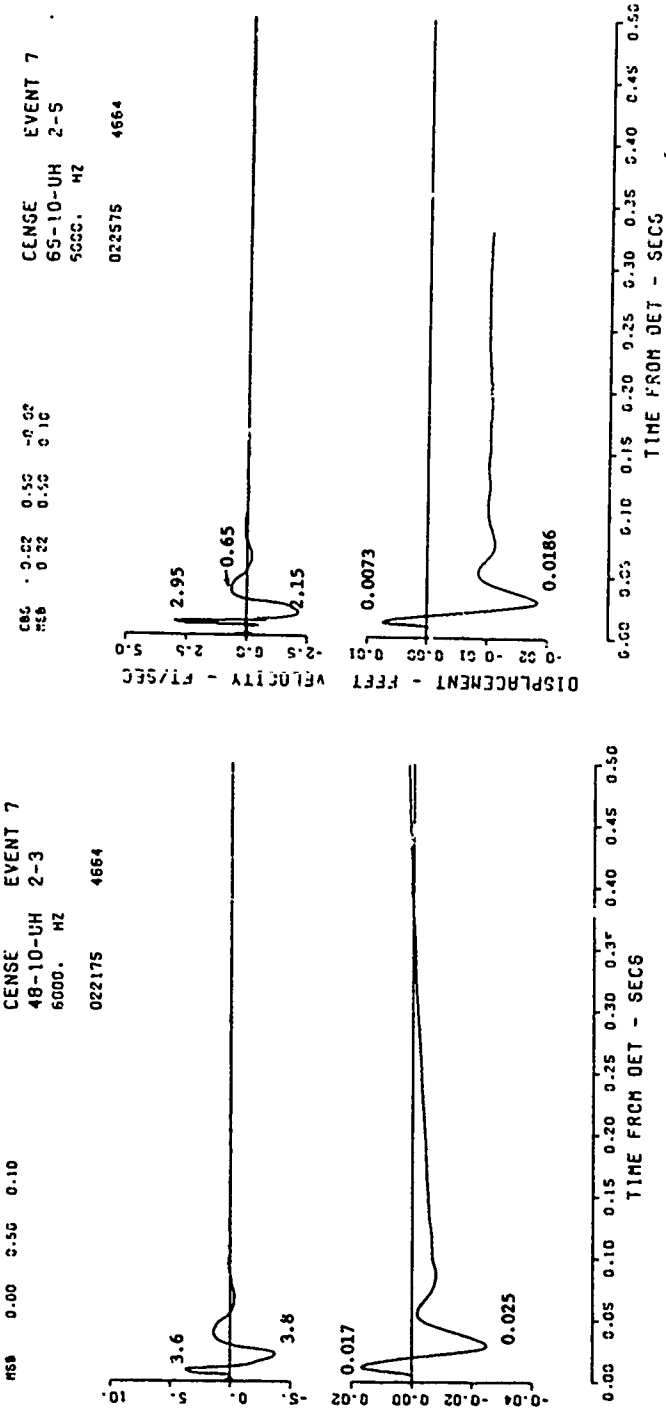

Figure B.23 (sheet 2 of 3).

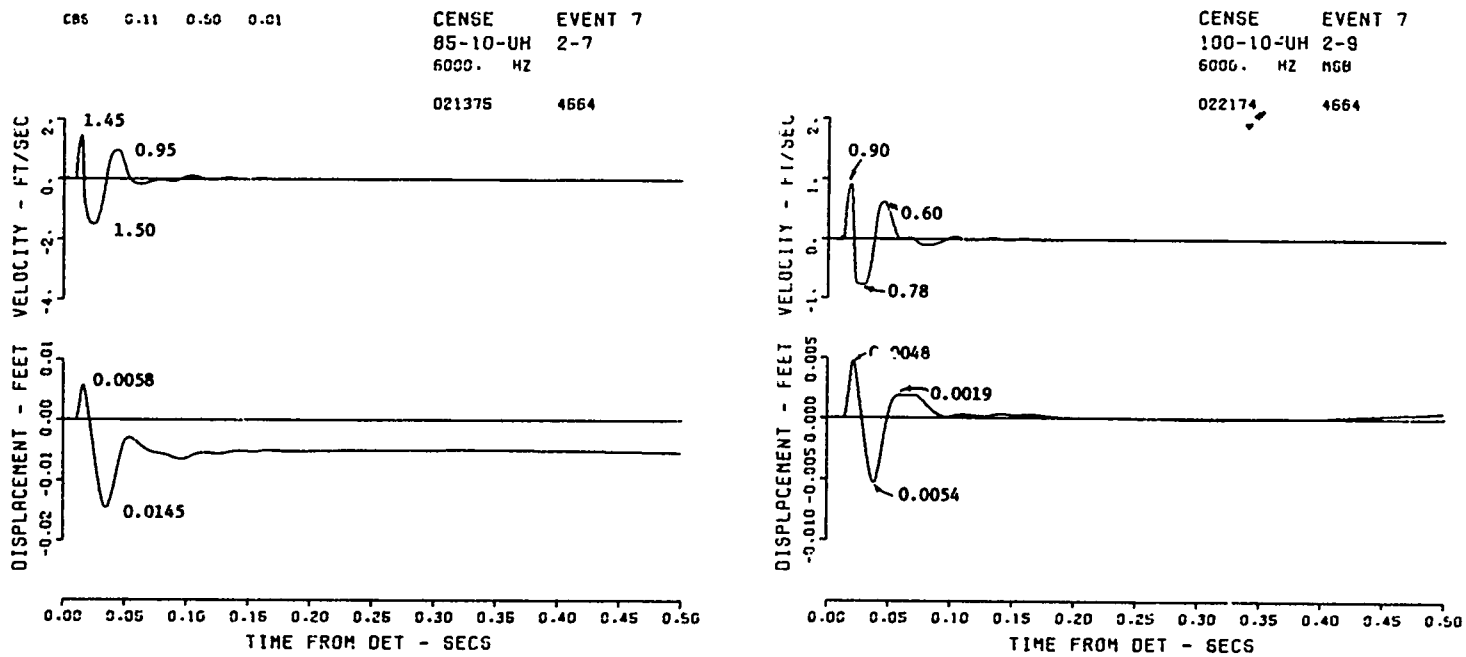

Figure B.23 (sheet 3 of 3).

APPENDIX C

NOTATION

AB	Surface airblast
AH	Horizontal particle acceleration
AV	Vertical particle acceleration
CG	Center of gravity of explosive charge
d_a	Apparent crater depth, feet
d_t	True crater depth, feet
DOB	Depth-of-burst below rock surface (to center of charge)
GZ	Ground zero
HE	High explosive
HOB	Height-of-burst above rock surface (to center of charge)
NM	Nitromethane explosive
r_a	Apparent crater radius, feet
r_t	True crater radius, feet
R	Slope of data with respect to distance
R_c	Charge radius = 1.5 feet
SZ	Surface zero
UH	Horizontal particle velocity
UV	Vertical particle velocity
v_a	Apparent crater volume, ft^3
v_t	True crater volume, ft^3
W	Charge weight (TNT equivalent), pound = 1140 pounds
$W^{1/3}$	Scaled charge weight = $(1140)^{1/3}$ = 10.45 $ft/lb^{1/3}$

In accordance with letter from DAEN-RDC, DAEN-ASI dated 22 July 1977, Subject: Facsimile Catalog Cards for Laboratory Technical Publications, a facsimile catalog card in Library of Congress MARC format is reproduced below.

Ingram, James K
CENSE explosion test program; Report 1: CENSE 1, explosions in sandstone / by James K. Ingram. Vicksburg, Miss. : U. S. Waterways Experiment Station, 1977.
164 p. : ill. ; 27 cm. (Technical report - U. S. Army Engineer Waterways Experiment Station ; N-77-6, Report 1)
Prepared for Office, Chief of Engineers, U. S. Army, Washington, D. C., under R&D Project 4A763734DT08, Task 09, Work Unit 008, Ground Shock from Multiple Bursts.
References: p. 66-67.

1. Air blast waves. 2. Cratering. 3. CENSE (Program). 4. Ground shock. 5. High explosives. 6. Sandstones. I. United States. Army. Corps of Engineers. II. Series: United States. Waterways Experiment Station, Vicksburg, Miss. Technical report ; N-77-6, Report 1.
TA7.W34 no.N-77-6 Report 1